Measurement of Transition Probabilities for Mn I Lines and the Manganese Solar Abundance

Thesis by

Thomas Russell Greenlee

In Partial Fulfillment of the Requirements

for the Degree of

Doctor of Philosophy

California Institute of Technology

Pasadena, California

1978

(Submitted April 17, 1978)

Acknowledgments

My thanks and praise must go above all to a person whom I met after my first year at Caltech, my Lord and Savior Jesus Christ. He has indeed "turned my mourning into dancing" and "put off my sackcloth and girded me with gladness." (Psalm 30:11) He has done this in several ways. First, He recognized that I was cut off from God by my thoughts, words and deeds, by the sins I committed by my own choice. I was "dead in trespasses and sins," a "child of disobedience" (Ephesians 2:1-2). And He cared enough about me to do something about that separation from God. First, He came to earth: "and the Word was made flesh, and dwelt among us." (John 1:14) And at the end of His life here, as Isaiah says, "Surely He has borne our griefs and carried our sorrows, yet we did esteem Him stricken, smitten of God and afflicted. But He was wounded for our transgressions; He was bruised for our iniquities; the chastisement of our peace was upon Him, and with His stripes we are healed. All we like sheep have gone astray; we have turned every one to his own way, and the Lord has laid on Him the iniquity of us all." (Isaiah 53:4-6) So Christ, when He was on the cross, paid the penalty for my disobedience and made it possible for me to have the kind of relationship with God that God wants me to have.

I accepted that payment by asking for His forgiveness and asking Him to come into my life as my Savior and Lord. Since that time He has given me "abundant life", meaningful, rewarding

life, just as He promised (John 10:10). He has given me peace about the future. I can rely on Him to provide everything I need here, and I need not fear death because He has given me eternal life. He has given me great joy in the present by providing many excellent friends who have encouraged and helped me and by enabling me to see that He has something to give me or show me every day; there are no worthless days. And He has given me a satisfaction about the past, especially the past six years, by showing me His reality, power and reliability in helping me to do far more than I could do on my own, especially in times of crisis when I was powerless. He transformed the crises into displays of His power and love.

One of the greatest blessings Christ has given me is my advisor, Ward Whaling. His provision of this thesis problem, his patient advice and perceptive criticism and his availability when I needed help have made this project possible. I have especially appreciated his concern not only for my research but also for my education as a physicist and for my personal welfare.

William Lennard helped me very much during my first year of research. He helped me learn how to use the equipment, the computer programs and the literature. Much of what he did in his thesis work was of use to me in this project.

Charles Barnes has been a great help and encouragement to me. He was my Modern Physics teacher during my first year, research advisor the following summer and teacher of my reading course the second year. Life at Caltech has been made much more

enjoyable because of his help and many good coffee-break discussions with him.

The people of Kellogg Lab have made the laboratory an excellent place to work. I am grateful for the help I have received from JoAnn Boyd, Paula Dunn, Evaline Gibbs, Gloria Laird, Jan Rasmussen, Kim Steiner and Marty Watson. Don Woshnak and Will Shick have patiently taught and retaught me machine-shop techniques and have helped me make many things in the shop. Laurie Graham, Al Massey, Fernand Meulmans and Myrl Warrick cheerfully initiated me into the knowledge of the mysteries of the electronics shop, tandem lab and chemistry lab. George Fox and Barbara Zimmerman have given me much assistance in the debugging and use of the lifetime measurement data-analysis program. Peggy Dyer and Mirmira Dwarkanath helped me to get acquainted with the equipment and people in Kellogg during my first summer at Caltech. Don McGrath assisted me often and cheerfully in maintaining the Van de Graaff generator, and he taught me the use of much of the equipment in room 200. All of the above people have, through their friendship, good humor and helpfulness, made work much more enjoyable than it would have been without them.

There are many people who have given me helpful advice during the course of this work, and for that advice I am grateful. These people include William Fowler, Jesse Greenstein, Ralph Kavanaugh, Guido Munch, Bill Russell, and Richard Ward. Robert Marcley has helped me learn about and use equipment ranging from amplifiers to programmable pocket calculators to vacuum pumps.

Don Skelton has taught me much about teaching and data analysis. The electronics workshop led by Irv Moskovitz and Tony Peitch was very helpful.

Nancy Durland, Ann Freeman, Iris Gimbrett, Polly Grandmontage and Marge Slight have been great morale boosters. Many good conversations with them have come at just the right time to cheer me up and get me back to work with renewed enthusiasm.

Special thanks are due to Sharon Vedrode for typing this thesis and to Diana Crozier for inking many of the figures.

Some of my most enjoyable times here were spent with hospitable friends who invited me to their homes for a meal and an evening of relaxation off campus. Those at Caltech who have nourished me with excellent food and even better company are Mark and Nicki Dumke, Bob and Christie Hatch, Mike and Margo Huffman, Bonnie Ludt and Bill and Kathy Russell. I enjoyed the friendship of Bill and Joann Westbrook, and the trips with Bill to Mounts Wilson and Palomar greatly enriched my life here and provided a needed rest, change of scene and break in the standard routine. I cannot list here all of those outside of Caltech whose hospitality I have enjoyed, but I must mention specifically Bonnie Abo, Pat Barnett, Anita Brewer, Valerie Clifton, Pam Cook, Terri Forshee, Ellen Heston, Jennifer Lisle, Maryann Olofsson, Jim Pearson, Althea Penner, Ron Pithart, Dennis and Susie Pool, Rosemary Swank, Carol Timms, Karen Ventimiglia and Norine Winters. Monte and Luana Withee, friends from my undergraduate

days, have made my vacations back home much more enjoyable through their hospitality.

The people of the Caltech Christian Fellowship and Lake Avenue Congregational Church have been a constant source of strength, love and encouragement to me. Don Page led me to see that I needed Christ and that He wanted to come into my life. Don, as friend, prayer partner, physicist and fellow-sufferer in running, taught me what it meant to delight in Christ, to serve Him and to enjoy physics simply because physics is neat stuff. Others who have helped me as prayer partners, running partners, friends and examples are Gary Yamamoto, Dave Fenska, Cary Huffman, Mike and Margo Huffman, Jeff Hamilton, Don Kuehne, Russ Potter and Jack Wisdom. Many at Lake Avenue Church, particularly Carl Garbe, Bruce Leafblad, Marv Jacobs, Chuck Miller, Ray Ortlund, Cecil Potter and Kent Tucker, have helped me as teachers and examples. Don and Natalie Gray have given me joy and strength through their wise advice, hospitality and designation of me as "uncle" to their children. I owe a lot to many people not named here for their prayers for me over the years.

Many of the people of Keck House have also made life more enjoyable here. Neil Gehrels, Dan Nadeau, Betty Vermeire and Ellen Williams have been good examples of service to others in their planning of parties and barbecues and baking cakes for special occasions. Irene Casey, Carmen de la Fuente and Robert Gang have made sure that the house was clean and in good repair. The students in Keck House have made it a fine place to live,

giving me privacy when I wanted privacy and good company when I wanted it.

My support during my first three years here came from the National Science Foundation in the form of a Graduate Fellowship, for which I am very grateful. Thanks are also due to the NSF for support of this research under grants PHY76-83685 and AST76-81607 and to the Office of Naval Research for grant N00014-75-C-0424. Caltech has helped me much through teaching assistantships and tuition scholarships.

Thanks go also to my teachers at Michigan Technological University and especially to Larry M. Julien, David Leddy, Dean C. Luehrs and Otto Ruehr for their conscientious teaching, encouragement and patient writing of many letters of recommendation both to graduate schools and to prospective employers.

Finally, I would like to thank my relatives and immediate family for their love and support. My aunt, Rachel Rooney, has helped me very much through hospitality and concern for me. Jim and Christie Greenlee and Dan and Linda Greenlee, my brothers and sisters-in-law, have encouraged me and stood behind me. My grandfather, Edward Allinger, has supported me with gifts and prayers.

My greatest debt, under Christ, is to my parents, Robert and Eloise Greenlee. It was through their teaching and guidance that I developed good study habits and a desire to do as well as I could in school. They did not direct me into an occupation, but when my interest turned to physics they encouraged me in my studies.

It has given me a great sense of security to know that they have always been willing to help me in any way they could. Their frequent letters, gifts and telephone calls have been cherished as reminders of their love for me. It is to them that this thesis is dedicated.

Abstract

Absolute transition probabilities have been measured for 81 lines from 14 upper levels of Mn I. Upper limits of transition probabilities for another 14 lines from 7 of these levels have also been measured. The method used was the measurement of relative transition probabilities (branching ratios) of lines from each upper level and the normalization of these relative probabilities to a scale set by the measured lifetime of the upper level. The lifetimes were measured by the technique of beam-foil spectroscopy. The transition probabilities of four lines were used with equivalent widths measured from the Preliminary Edition of the Kitt Peak Solar Atlas (Brault and Testermann 1972) and the model atmosphere of Goldberg et al. (1960) to calculate a value for the solar abundance of manganese of $A_{Mn} = 5.44 \pm .10$. The ratios of abundances of manganese, iron and nickel, values for the latter two elements taken from the table of Ross and Aller (1976), were compared with corresponding ratios predicted by four models of nucleosynthesis. The closest agreement with the observations was obtained from models using combinations of explosive oxygen burning, explosive silicon burning and the e process with α-rich freeze-out.

Table of Contents

Table of Contents (Continued)

Table of Contents (Concluded)

1. Introduction

1.1 The Definition of Solar Abundance

The abundance of an element in the solar photosphere is determined by an examination of the absorption lines this element produces in the solar spectrum. Spectra of the sun record the strength of absorption lines with respect to the continuum level of radiation. From wavelengths of about 4000 Å to 16000 Å this continuum level is determined by the formation and dissociation of H^-, which depends on the density of H in the photosphere. Hence the intensity relative to the continuum is a measure of the number density of atoms and ions of an element compared to that of hydrogen atoms and ions. So the number to which we refer as the solar abundance of element X is

$$A_X \equiv \log_{10}(N_X/N_H) + 12.00 \quad , \qquad (1\text{-}1)$$

where N is the number density of each element. The addition of 12 is a convention introduced by Claas (1951) to avoid negative numbers as abundances.

1.2 The Motivation for this Project

One of the chief motivations for determining abundances in general is the need to test theories of stellar nucleosynthesis. Since the classic paper by Burbidge et al. (1957) many workers have presented calculations of how different elements have been produced. (See Trimble 1975 for a review of models of nucleosynthesis.) The only way to test those theories and to determine

the physical conditions at the time of element formation is to examine the chemical composition of the present universe. As Woosley (1976) notes, "The experimentally determined abundance pattern of the chemical elements has always constituted the primary input and chief constraint upon theories of elemental nucleosynthesis." Among the objects which are examined are meteorites, the sun and other stars.

The sun is an interesting object of study because it is believed that the composition of the solar photosphere, except for the elements Li, Be and B, is the same as that of the original nebula which condensed to form the solar system (Cameron 1973). This nebula was the product of nuclear burning processes in stars and subsequent ejection of matter from stars into the interstellar medium. So the composition of the solar photosphere gives us information about nuclear processes and physical conditions in the stars which ejected the material.

Meteorites are believed to be composed of the nonvolatile elements of the original solar nebula (Cameron 1973). It is interesting to compare abundances of elements in the sun and in meteorites not only to test the consistency of the results but also to check the chemical fractionation which has occurred in the formation of meteorites. Urey (1967) discusses the questions which arise if solar and meteoritic abundances disagree.

Manganese is an interesting element to study because it is a member of the iron group of elements (roughly vanadium through nickel) and shares some characteristics with the rest of the

group which make the abundance determination important. The nucleosynthesis processes which produce iron group elements are hydrostatic C, O and Si burning, C detonation in degenerate cores, explosive O and Si burning and the e-process (Trimble 1975), so the comparisons of calculated and measured relative abundances test theories for these processes.

The iron group elements are relatively abundant in the sun and in most stars. (See, for example, the solar abundance table of Ross and Aller 1976.) This abundance combined with other properties of the atoms can have significant effects in stars. Because of the abundance and atomic numbers of iron group elements (roughly 23-28), these elements affect the opacity in many types of stars. In the outer layers of many stars the continuum opacity is determined by the dissociation and recombination of the H^- ion, and the continuum opacity depends on the electron pressure. So, although the continuum absorption by metal atoms and ions themselves is slight, their abundances affect the opacity through their contribution to the electron pressure (Ross and Aller 1976). Watson (1969) has demonstrated that the abundance of iron affects the opacity near the core of the sun through the bound-free transitions of highly charged iron ions. He reported that an increase in N_{Fe} by a factor of 10 would double the calculated neutrino flux from the sun. Other iron group elements would have a similar influence on the opacity in proportion to their abundances.

Because of the abundances and the rich spectra due to the several equivalent 3d electrons of iron group elements, lines from

atoms and ions of these elements dominate the spectra of many stars. For example, over half of the lines identified in the solar spectrum (Moore et al. 1966) of solar origin are from iron group elements. These lines must be taken into account for accurate model atmospheres analysis (Mihalas 1970), and, therefore, the abundances of the elements producing the lines must be known.

Determinations of the manganese solar abundance have been made by other workers with varying results (see Table 1), but another determination was judged to be worthwhile for at least two reasons. One of these reasons is the uncertainty regarding oscillator strengths of Mn I lines. The abundance in the photosphere is determined by measuring the amount of radiation absorbed in spectral lines and by calculating the number density of atoms or ions which would absorb the observed amount of radiation. The strength of an absorption line is a function of $N_\ell g_\ell f_{\ell u}$, where N_ℓ is the number density of manganese atoms or ions in the lower level, g_ℓ is the statistical weight of the lower level and $f_{\ell u}$ is the oscillator strength of the ℓ-u transition. (See the Atomic Physics section for the definition of oscillator strength.)

The abundances of iron group elements have been very uncertain because of different oscillator strengths used. (See Table 1 for the sources of oscillator strengths used in earlier determinations of A_{Mn}.) Concerning abundance determinations, Pagel (1973) wrote, "The skeleton in the cupboard, so far as photospheric abundances are concerned, is undoubtedly the oscillator strengths,

especially for elements in the iron group for which no decent theory is available..."

One of the reasons for the uncertainty in transition probabilities of iron group elements is the difficulty of producing a known concentration of a given energy level. Conventional methods of measuring absolute oscillator strengths have depended on the measurement of vapor pressure, the weighing of an atomic beam, or the determination of the temperature of a flame, all difficult measurements. The production of a vapor of known concentration is especially difficult, and gaseous compounds of iron group elements are difficult to produce, dangerous to use and unstable, so that their use in spectroscopy has been limited.

The relatively new method of measuring oscillator strength proposed by Kay (1963) and Bashkin (1964) by measuring the mean radiative lifetime of excited states is free of the difficulties of the other methods; there is no determination of the temperature of a flame or the density of atoms in a given energy level. The lifetime of an upper level provides an absolute scale to which to adjust relative oscillator strengths of emission lines from the upper level.

All measurements of oscillator strengths used in abundance determinations have involved the measurement of relative oscillator strengths and the normalization of these relative strengths to an absolute scale. In the work of others the measurement of relative oscillator strengths has depended on the measurement of the temperature of an arc or furnace and the assumption of local

thermodynamic equilibrium, and the whole series of relative values have been normalized using the absolute oscillator strengths of from one to three lines. Our method of measuring relative oscillator strengths involves no determination of temperature, since the relative strengths are measured only for lines from the same upper level and are normalized using the lifetime of that upper level. Therefore, we avoid the errors that may occur in relative oscillator strengths due to errors in temperature determination or deviations from local thermodynamic equilibrium in an arc.

In response to the need for additional independent determinations of f-values and solar abundances, Caltech has carried out a program of measurement of absolute f-values of lines of iron group elements in the solar spectrum. This program has included Fe (Whaling et al. 1969, Smith 1972), Ni (Lennard 1974), Cr (Cocke et al. 1973) and Ti (Whaling et al. 1977), and a study of Co is under way. The investigation of Mn was a logical step in this program because, as Woosley (1976) observes, it is the pattern of abundances rather than any single abundance which is critical to the evaluation of nucleosynthesis theories. We consider our Mn abundance in relation to the abundances of other iron group elements.

Therefore, the objective of this project was to select lines well-suited for the determination of A_{Mn} and to make a completely independent determination of their absolute oscillator strengths. This objective has been achieved, and these oscillator strengths have been used to determine A_{Mn}.

Another reason that this determination of the Mn abundance was needed concerns the choice of lines in the solar spectrum from which abundances have been calculated. Other investigations have used, for the most part, lines on the saturation or damping parts of the curve of growth. (See Chapter 4 regarding the curve of growth, and see the equivalent widths in Table 1.) For these lines the abundance depends on the value of the microturbulence velocity used; the abundances are thus dependent on the model atmosphere. The use of such lines is especially hazardous with manganese because the hyperfine structure can affect the abundance calculated from such lines (Heide 1968). In this investigation only lines on the linear portion of the curve of growth are used for abundance determination. These lines give results which are very little affected by the model used or by hyperfine structure. We have further restricted our selection to $\lambda > 4000$ Å, a region of the solar spectrum where the continuum is well defined and where equivalent widths can be measured accurately.

1.3 Atomic Physics

The quantity which we set out to determine for many lines in the manganese spectrum is the absolute transition probability $A_{u\ell}$. This is the probability per unit time for a spontaneous decay from level u to level ℓ, where E_u, the energy of level u, is greater than E_ℓ. If there are N_u atoms in level u at a certain time the number of transitions per second to ℓ is $N_u A_{u\ell}$. As shown in Sobel'man (1972),

$$A_{u\ell} = \frac{1}{2J_u + 1} \frac{4\omega_{u\ell}^3}{3\hbar c^3} |(\ell \| D \| u)|^2 \qquad (1\text{-}2)$$

where $\omega_{u\ell} = \frac{E_u - E_\ell}{\hbar}$ c is the speed of light, $\hbar$ is Planck's constant divided by 2π, J_u is the angular momentum of level u, and $(\ell \| D \| u)$ is the reduced matrix element of the dipole moment operator.

The quantity often used in abundance determinations is the Ladenburg oscillator strength $f_{\ell u}$. This is easily calculated using the transition probability

$$g_\ell f_{\ell u} = \frac{mc^3}{2e^2 \omega_{u\ell}^2} g_u A_{u\ell} = 1.499 \times 10^{-16} \lambda_{u\ell}^2 g_u A_{u\ell} \quad , \qquad (1\text{-}3)$$

where g_u, the statistical weight of level u, is $2J_u + 1$, m and e are the electron mass and charge, respectively, and $\lambda_{u\ell}$ is the wavelength of the transition in Å. Hereafter the product $g_\ell f_{\ell u}$ will be referred to as gf.

To find the transition probabilities we had to measure the mean lives of several upper levels. The mean life of a level u is

$$\tau_u = \left(\sum_\ell A_{u\ell} \right)^{-1} \quad . \qquad (1\text{-}4)$$

If one starts at t = 0 with $N_u(0)$ atoms in level u and if there is no replenishment of level u then the number of atoms in u at time t is

$N_u(0)e^{-t/\tau_u}$. The number of photons per second of wavelength $\lambda_{u\ell}$ emitted at t is $N_u(0)A_{u\ell}e^{-t/\tau_u}$.

Later in this thesis we make use of the fact that when LS coupling is a good approximation τ_u is the same for every level of a term ^{2S+1}L, where L represents the total orbital angular momentum of the electrons, and S is the total spin angular momentum quantum number of the electrons. The demonstration of this equality of lifetimes is presented in Appendix A.

The other quantity which was measured was the branching ratio, $BR_{u\ell}$, for each transition of interest. This is defined as

$$BR_{u\ell} \equiv \frac{A_{u\ell}}{\sum_k A_{uk}} \quad . \tag{1-5}$$

So the branching ratio is the fraction of transitions from level u that go to level ℓ.

1.4 Summary of the Method

The first step of this project was to measure the lifetimes of the upper levels of interest by the technique of beam-foil spectroscopy as described in Chapter 2. Next, the branching ratios were measured using a hollow-cathode light source and the 5-meter Paschen-Runge spectrometer in Bridge Laboratory. From the lifetimes and branching ratios the $A_{u\ell}$'s and gf's were calculated: $A_{u\ell} = BR_{u\ell}/\tau_u$. The branching ratio measurements and gf results are presented in Chapter 3. Then, using the preliminary solar atlas from the Kitt Peak National Observatory, the model

atmosphere of Aller and Pierce (1952) and our measured gf's, we calculated A_{Mn} as described in Chapter 4.

The basic outline of this project is similar to that of previous Caltech work on other elements. However, the approach taken was a bit different, and manganese presented some difficulties not encountered with other elements. Our Mn study differed from earlier Caltech studies of iron group elements in the following ways:

(1) The selection of levels for lifetime measurements. The Caltech study of other elements commenced with a survey spectrogram of the beam-foil spectrum, and lifetime measurements were carried out for the strong well-separated lines. In this work we limited our search to upper levels of lines useful for solar abundance determination by first examining the solar spectrum (Moore, 1966) for useful lines, then finding the upper levels of these lines and finally finding strong lines from these upper levels which were suitable for lifetime measurement.

(2) One of the difficulties encountered with manganese was the blending of lines in the same multiplet. Due to the close spacing of levels in the terms which were studied (≤ 235 cm^{-1} between adjacent levels) many lines in the beam-foil spectrum were blended with lines of the same multiplet, and lifetime measurements had to be made using lines from different upper levels of the same term. The effect of using such blends had to be determined to give meaning to the results of the lifetime measurements. (See Chapter 2.)

(3) Manganese has a large nuclear magnetic moment (3.47 nuclear magnetons), and, therefore, some lines of the spectrum show large hyperfine structure. Such structure is important for some lines in the determination of solar abundances (Heide, 1968) and had to be considered. (See section 3B of Chapter 4.)

(4) Spectroscopically pure manganese, unlike Fe and Ni, is not available in solid form suitable for constructing a hollow cathode. It is available as a fine powder. A method was devised to make a suitable cathode for the hollow cathode lamp from this powder.

Some instrumentation was changed for this project. The monochromator used in the lifetime measurements was a Jarrell-Ash model 82-210, a .25 M Ebert monochromator, rather than the McPherson 218 monochromator used in the Fe and Ni work. The Jarrell-Ash instrument was faster (f/3.5) than the McPherson (f/5.3), which is important for beam-foil work because of the weakness of the light source. Also, in measuring the upper limits of branching ratios of lines near 2200 Å with the Paschen-Runge spectrometer a D_2 discharge lamp was used to calibrate the system in the ultraviolet since the tungsten-filament standard lamp is too weak at that wavelength. This was our first use of the D_2 discharge lamp as a calibration standard.

2. Lifetime Measurements

2.1 The Selection of Lines for Study

Since the goal of this experiment was to determine the solar abundance of manganese, the lifetime measurements were limited to upper levels of Mn I lines in the solar spectrum. A search was made in The Solar Spectrum (Moore et al. 1966) for unblended Mn I lines with wavelengths between 4000 Å and 8770 Å. This search yielded 77 lines.

From the lists of solar lines the best upper levels for study were chosen. These were levels with at least two usable branches or one very clean (approximately .17 Å or more from neighboring lines) unblended usable solar line per level. This narrowed the investigation to eight upper levels producing thirteen useful solar lines. These lines and their upper levels were:

upper level	λ_{Moore} (Å)
$z^6F^o_{7/2}$	5004.894
$z^4F^o_{9/2}$	5255.325 5260.778
$z^4F^o_{5/2}$	4671.687
$z^4F^o_{3/2}$	4739.113 4761.528
$z^4D^o_{5/2}$	5348.070 6440.934
$e^4S_{3/2}$	5377.614 5399.479
$e^4P_{3/2}$	4825.604 4854.616

upper level	λ_{Moore} (Å)
$e^6D_{9/2}$	8741.68

The Revised Multiplet Table (Moore 1945) was used to find the branches from these upper levels. Then the strongest branches of each upper level of interest were found from Corliss and Bozman (1962). Although the absolute transition probabilities of Corliss and Bozman are known to be in error, these tables provide a rough guide to the relative strengths of lines from the same upper level. Since the beam-foil light source is very weak, only the strongest branches of an upper level can be used for the lifetime measurements.

Then a search was made of our beam-foil spectrum for strong lines from the chosen upper levels. The lines from two of the upper levels of interest ($e^6D_{9/2}$, $e^4S_{3/2}$) were not seen, and those from the $e^4P_{3/2}$ level were very weak. So our efforts were limited at first to finding the lifetimes of the remaining five levels ($z^6F^o_{7/2}$, $z^4F^o_{9/2,5/2,3/2}$, $z^4D^o_{5/2}$). The measurements were extended to lines from the other levels of the z^6F^o, z^4F^o and z^4D^o terms either because they were blended with the lines of interest or because the line from the level of interest was too weak for lifetime measurements or in order to check on the equality of lifetimes of levels within a term.

2.2 Method and Equipment

Since 1964 (Bashkin) the beam-foil method has been used to measure the lifetimes of excited levels of many elements. In this method ions are accelerated (by a Van de Graaff generator in our experiment), passed through a thin foil, usually carbon, and come out of the foil in many states of excitation and ionization. As the excited ions travel downstream from the foil they undergo radiative de-excitation. The intensity of light from a particular transition is measured at different distances past the foil, and the distance scale is converted to a time scale by means of the velocity of the beam downstream from the foil. Figure 1 is a schematic of the beam path, the spectrometer and the electronics used. This method has been used at Caltech by Whaling et al. (1969) for Fe I, Smith (1972) for Fe II and Lennard (1974) for Ni I. The method has been reviewed by Bashkin (1974).

The ion source is similar to the one described by Magnuson et al. (1965). Figure 2 is a drawing of the furnace. Current was passed through a 25 mil tungsten wire, heating both the furnace and the wire until the wire emitted electrons. Spectroscopically pure manganese powder placed in depressions drilled in the bottom of the furnace was heated to raise its vapor pressure to a few millitorr. Atoms of manganese in the vapor were ionized by electrons from the filament which were accelerated by a voltage difference between the wall of the furnace and the filament. A magnetic field was applied to lengthen the path traveled by the electrons through the manganese vapor. Another tungsten coil was used to provide

more heat when needed. The tantalum heat shields around the furnace, which had been used by Smith and Lennard, were removed to lower the furnace temperature. The lower temperature was necessary because otherwise a charge of manganese in the source was quickly exhausted in initially large (5-6 μamps) but quickly diminishing beams.

The ion source was in the terminal of the 2MV Van de Graaff generator in Kellogg Laboratory. Two beam energies were used in these measurements: approximately 300 keV and 500 keV. For both energies sixteen of the thirty-four resistors in the column were shorted out with a shorting strap to improve the electrostatic focus of the ion beam at the low terminal voltage. On the 300 keV runs an extension was added to the voltage regulating probe to increase the regulator current and improve the voltage stability.

The ions were extracted through a hole in the bottom of the furnace and accelerated down the column of the Van de Graaff. Mn^+ ions were separated from contaminants in the beam (primarily C and H) by a magnetic field. The resolution of the mass analyzer was better than 5%. Then the ions were separated by energy by an electrostatic analyzer calibrated by Lennard to ± .5% in energy using the 340.46 keV resonance of $^{1}H(^{19}F, \alpha\gamma)^{16}O$. Therefore, the ion velocity was known to ± .25%. The beam was collimated by micrometer-adjusted slits in front of the target chamber.

The target chamber contained carbon foils of thickness 5 or 10 $\mu g/cm^2$ (± 40%). These were mounted on tungsten mesh as

described by Smith (1972). The frames holding the foils were held by a rod which could be rotated, raised or lowered to place new sections of foil in the beam path. The 10 $\mu g/cm^2$ foils lasted about 5 minutes under bombardment by a 1-3 μamp manganese beam. The pressure within the target chamber was kept at approximately 10^{-6} torr, which gives a mean free path on the order of 100 meters for collisions of beam atoms with residual gas atoms. The beam was observed no more than 11 cm from the foil, so the probability of de-excitation by collisions with residual gas atoms was negligible. On one side of the target chamber was a window of GE 151 quartz through which the spectrometer viewed the beam.

The spectrometer was a Jarrell-Ash .25 meter Ebert monochromator mounted on a lathe bed to enable it to travel parallel to the beam. The monochromator had two gratings, one ruled with 1180 grooves/mm and blazed at 5000 Å, the other ruled with 2360 grooves/mm and blazed at 3000 Å. The speed of the monochromator was f/3.5. Figure 3 shows the monochromator optical system. Appendix 2 describes the alignment of the optical axis of the monochromator perpendicular to and at the same level as the beam.

An EMI 6256S phototube was placed at the exit slit of the monochromator. The photomultiplier was wired for pulse-counting, with the cathode at ground potential. The PMT was refrigerated with solid CO_2. A light pipe made from a 3 cm length of pyrex tube (1 cm I.D.) sealed at each end with quartz windows and filled with dry argon was used to conduct light through the wall of the refrigerator. The inner wall of the pyrex tube was lined with

aluminum foil to provide internal reflection in the light pipe. The anode of the photomultiplier tube was connected to the high-voltage power supply and to a preamplifier which led to the amplifier and scaler. (See Figure 1.)

Another photomultiplier tube, an RCA 8575, was used to monitor the amount of beam which passed through the foil. In this way the same amount of beam was used for each intensity reading in a given lifetime measurement. A light pipe was positioned out of the beam path downstream of the foil. This pipe conducted light of many wavelengths given off by the beam to the photocathode of the monitor photomultiplier. The signal current went to an Elcor A308C current integrator. A pulse from the integrator moved the beam stop into the beam when a preset amount of charge from the photomultiplier had been collected. This pulse also stopped the counting scaler and a timing scaler which was receiving pulses from a clock pulse generator in order to time each reading.

2.3 Procedure

For each line selected for measurement a scan was made of the beam foil spectrum in the vicinity of the line. The monochromator pass band (slit widths) and the Doppler width (acceptance angle) were set as large as possible without introducing interference from neighboring lines. Then the current integrator was set to give 2000-3000 counts at a distance .05-.10 inch from the foil. The photon counts for this integrated beam current were measured at different distances past the foil, usually in intervals of .20 inch.

Then the monochromator was moved back near the foil and readings were made between the first readings, so there were data for every .10 inch past the foil. The readings were stopped when a distance was reached for which the signal was approximately .05× the original signal, indicating that the beam had been observed for at least 3 mean lives of the state of interest.

Two kinds of background had to be subtracted from the raw data. Every 5-10 readings the dark counts from the pulse-counting photomultiplier were measured with the beam stopped. After the intensity readings were finished the spectrometer passband was set at a wavelength in a flat region of the spectrum near the line, and intensity readings were taken of this beam-dependent background at several distances past the foil. The dark background was measured for these readings, also. Figure 4 shows the spectrum near the line at 3806.715 Å from the $z^6F^o_{11/2}$ upper level. The raw counts minus dark background are plotted on the semilog scale versus distance from the foil. The lower curve shows the variation of counts at 3795 Å minus dark counts with distance.

2.4 Corrections to the Data

There were several corrections which had to be made to the data before they could be used to find the lifetimes. The dark background had to be subtracted from the raw data. If the dark background reading took time T_D to record N_D counts and a time T_S was used for a given signal intensity measurement, then $\frac{T_S}{T_D} N_D$ counts were subtracted from the signal as dark background. Dark

background also had to be subtracted from the beam-dependent background counts in the same way before the latter could be subtracted from the signal. So if N_S is the signal at the line peak for a certain position of the spectrometer and if N_B, T_B, N_{DB} and T_{DB} are quantities for the beam-dependent background measurements analogous to N_S, T_S, N_D and T_D, respectively, then the first correction to the data involved the calculation of

$$N_S - \frac{T_S}{T_D} N_D - \left(N_B - \frac{T_B}{T_{DB}} N_{DB} \right).$$

The energy of the beam before it hit the foil was determined by the electrostatic analyzer, but the energy loss of the beam in the foil was nonnegligible. This energy loss had to be calculated so that the velocity of the beam past the foil could be used to convert the distance scale to a time scale. The two types of interactions which need to be considered are the slowing down of the ion by its interaction with the electrons of the target material and the scattering of the ion by nuclei of the target. Hvelplund and Fastrup (1968) measured the energy loss for Mn ions through carbon foils and subtracted the nuclear scattering part of that energy loss using the theory of Lindhard et al. (1963) to find $\left(\frac{dE}{dx}\right)_e$, the electronic stopping cross section. They found that $\left(\frac{dE}{dx}\right)_e = kE^{.55}$, where k is 1.09×10^8 eV/(gm/cm^2). We have used this electronic stopping cross section with the theoretical nuclear stopping cross section of Lindhard et al. to calculate the energy lost by Mn ions in passage through the carbon foils. At 300 keV the total energy loss was approximately 6 keV/(μgm/cm^2).

The calculations were checked by a direct measurement of the beam velocity using a Doppler shift measurement. Since the Doppler shift of a photon of wavelength λ emitted at an angle θ with respect to the direction of motion of an atom moving at velocity v is $\Delta\lambda = \lambda \frac{v}{c} \cos\theta$, where c is the speed of light, one can measure the Doppler shift by viewing the beam head-on ($\theta = 0$) and from the side ($\theta = 90^{o}$). The $\theta = 0$ measurement was made by placing a mirror in the beam path at 45^{o} to the beam axis. A scan was made of the Doppler-shifted line, and then the monochromator was moved forward to measure the line at $\theta = 90^{o}$. The results of the measurements are listed in Table 2 with the Doppler shifts calculated from the energy loss analysis given above.

The foil not only reduces the beam energy but also scatters some ions out of the viewing area of the monochromator. As the downstream distance increases the monochromator will see a smaller and smaller fraction of the beam because the scattered ions will be at greater distances from the axis of the beam. The fraction of the beam seen by the spectrometer had to be computed for each distance past the foil, and the data with background subtracted were multiplied by the inverse of that fraction. The fraction was computed using the method described by Lennard (1974). The Blaugrund (1966) approximation for $\langle \theta_x^2 \rangle$, the mean square scattering angle in any given plane through the beam axis, was used with the Hvelplund and Fastrup (1968) and Lindhard et al. (1963) energy loss calculations to find the desired correction factor. The

largest correction factor used in any lifetime measurement was 1.23 for a distance 4.07 inches past the foil.

To make sure that no error was introduced by this procedure the lifetime of the $z\,^4D^o_{7/2}$ level was measured using the 4451.575 Å line and three different arrangements of the lens system to produce demagnifications of the image of the beam on the entrance slit ranging from 1/2 to 2/7. The lifetime measurements were also made at energies of approximately 300 and 500 keV and foil thicknesses of 5 and 10 $\mu g/cm^2$ to vary the calculated correction factor for a given distance past the foil. No systematic difference in lifetime with lens arrangement, foil thickness or energy was observed.

2.5 Analysis of the Data

The raw data read into the data analysis program were the readings of the monochromator position in inches, numbers of counts for a given integrated beam current, dark background for each reading, beam-dependent background, wavelength of the line used, magnification of the lens system, foil thickness and the energy of the beam read from the electrostatic analyzer setting. The program subtracted the background from the raw data, calculated the correction for scattering at each reading position, calculated the true beam energy based on the electrostatic analyzer calibration and subtracted the energy loss caused by passage through the foils. The corrected data were then fit to a single exponential or to a sum of exponentials,

$$I(x) = P_1 e^{M_1 x} + P_2 e^{M_2 x}$$

by a computer code which went through a series of iterations to minimize

$$\chi^2 = \sum_i \frac{[I_c(x_i) - I_m(x_i)]^2}{I_c(x_i)}$$

where the sum is over the readings taken, x_i is the distance past the first reading, I_c is the number of counts calculated, and I_m is the measured number of counts corrected for background and scattering of the beam.

The data were fit to a sum of exponentials because the equation governing the population of a given upper level u is

$$\frac{dN_u}{dt} = -N_u(t) \sum_i A_{ui} + \sum_j N_j(t) A_{ju} \qquad (2\text{-}1)$$

where i denotes levels lower in energy than u and j denotes levels higher than u. If the excitation occurs in a time interval very small compared with the lifetimes of the excited states then it can be said that the excitation populates a given level with N(0) atoms at time t = 0. If the second sum on the right side of (2-1) is negligible compared with the first, then

$$N_u(t) = N_u(0) e^{-t/\tau_u}$$

where

$$\tau_u \equiv \left(\sum_i A_{ui} \right)^{-1} .$$

If only one level j of lifetime τ_j contributes significantly to the second sum then

$$N_u(t) = N_u(0)e^{-t/\tau} \left\{ 1 + \frac{A_{ju} N_j(0) \tau_u \tau_j}{N_u(0)(\tau_u - \tau_j)} \right\} + e^{-t/\tau_j} \frac{A_{ju} N_j(0) \tau_u \tau_j}{\tau_j - \tau_u} .$$

The most general solution to (2-1) is a sum of exponentials with the number of terms in the sum depending on the number of non-zero N_j.

The quantity observed is the intensity of light of wavelength λ_{ui} emitted in the u-i transition. This intensity is $I_{ui}(t) = N_u(t)A_{ui}$, so the observed intensity should be one or a sum of exponentials. Since x = vt, where v is the velocity of the beam, each fitting parameter $M_k = \frac{-1}{v\tau_k}$, where τ_k is the mean life associated with the appropriate decay.

2.6 Possible Sources of Error

The beam-foil source produces atoms and ions in many states of ionization and excitation. Therefore, the beam-foil spectrum includes lines from several ionization states, and one must check to make sure that these lines do not affect the measured lifetime. We checked Inglesias and Velasco's (1964) list of Mn II lines to determine whether our lines of interest were blended with known Mn II lines. The lifetime measurements were also made at two

energies. Since the fraction of Mn I atoms in the beam decreases rapidly as the energy increases, measurements at different energies should reveal the presence of unknown lines (from Mn II or multiply charged ions) at the same wavelength as the line of interest. No systematic change in lifetimes was observed as the beam energy was changed. Also, the scans of the spectra at and around lines of interest gave no indication that lines from other charge states were contributing to the beam-dependent background.

Another possibility which must be considered is the replenishment of the upper level of interest by transitions from still higher levels. This is called cascading, and it has been responsible for many erroneous lifetime measurements by beam-foil spectroscopy. If there is no cascading, the data can be fit well to a single-exponential curve. The use of two or more exponentials to fit the data implies that cascading is present.

Curtis et al. (1970) have defined the replenishment ratio, R(t), which is the ratio of the rate of replenishment at time t of an upper level by cascades into it to the depopulation of that level by decays from it. For data fitted to a multi-exponential decay curve in which the first exponential contains the lifetime of the level of interest,

$$I(t) = \sum_{k=1}^{n} P_k e^{-t/\tau_k} \quad ,$$

the replenishment ratio

$$R(t) = \left[\sum_{k=2}^{n} \left(1 - \frac{\tau_1}{\tau_k}\right) P_k e^{-t/\tau_k} \right] \Big/ \sum_{k=1}^{n} P_k e^{-t/\tau_k} \quad .$$

R(t) is zero for a single exponential decay.

A convenient measure of the importance of cascading is R(0), the replenishment ratio at t = 0. For a sum of two exponentials this is $R(0) = \left(1 - \frac{\tau_1}{\tau_2}\right)\left(\frac{P_2}{P_1+P_2}\right)$. The slope of the decay curve at t = 0 is $\frac{dN(t)}{dt}\Big|_{t=0} = \frac{-N_1(0)}{\tau_1}[1 - R(0)]$. If $R(0) \ll 1$ the level is essentially unreplenished. If $R(0) \sim 1$ cascading is large and a multiexponential fit is required. If $R(0) > 1$ the decay curve will rise initially and cascading will dominate the observed intensity.

The measurements of lifetimes were actually started 2-4 nanoseconds from the foil, so the "R(0)" listed in Table 3 are actually R(2-4ns). It is seen that these "R(0)" are always much less than 1, with many of the decays being well fit with single exponentials. If the cascade lifetime is longer than the lifetime of interest, R(0) should be the minimum replenishment ratio, so R(2-4ns) is as good an indicator of cascade repopulation as R(0) would be since R(2-4ns) is at least as large as R(0). If the decay curve initially rose and reached its peak sooner than 4 ns from the foil the initial rise would be missed, but the observed lifetime would not be affected.

Another way of testing for cascading is to measure the lifetime using different beam energies, producing, one would expect, different distributions of atoms among the upper levels. This was

done, and, within the precision of the beam-foil method, no systematic differences in the measured lifetimes were observed. We conclude that cascading has not affected our lifetime measurements.

2.7 The Equality of Lifetimes of Levels within a Term

One of the problems encountered with manganese arose from the very close spacing of levels within the same term. There are energy differences of ≤ 240 cm^{-1} ($\sim .03$ eV) between adjacent levels in each of the z^6F^o, z^4F^o and z^4D^o terms. Therefore, lines in the same multiplet are often less than 1 Å apart and are blended in beam-foil spectroscopy. (See Figure 4.) The lines we have used in the lifetime measurements are blends of two or more lines from different upper levels of the same term. The significance of a lifetime measurement using such a blended line must be determined.

There are different possible interpretations of the light decay curve of a blended line when the curve is fit to a sum of exponentials. If the curve is well-fit by a single exponential, $I(x) = Pe^{Mx}$, it is apparent that there are no significant cascades and that either the upper levels of both lines have approximately the same τ or one component of the blend is much weaker than the other and contributes insigificantly to the intensity.

If the intensity decay curve is fit by a sum of two exponentials, $I(x) = P_1e^{M_1x} + P_2e^{M_2x}$, there are three possible interpretations. Either (1) there is a cascade or (2) the lifetimes of the upper levels of lines in the blend are different and the second

exponential represents the decay of one component of the blend. The third possibility is that both a cascade and the second component of the blend produce the second exponential.

If LS coupling is a good approximation in Mn for the relevant upper and lower levels the lifetimes of all levels of a term will be approximately equal, and that lifetime can be determined by using a blend of two lines from the same upper term. Some experimental evidence that LS coupling holds or that the lifetimes of the levels are the same within a term has been obtained.

One of the clearest pieces of evidence for the validity of LS coupling is the absence of intersystem ($\Delta S \neq 0$) transitions. For the levels from the terms of interest none of the branching ratios of intersystem transitions is $> 2\%$. Garstang (1977) has advised us that a lack of strong intersystem transitions is a very good sign that LS coupling holds and that the level lifetimes should be equal for levels within the same term.

The results for the blend of lines 3823.508 ($J_u = 9/2$) and 3823.891 ($J_u = 5/2$) provide a good example of the evidence for the equality of level lifetimes from beam-foil measurements. These lines are only 0.4 Å apart, while the full width at half maximum for a line is 2.2 Å when the 100 μ slits and low blaze grating are used in the Jarrell-Ash monochromator. This is the instrumental linewidth and does not include the Doppler width of the line. Therefore, both lines should contribute significantly to the intensity observed. For none of these measurements is $P_2 > .03\ P_1$, while from relative intensity measurements of the lines one would expect

I(3823.891) = .26 I(3823.508). From the R(0)'s listed in Table 3 it is seen that the intensity curves are essentially single exponentials [R(0) < .003]. The absence of a second exponential when one would be expected if $\tau_{9/2}$ and $\tau_{5/2}$ were different indicates that $\tau_{9/2} \approx \tau_{5/2}$.

The reasoning is similar for the other blends. The replenishment ratios are always < .07. Where the lines are closely blended P_2 is always much smaller than would be expected if the weaker component of the blend were causing the second exponential. In the 3806.715-3809.593 blend and that of the lines 3839.779, 3841.074 and 3843.988, one component is far enough from the other(s) that it could be argued that the component does not contribute significantly to the intensity measurement and may still decay at a rate different from that of the other components of the blend. However, in both cases measurements using other lines from the upper level of the weaker component of the blend indicate that the upper level lifetime is, within the experimental uncertainties, equal to the lifetime of the upper level of the stronger component.

For the z^4F^o term the strong lines from different levels were so closely spaced that there was no opportunity to measure different blends as was the case with the z^6F^o term. However, from Table 3 it is seen that all but one of the measurements of the 4761-4766 Å blend are nicely fitted with 1-exponential curves. For the one two-exponential fit $P_2 = .02\ P_1$ and $|M_2| < .25\ |M_1|$. The lifetime measured on the short-λ side of the peak (17.80 ns) is

about 14% ± 8% greater than that measured on the long-λ side of the peak (15.33 ns). The conclusion is that the lifetimes of the z^4F^o levels differ by less than 22%.

Because of the weakness in the beam-foil spectrum of lines from the z^4D^o term other than the 4451.575-4453.013 Å blend, only this blend is used in lifetime measurements for this term. Many of the fits used two exponentials, but R(0) is always less than .05, and $P_2 < .06\ P_1$. The M_2's vary widely and have little effect on M_1. From this it is seen that either 4453.013 Å contributes insignificantly to the intensity of the blend or $\tau_{7/2} \approx \tau_{1/2}$.

Measurements of Total Intensities

It was also possible to use the hollow-cathode lamp and the Paschen-Runge spectrometer described in Chapter 3 to test the equality of level lifetimes within a term, even though such measurements cannot reveal the values of the lifetimes. This test was motivated by the following considerations. The intensity in photons per second in the line at $\lambda_{u\ell}$ is $I_{u\ell} = N_u A_{u\ell} = C g_u A_{u\ell} e^{-E_u/kT}$, where C is proportional to a partition function. In Chapter 1 it was mentioned that

$$\frac{1}{\tau_u} = \sum_{\ell} A_{u\ell} \quad ,$$

so

$$\sum_{\ell} I_{u\ell} / [C g_u e^{-E_u/kT}] = \frac{1}{\tau_u} \quad .$$

Then

$$\frac{1}{g_u} \sum_{\ell} I_{u\ell} = \frac{C}{\tau_u} e^{-E_u/kT} \quad ,$$

or

$$\ell n \left(\frac{1}{g_u} \sum_{\ell} I_{u\ell} \right) = \ell n \left(\frac{C}{\tau_u} \right) - E_u/kT \quad . \tag{2-2}$$

Therefore, if we measure a quantity Q_u proportional to

$$\frac{1}{g_u} \sum_{\ell} I_{u\ell}$$

for each u of an upper term while keeping T constant, $\ell n\ Q_u$ plotted vs E_u should be a straight line if all τ_u are equal. If $\tau_u \neq \tau_{u'}$ one would not expect all of the points to fall on the same straight line.

In the experimental work with the Paschen-Runge spectrometer two detecting channels were used simultaneously. The stepping channel was used to scan different lines while the monitor channel was set at the peak of one strong line from the given upper term. $s_{u\ell}$ is the signal from the stepping channel at the peak of the line for the u-ℓ transition. $M_{u'\ell'}$ is the signal of the monitor channel at the peak of the u'-ℓ' line. $BR_{u\ell} = A_{u\ell} / \sum_k A_{uk}$, where the sum is over all lower levels.

To measure the total intensity of lines from the levels of a term, $s_{u\ell}/M_{u'\ell'}$ was measured for one line from each level of the upper term, with all measured lines in the same wavelength

region (within 40 Å of each other) and with all measurements for that term using the same monitor line $\lambda_{u'\ell'}$, and the monitor signal was kept approximately (within ± 4%) constant. The branching ratios $BR_{u\ell}$ were measured for all lines from all levels of the term.

The data were $s_{u\ell}$, $M_{u'\ell'}$, and the BR's. To convert them into the Q_u previously mentioned involved the following. $s_u = KI_{u\ell}$, where K is a constant. For lines in the same wavelength region no correction need be made for filter transmission or spectrometer response, so K is the same for all measured lines from the same term. $M_{u'\ell'} = K'I_{u'\ell'}$. Then

$$\frac{1}{g_u BR_{u\ell}} \frac{s_{u\ell}}{M_{u'\ell'}} = \frac{K}{K'N_{u'}A_{u'\ell'}} \frac{1}{g_u} \sum_k I_{uk} \quad .$$

If the monitor signal is constant $N_{u'}$ is constant, so $\frac{1}{g_u BR_{u\ell}} \frac{s_{u\ell}}{M_{u'\ell'}}$ is the quantity Q_u desired. Plots were made for each term of

$$\ell n\left(\frac{1}{g_u BR_{u\ell}} \frac{s_{u\ell}}{M_{u'\ell'}}\right) = \ell n\left(\frac{1}{g_u} \sum_k I_{uk}\right) + \ell n\left(\frac{K}{K'N_{u'}A_{u'\ell'}}\right)$$

$$= -\frac{E_u}{kT} - \ell n\left(\frac{\tau_u}{C}\right) + \ell n\left(\frac{K}{K'N_{u'}A_{u'\ell'}}\right)$$

[from (2-2)]

This was plotted against $E_u - E_{u'}$. If T is a constant and τ_u is the

same for each upper level of the term one expects this plot to be a straight line with slope $-1/kT$.

Figure 5 shows the results. The plot for the z^6F^o term is a straight line with a slope indicating a temperature of 1424 ± 128^oK. The z^4F^o term's plot is a straight line with a slope which would be produced by a temperature of 5308 ± 1146^oK. The slope of the plot for the z^4D^o term gives a temperature of 5156 ± 1146^oK.

It is not clear why the slope of the z^6F^o plot is different from slopes for the z^4D^o and z^4F^o plots. Little is known about the details of excitation processes in the hollow-cathode lamp, so we have assumed only that the relative populations of levels within a term go as $\frac{g_u}{g_{u'}} e^{-\gamma(E_u - E_{u'})}$, where γ is a constant characteristic of the term. It would be a remarkable coincidence if this were not true and the lifetimes of levels within the terms varied in such a way as to give the straight lines shown.

These results indicate that either τ_u is proportional to $e^{\beta E_u}$, which would also give straight line plots, or τ_u is approximately constant for all u in a given term. The beam-foil results for the z^6F^o term show that if $\tau_u \propto e^{\beta E_u}$, then

$$|\beta| \leq \left| \frac{\ell n (\tau_{11/2}/\tau_{5/2})}{E_{11/2} - E_{5/2}} \right| = 2.53 \times 10^{-4} \text{ cm} = 2.04 \text{ eV}^{-1} .$$

No evidence has been found that the lifetimes of the upper levels vary within a term by more than 22% for the three terms of interest to this investigation. It is consistent with all of the

evidence to assign the same lifetime to all levels of a term and to designate the uncertainty in that lifetime value as 15%.

2.8 The Results of Other Lifetime Measurements

Table 3 shows the results of Martinson et al. (1973) and Pinnington and Lutz (1974) along with the CIT results. The above authors are beam-foil spectroscopists who have also investigated Mn I. Their values and ours are in good agreement (within 15%) for the z^6F^o and z^4F^o terms. There is an approximately 20% disagreement between their work and this work for the z^4D^o lifetime. The cause of this disagreement has not been determined, but we have noticed that our result agrees with theirs if we do not subtract the beam-dependent background in analyzing the data. It is worthwhile to note that the solar abundances calculated from the z^4D^o lines agree very well with those calculated from the z^4F^o and z^6F^o lines. (See Table 6.)

3. Branching Ratios, Transition Probabilities and Oscillator Strengths

3.1 Summary of the Method

The purpose of this stage of the experiment was to measure the branching ratios for all transitions from the upper levels of interest. Since the branching ratio $BR_{u\ell}$ of a transition from upper level u to lower level ℓ is $BR_{u\ell} \equiv A_{u\ell} / \sum_{\ell'} A_{u\ell'}$, where the sum is over all lower levels, the absolute transition probability $A_{u\ell} = BR_{u\ell}/\tau_u$. The method of measuring the branching ratios was to measure the emission line intensity $I_{u\ell} = KN_u A_{u\ell}$, where K is a constant and N_u is the number density of atoms in level u. This was done for every detectable line from each upper level of interest, and the branching ratios were found by summing intensities of lines from the same upper level and dividing the intensity of each line by the sum.

Two sources of information were of use in listing the branches, since it was found that the Revised Multiplet Table (Moore 1945) was not complete. A computer program written by Lennard used the energy levels given in Moore (1971) and the selection rules $|\Delta L| \leq 1$, $|\Delta J| \leq 1$ and $J = 0 \not\leftrightarrow J = 0$ to compute wavelengths of possible transitions and to group the branches by upper level. Another run of the program gave branches for which $|\Delta L| = 2$. Using these lists of branches, we searched the spectrum in Catalan et al. (1964) to find those branches which were actually seen in the arc spectrum of manganese. This collection of

branches seen by Catalan was given the highest priority in our measurements.

3.2 Apparatus

The light source providing the manganese spectrum was a hollow cathode discharge (Figure 6). The operation of such a source has been described by Tolansky (1947) and more recently by Falk and Lucht (1976). The anode is a cylindrical shell coaxial with the cathode. The cathode is made of the material to be studied, unless the carrier gas is to be studied, in which case the cathode is made of a material which does not sputter easily and which has few lines in its spectrum. Carrier gas flows into the source and is pumped out by a mechanical roughing pump. The gas is ionized, and the ionized gas is accelerated towards the cathode. When a carrier gas ion hits the cathode it sputters atoms from the cathode. These sputtered atoms are then excited by collisions with electrons which are accelerated by the field at the cathode. When the mean free path of the electrons is less than or approximately equal to the diameter of the hole in the cathode, the sputtering and excitation processes take place almost entirely within this hole, producing a small, bright spot of light (Sawyer 1963).

Since spectroscopically pure Mn is not sold in solid bars or rods but as a powder, a new method had to be found by which to make an Mn cathode. The most effective method involved the use of the bell jar in Kellogg Laboratory. Pure (.999+) manganese

powder was pressed inside a ceramic tube of inside diameter approximately .20". The ceramic tube was placed inside a spiral of tungsten wire. The wire was placed across the electrodes of the bell jar, and the bell jar was evacuated. Then current was passed through the wire, heating up the tube. The most effective sequence used was 62 amps at 10 volts, with 1 minute to go from 0 to 62 amps, 5 minutes at that current and the current promptly turned to 0 amps after that. The slug was then allowed to cool in the vacuum. When the tube was removed from the bell jar the slug of Mn was pushed out of the ceramic tube with a brass rod. The slug was then machined with great care, since it tended to come apart in the lathe.

After most of the work with the hollow cathode source had been completed, a more easily constructed Mn source was tested and found to be suitable for some measurements. The cathode was made by our machining an aluminum cathode and placing Mn powder in the hole. After 1-2 hours of operation the lamp emitted a spectrum which consisted principally of manganese lines. Although aluminum is hard to sputter and has few lines, a comparison of this spectrum with that emitted by the pure Mn cathode revealed some lines which could only have come from aluminum.

Two carrier gases were used. Helium was best for most measurements, since there are fewer lines in its spectrum than in the spectra of most gases, so there is less chance of blending of a helium line with a manganese line. Also, helium produced a useful intensity of signal from the source, greater than 100 na (for

the stepping channel, see below) for the strongest branch from each upper level. However, for some measurements of very weak lines argon was used to produce a more intense signal due to its better sputtering of the manganese.

The source was operated using carrier gas pressures of 1.8-3.3 torr for He and 0.8-2.0 torr for Ar. The voltage from the power supply was 300-370 v.d.c., and the discharge currents were in the range 50-110 ma. Since the ballast resistor in series with the source was 1100 Ω, the voltage across the source was about 250-300 v.d.c.

The spectrometer used for the branching ratio measurements was the Paschen-Runge spectrometer in Bridge Laboratory. For measurements at wavelengths less than 8460 Å the north entrance slit was used. (See Figure 7.) Table 4 gives the specifications for the mirror, slits, grating, Rowland circle, detectors, filters and electronics. The concave mirror focuses light from the hollow cathode onto the entrance slit. The entrance slit used most often was the 50 μ slit, which gives a line width of .146 Å FWHM. The concave grating diffracts the light and focuses it along the Rowland circle. The wavelength corresponding to a given detector position can be read from a steel tape stretched along the circular track which supports the detector.

In the branching ratio measurements two photomultiplier tubes were used simultaneously as detectors, with their signals going to independent current amplifiers connected to the inputs of a two channel strip chart recorder. One of these photomultipliers was

the scanning channel, which was used to scan the line being measured. For wavelengths of less than 6600 Å the photomultiplier was an EMI 9783B (Cs-Sb photocathode) refrigerated with dry ice. It was mounted on a platform driven at scanning rates of .1, 1.0 or 10 Å/minute by a stepping motor. For wavelengths greater than 6600 Å the detector was a dry-ice-refrigerated RCA 4832 photomultiplier tube (Ga-As photocathode) driven by a multi-speed motor. The speed frequently used for slow scans was .35 Å/minute.

The other detector was positioned at the peak of a strong line from the upper level of interest. Its purpose was to monitor the population of the upper level by providing a signal proportional to that population. This detector was an unrefrigerated EMI 9783B, and it was placed on the portion of the Rowland circle which received light from the -1 order from the grating. In this position the monitor channel does not interfere with the positioning of the scanning channel. The carriage holding the phototube had an adjustable exit slit which was set at 200 μ to provide a large enough signal and a flat peak to the line so the monitor detector could be set reproducibly on the line peak.

The calibration of the detection efficiency of the spectrometer is described in Appendix 3.

For wavelengths greater than 8460 Å it was necessary for us to use the south entrance slit. (See Figure 8.) This entrance slit was adjusted to a 300 μ width. The scanning detector was a refrigerated Hamamatsu R406 photomultiplier (S-1 photocathode response) mounted on a carriage similar to that for the monitor

detector mentioned above. The exit slit width was adjusted to 400 μ. The refrigerated EMI 9783B on the stepping channel carriage was used as a monitor since it was desired to keep the dark current in the monitor channel as low as possible. A low dark current in the monitor channel was desired because it was not known what intensities the monitor lines would have in third order.

The calibration of the spectrometer in the south-entrance-slit configuration is also described in Appendix 3, and the electronics for the spectrometer system are listed in Table 4.

3.3 Procedure

First, the lists were made of branches from each level as mentioned in section 1. Then scans were made of the relevant wavelength regions to locate and identify the lines. Figure 9 is such a scan.

The first step in the actual branching ratio measurement was the setting of the monitor detector on a strong line from the relevant upper level. For wavelengths of less than 8460 Å the uncooled EMI 9783B mentioned above was used to scan the wavelength region of interest in the -1 order. When the correct line had been located, the monitor was set at its peak. In the measurements of upper limits on the intensities of lines at wavelengths greater than 8460 Å the stepping-motor channel was set at the third order 4451.575 Å $z^4D^o_{7/2}$ line so that the monitor channel

carriage would not interfere with the scanning of the 9050-9250 Å region by the R406.

Once the monitor channel was in position and the scanning channel carriage had been moved by hand to the appropriate λ region, the scanning channel was moved (scanning at a rate of 10 Å/minute or 7.40 Å/minute for the EMI 9783B or RCA 4832 photomultipliers, respectively) to the line of interest. Then the scanning speed was set at 1 Å/minute (EMI PMT) or .35 Å/minute (RCA PMT), and the time constant for the current amplifier was set to be much less than the time required for the photomultiplier to scan the line. Figure 10 shows such a scan. All lines in the wavelength region from a given upper level were scanned. Then the monitor detector was shifted to a line from another level of the term, and all of the lines in the wavelength region from this upper level were measured. This process was repeated until all of the lines in that wavelength region from the upper term had been measured. For the z^6F^o term only one monitor line was used in all measurements of branches from that term because of the closeness of the spacing ($E_J - E_{J+1} < 115$ cm^{-1}) of levels in the term. The ratio of the scanning channel signal to the monitor channel signal was usually reproducible to better than 5% when a line was measured before and after the monitor detector was shifted off of the peak of the monitor line and then brought back to the peak. This is about the same as the reproducibility of measurements of the same line with the monitor detector stationary.

3.4 Analysis of the Data

The data were the filter transmissions $t(\lambda)$, spectrometer response $\mathcal{E}(\lambda)$, monitor signal levels and scanning channel signal levels. The filter transmissions were measured by recording the attentuation in signal from the standard lamp as the filter was placed in front of the entrance slit. The spectrometer response was measured as described in Appendix 3. The relevant monitor signals were those at the peak of the monitor line and at a flat region of the spectrum near the monitor line. The signal from the flat part of the spectrum was due to the monitor dark current and any continuum emitted by the lamp. The scanning channel signals used were also the signals at the peak of the line and at a flat place in the spectrum near the line.

The first step in the analysis of these data was the subtraction of the background from the monitor and scanning signals at the peaks of the lines. The resulting monitor signal $M_{u\ell'} = K'N_u A_{u\ell'}$, where K' is a constant, N_u is the population of the upper level and $A_{u\ell'}$ is the spontaneous transition probability of the u-ℓ' transition. The resulting scanning channel signal is $s_{u\ell'} = t(\lambda)\mathcal{E}(\lambda)KN_u A_{u\ell}$, where K is another constant. Actually, as Smith (1972) notes, the intensity in a given line is proportional to the area under the line, but since in our scans of lines the full width at half-maximum is very nearly equal to $\frac{d\lambda}{d\ell}\Delta\ell$, where $\frac{d\lambda}{d\ell}$ is the reciprocal dispersion along the Rowland circle and $\Delta\ell$ is the width of the image of the widest slit (entrance or exit) on the circle, we are justified in using the peak heights rather than areas. Note that the width of

the line in Figure 10 is .144 ± .006 Å in agreement with the value expected for the 50 μ slit width.

The next step in calculating the branching ratio was to divide $s_{u\ell}$ by $M_{u\ell'}$, $t(\lambda)$ and $\mathcal{E}(\lambda)$. $\frac{s_{u\ell}}{M_{u\ell'}T(\lambda)\mathcal{E}(\lambda)} \equiv \frac{S_{u\ell}}{M_{u\ell'}} = \frac{K}{K'}\frac{A_{u\ell}}{A_{u\ell'}}$. Then $\frac{S_{u\ell}}{M_{u\ell'}} / \frac{S_{us}}{M_{u\ell'}} \equiv R_{u\ell} = \frac{A_{u\ell}}{A_{us}}$ was calculated, where the subscript us denotes the strongest transition from u. This was done so that it was not necessary to measure all of the lines from a given upper level in one day; it was sufficient to normalize the results of the day to the average of $\frac{S_{us}}{M_{u\ell'}}$ measured at the beginning and end of the day's run and calculate the $R_{u\ell}$ for the lines measured that day. These R's could then be compared with those of lines measured on other days. If $S_{us}/M_{u\ell'}$ varied by more than 10% during the day, that day's measurements were thrown out.

The branching ratio $BR_{u\ell} = R_{u\ell} / \sum_k R_{uk}$, where the sum is over all branches from u. The transition probability is simply $A_{u\ell} = BR_{u\ell}/\tau_u$.

3.5 The Assignment of Uncertainties

Several factors contributed to the uncertainties in the transition probabilities. The analysis of uncertainties in the lifetime measurements has been given above. The uncertainties in the branching ratios arise from uncertainties in signals (scanning and monitor channels), filter transmissions and spectrometer responses.

$$\left(\frac{\Delta BR_{u\ell}}{BR_{u\ell}}\right)^2 = \left(\sum_{k\neq\ell} BR_{uk}\right)^2\left(\frac{\Delta R_{u\ell}}{R_{u\ell}}\right)^2 + \sum_{k\neq\ell} BR_{uk}^2\left(\frac{\Delta R_{uk}}{R_{uk}}\right)^2$$

$$= (1 - BR_{u\ell})^2\left(\frac{\Delta R_{u\ell}}{R_{u\ell}}\right)^2 + \sum_{k\neq\ell} BR_{uk}^2\left(\frac{\Delta R_{uk}}{R_{uk}}\right)^2$$

Since

$$R_{u\ell} = \frac{S_{u\ell}}{M_{u\ell'}} \Big/ \frac{S_{us}}{M_{u\ell'}} = \frac{s_{u\ell}}{M_{u\ell'}t(\lambda_{u\ell})\mathcal{E}(\lambda_{u\ell})} \Big/ \frac{s_{us}}{M_{u\ell'}t(\lambda_{us})\mathcal{E}(\lambda_{us})} \quad ,$$

$$\left(\frac{\Delta R_{u\ell}}{R_{u\ell}}\right)^2 = \left(\frac{\Delta s_{u\ell}}{s_{u\ell}}\right)^2 + \left(\frac{\Delta M_{u\ell'}}{M_{u\ell'}}\right)^2 + \left[\frac{\Delta[t(\lambda_{us})/t(\lambda_{u\ell})]}{t(\lambda_{us})/t(\lambda_{u\ell})}\right]^2$$

$$+ \left[\frac{\Delta[\mathcal{E}(\lambda_{us})/\mathcal{E}(\lambda_{u\ell})]}{\mathcal{E}(\lambda_{us})/\mathcal{E}(\lambda_{u\ell})}\right]^2 + \left(\frac{\Delta s_{us}}{s_{us}}\right)^2 + \left(\frac{\Delta M_{u\ell'}}{M_{u\ell'}}\right)^2 \quad .$$

In this equation $\Delta s_{u\ell}$ and $\Delta M_{u\ell'}$ are the uncertainties in line peak height and monitor signal level, respectively, for a given measurement. If there were several measurements of the same transition the mean of $s_{u\ell}/M_{u\ell'}$ and a Δ large enough to include the day's measurements were used. For lines within the same wavelength region as the strongest branch (within ± 100 Å), $\Delta\left[\frac{\mathcal{E}(\lambda_{us})}{\mathcal{E}(\lambda_{u\ell})}\right] = 0$. $\Delta\left[\frac{t(\lambda_{us})}{t(\lambda_{u\ell})}\right] = 0$ for lines within ± 100 Å of the strongest branch which were measured with the 10% neutral density filter, since the strongest lines required the use of the 10% filter. $\Delta\left[\frac{t(\lambda_{us})}{t(\lambda_{u\ell})}\right] \Big/ \frac{t(\lambda_{us})}{t(\lambda_{u\ell})} = 4\%$ for lines measured without the 10% filter. This was determined by measuring the transmission of the 10%

filter several times during the series of BR measurements. $\Delta\left[\frac{t(\lambda_{us})}{t(\lambda_{u\ell})}\right]$ is negligibly small (1-2%) for filters other than neutral density filters. $\Delta\left[\frac{\mathcal{E}(\lambda_{us})}{\mathcal{E}(\lambda_{u\ell})}\right] \Big/ \frac{\mathcal{E}(\lambda_{us})}{\mathcal{E}(\lambda_{u\ell})} = 7\%$ for $|\lambda_{u\ell} - \lambda_{us}| > 100$ Å. This is due to the uncertainty in the calibration of the standard lamp. Note that for the levels of interest the branches were either within 100 Å of the strongest branch or more than 400 Å from the strongest branch.

Once the uncertainties in the branching ratios were found, the calculation of uncertainties for the transition probabilities and oscillator strengths was straightforward. $A_{u\ell} = BR_{u\ell}/\tau_u$, so

$$\frac{\Delta A_{u\ell}}{A_{u\ell}} = \sqrt{\left(\frac{\Delta BR_{u\ell}}{BR_{u\ell}}\right)^2 + \left(\frac{\Delta \tau_u}{\tau_u}\right)^2} \quad .$$

$$\Delta \log gf = \frac{\log\left(1 + \frac{\Delta A_{u\ell}}{A_{u\ell}}\right) - \log\left(1 - \frac{\Delta A_{u\ell}}{A_{u\ell}}\right)}{2} \quad .$$

3.6 Tests for Possible Errors in Method

A. The use of a monitor line from an upper level different from that of the line measured

In the measurements of BR's for lines from the z^6F^o term only one monitor line was used. In measurements for lines of the $z^4F^o_{7/2}$ and $z^4F^o_{5/2}$ upper levels the monitor lines were not fully resolved from each other by the spectrometer. In each of these cases $s_{u\ell}/M_{u'\ell'}$ depends on $e^{-(E_u - E_{u'})/kT}$, assuming a Maxwell-Boltzmann distribution of levels within a term, and therefore

$s_{u\ell}/M_{u'\ell'}$ varies with temperature, while for $u = u'$ there is no temperature dependence in $s_{u\ell}/M_{u'\ell'}$. It must be determined whether $s_{u\ell}/M_{u'\ell'}$ varies enough with temperature to introduce significant error into the results for the range of temperatures used. "Significant" means greater than the uncertainties already associated with the s/M measurement.

Since the variation in temperature cannot be measured directly, it is more useful to calculate the relative change in $s_{u\ell}/M_{u'\ell'}$ with respect to the relative change in monitor signal, $\Delta M_{u'\ell'}/M_{u'\ell'}$, which one can measure directly. For the details of these calculations, see Appendix 4. The results are, for u' different from u in the z^6F^o term with 3834.368 ($J_u = 7/2$) as the monitor line, that $\left|\frac{\Delta(s_{u\ell}/M_{u'\ell'})}{s_{u\ell}/M_{u'\ell'}}\right| \leq .005 \left|\frac{\Delta M_{u'\ell'}}{M_{u'\ell'}}\right|$, demonstrating that the change in s/M is not significant for the range of monitor signals used.

With the z^6F^o term the 3834.368 Å line was blended with 3833.865 from the $J_u = 3/2$ level. In the z^4F^o term the line at 4766.426 Å ($J_u = 7/2$) was not fully resolved by the monitor from the $J_u = 5/2$ line at 4765.856 Å. For a blended monitor line

$$M_{u'\ell'} = K' \frac{1}{U_o}\left(g_{u'}A_{u'\ell'}e^{-E_{u'}/kT} + \alpha g_{u''}A_{u''\ell''}e^{-E_{u''}/kT}\right)$$

where α is a constant which describes how well the lines are resolved by the monitor system. α is 0 for no blending. $M_{u'\ell'}$ is measured at the peak of the $u'\ell'$ line. By calculations similar to those in Appendix 4 it is found that $\left|\frac{\Delta(s_{u\ell}/M_{u'\ell'})}{s_{u\ell}/M_{u'\ell'}}\right| < .0085 \left|\frac{\Delta M_{u'\ell'}}{M_{u'\ell'}}\right|$.

The data are consistent with the calculations. For the z^6F^o term $s_{u\ell}/M_{u'\ell'}$ was measured with the lines at 3839.779 Å (J_u = 1/2), 3834.368 Å (J_u = 7/2) and 3806.715 Å (J_u = 11/2) as the $u\ell$ lines and 3834.368 as the monitor line. The relevant ratio is $F(\lambda) \equiv \frac{s_{u\ell}(\lambda)}{M_{u'\ell'}} / \frac{s_{u'\ell'}(3834.368)}{M_{u'\ell'}}$ since for this ratio any fluctuations in s/M not caused by changes in the lamp will cancel out. $F(\lambda)$ was measured for monitor currents from 13 na to 160 na. A systematic decrease in F(3806.715) of 13% was observed over this range, and F(3839.779) decreased systematically by 7% over the same range. However, for the range of monitor currents used in the branching ratio measurements (34-96 na) the variation in each F was 3-4%. The uncertainty in each F was 2-4%.

For the z^4F^o term $\frac{s(4701.150)}{M} / \frac{s(4761.527)}{M}$ was measured, once with 4762.376 as the monitor line and then with 4761.527 as the monitor line. Both 4701.150 and 4761.527 are from the J = 3/2 level, while 4762.376 is from the J = 9/2 level. Thus, ΔE was the greatest possible for this term, 526 cm^{-1}, greater than it was during any of the BR measurements for which blended lines were used. Also, the temperature was higher for the $\frac{s(4701.150)}{M(4762.376)}$ measurement than for the $\frac{s(4761.527)}{M(4762.376)}$ since for the former M = 1.70 M for the latter. The two measurements of $\frac{s(4701.150)}{M} / \frac{s(4761.527)}{M}$ agreed to better than 4%, which is within the range of variation of s/M measured using a monitor line from the same upper level as the line measured.

From the above we conclude that neither the use of a monitor line from a different upper level in the same term as the upper

level of interest nor the use of blended monitor lines introduced significant error into the measurements.

B. Self-absorption

The hollow cathode discharge is a light source of finite depth, so there is a chance that before a photon from the u-ℓ transition can escape the source it will be absorbed by an atom in level ℓ. If the fraction of radiation absorbed, $dI_{u\ell}/I_{u\ell}$, is different for different lines the observed relative intensities of those lines will not be the true relative intensities, and the branching ratios computed from the observations will be incorrect.

The decrease in intensity $I_{u\ell}$ is $dI_{u\ell} = \alpha I_{u\ell} N_\ell B_{\ell u}$, where $B_{\ell u}$ is the Einstein absorption coefficient $(g_u \lambda_{u\ell}^3 / g_\ell 8\pi h) A_{u\ell}$ and α is a constant. So

$$dI_{u\ell} = \alpha I_{u\ell} N_\ell \frac{g_u \lambda_{u\ell}^3}{g_\ell 8\pi h} A_{u\ell} \quad .$$

Let

$$k_{u\ell} = \frac{g_u \lambda_{u\ell}^3}{g_\ell 8\pi h} \quad .$$

The observed intensity is $I'_{u\ell} = I_{u\ell} - dI_{u\ell} = I_{u\ell}(1 - \alpha k_{u\ell} N_\ell A_{u\ell})$. For $\alpha k_{u\ell} N_\ell A_{u\ell} \ll 1$ changes in N_ℓ will not change $I'_{u\ell}/I_{u\ell}$ significantly, and $I'_{u\ell}/I_{u\ell} = 1$. But if $\alpha k_{u\ell} N_\ell A_{u\ell} \sim .1$, for example, doubling N_ℓ changes $I'_{u\ell}/I_{u\ell}$ from .9 to .8. Therefore, if $I'_{u\ell}$ is compared with I'_{uk} for a transition u-k with little self-absorption, the ratio of observed intensities $I'_{u\ell}/I'_{uk}$ should change as N_ℓ changes.

In planning an experimental test for self-absorption one needs to assess the effect it should have if it is present. Among the lines measured $A_{u\ell}$ varied by a factor of approximately 10^3 for lines from the same upper level, while $\lambda_{u\ell}$ varied by a factor of approximately 2. Therefore, $\alpha N_\ell A_{u\ell} k_{u\ell}$ should be much less for weak lines even though these lines are usually at longer wavelengths than the strong lines. The ratio of the observed intensities of a strong line $\lambda_{u\ell}$ and a weak line λ_{uk} from the same upper level is $\frac{I'_{u\ell}}{I'_{uk}} = \frac{I_{u\ell}}{I_{uk}} \frac{(1 - \alpha k_{u\ell} N_\ell A_{u\ell})}{(1 - \alpha k_{uk} N_k A_{uk})}$. If this ratio is observed under different lamp operating conditions yielding different N_ℓ and if there is appreciable self-absorption, the ratio should decrease systematically with increasing N_ℓ. For negligible self-absorption the ratio should remain the same.

Such a series of measurements was made for strong transitions to the a^6D and a^4D terms. The a^6D term is the lower term for strong lines from the z^6F^o term, and the a^4D term is the lower term for strong lines from the z^4F^o and z^4D^o terms. The test for self-absorption by a^6D levels involved the lines 3841.074 and 3799.256 from the $z^6F^o_{5/2}$ level, with BR(3841.074) = .577 while BR(3799.256) = .0236. $s_{u\ell}/M_{u\ell'}$ was measured for both of these lines using 3841.074 as the monitor line and using a range of monitor currents from approximately 80 na to 5 na. The ratio $\frac{s}{M}(3841.074)/\frac{s}{M}(3799.256)$ remained the same, within experimental uncertainties (about 6%) for all of the measurements. No systematic change in this ratio is observed.

For lines to the a^4D term a similar test was made using the lines 4762.376 and 5255.330 from the $z^4F^o_{9/2}$ level. 4762.376 has a $a^4D_{7/2}$ as its lower level and has a branching ratio of .924, while 5255.330 has a $a^4G_{11/2}$ as its lower level and has a BR of .049. 4762.376 was used as the monitor line. No systematic variation of $\frac{S}{M}(5255.330)/\frac{S}{M}(4762.376)$ over the range of monitor currents from 300 na to 15 na was observed. The spread in $\frac{S}{M}(\lambda_{uk})/\frac{S}{M}(\lambda_{u\ell})$ was about 5%. Therefore, no self-absorption was detected in strong lines to the a^6D and a^4D terms.

None of the lines of interest go to the ground level except for the 2 UV lines 2184.912 and 2176.014 which are transitions with $\Delta S = 1$, $\Delta L = -2$ and are so weak that we could establish only an upper limit on their intensities. Therefore, self-absorption by the ground level was not investigated.

If self-absorption did affect the BR measurements the calculated $A_{u\ell}$ for weak lines should be too large, and the solar abundance of manganese calculated using those lines should be too small. Comparison of our abundance results with those of others recently published suggests that the $A_{u\ell}$ are not too large and therefore that self-absorption has not been a problem.

C. Linearity of the scan/monitor ratio

The assumption in calculating branching ratios has been that $S_{uk}/M_{u\ell} = \frac{K}{K'A_{u\ell}} A_{uk}$, where $\frac{K}{K'}$ is independent of S and M. If $\frac{K}{K'}$ is dependent on S or M, then the ratio of the transition probabilities for two lines will not be $\frac{S_{uk}}{M_{u\ell}} / \frac{S_{uj}}{M_{u\ell}}$ because the $\frac{K}{K'}$ will not cancel

out. Therefore some check was needed to make sure that $\frac{K}{K'}$ did not vary with S or M.

The test, performed by W. Whaling, made use of the tungsten filament standard lamp. The monitor and scanning channels were set at 3834 Å, and the tungsten filament lamp was adjusted to give the desired monitor signal. A neutral density filter was placed in front of the stepping channel to reduce the signal below 100 na. For a given lamp current S/M was measured with no filter in front of the entrance slit and with the 10% neutral density filter in front of the entrance slit. This cut both S and M by the same amount, approximately a factor of 10. No systematic difference between S/M measured with and without the 10% filter was seen for a range of monitor currents (measured without the 10% filter) from 64 na to 855 na. Taking into consideration the M's measured with the 10% filter we can say that S/M did not vary systematically as the monitor current was changed from approximately 7 to 855 na. Therefore $\frac{K}{K'}$ does not vary over this range of monitor currents for scanning channel signals of under 100 na.

D. Linearity of stepping channel response

During the branching ratio measurements it was always assumed that $s = KL$, where K was a constant and L was the illumination falling on the slit. If this were not so, then the BR measurements would be in error.

The test of the linearity of the stepping channel was performed by W. Whaling and Craig Lage. A mask with several .375"

diameter milled holes was placed to intercept the beam between the mirror and the entrance slit. Each hole could be covered with black electrical tape so that light from any combination of holes could illuminate the entrance slit. Current through the tungsten filament lamp was adjusted to give a signal of approximately 250 na for illumination from a certain hole. The signal current s was measured for illumination from each hole: $s = K(s)L_n$, where L_n is the illumination through hole n. For the small s (100-250 na) due to each single hole K(s) was assumed to be a constant, $K(s_o)$. The signal s was measured for various combinations of holes. $s_{n+m} = K(s_{n+m})(L_n + L_m) = K(s_{n+m})[s_n/K(s_o) + s_m/K(s_o)]$, so $K(s_{n+m})/K(s_o) = s_{n+m}/(s_n + s_m)$. This ratio was measured for $s_o \leq 250$ na and $s_{n+m} = 500$-950 na. A plot of $K(s)/K(s_o)$ versus s showed that the ratio decreased linearly from s = 250 na to s = 950 na, with K(950 na) = .98K(250 na). Extrapolating this back to the 0-100 na region shows that K should vary less than .5% between 0 and 100 na, which is well within the uncertainty of our measurements. Therefore, the assumption of detector linearity is justified for the range of signals which we used.

E. Scattered light

In every spectrometer some light will be scattered from the walls and from mountings of optical parts as well as from the parts themselves. Because of this scattering, at any position on the track the detector will receive not only light of the appropriate wavelengths diffracted from the grating but also some light of

different wavelengths which is called scattered light. Scattered light is not a great concern when one is using a line source because it will show up, along with any continuum produced by the source, as a slowly-varying background which is usually much less intense than the lines. This background can be subtracted from the line to give the signal produced by the line. But when one is using a continuum source it is not apparent what part of the signal is due to diffracted light of the desired wavelength and what part is due to scattered light. This difficulty is aggravated in the use of the tungsten filament standard lamp by the lamp's spectral distribution of radiation since the number of photons cm^{-2} (of source) $\mathring{A}^{-1}$ $stearad^{-1}$ sec^{-1} increases with increasing wavelength up to about 12000 $\mathring{A}$. For instance, the brightness at 7000 $\mathring{A}$ is 78 times the brightness at 3700 $\mathring{A}$. So a small fraction of long-wavelength light scattered to the short-wavelength part of the track can alter the signal significantly. The result would be to assign too high a response to the spectrometer at short wavelengths and thus make the branching ratios of short-wavelength lines too low. So it is important to make sure that scattered light is not discernably affecting the calibration.

The first step in the laboratory test for scattered light was the measurement of the transmission of a Corning 7-59 filter with a line source, a small nickel hollow cathode lamp with neon as the carrier gas. The line used was 3858.30 $\mathring{A}$. The transmission was also measured at that wavelength with the same continuum source used in the calibration measurements, the tungsten filament standard

lamp with 35.0 amps a.c. through the filament. After the filter transmission measurements a Corning 2-60 filter was placed in front of the entrance slit while the tungsten filament lamp was on and the 7-59 filter was in front of the stepping photomultiplier tube.

The 7-59 filter cuts off all light below approximately 2900 Å. Its transmission reaches a maximum of 0.84 at 3700 Å and then falls until it cuts off light above 5000 Å. It transmits again in the 6900-12500 Å region and in some regions of longer wavelength. The 2-60 filter cuts out light below 6100 Å and has a transmission of about 0.88 from about 6650 Å upward.

With the line source and with a filter in front of the entrance slit to eliminate second order lines the signal at the peak of the line is $s(\lambda)$. With the 7-59 filter in place in front of the stepping channel the signal is $s_f = s(\lambda)t(\lambda)$ so $t(\lambda) = s_f/s(\lambda)$. However, with the continuum source and a filter to eliminate second order radiation the signal (after dark background has been subtracted) is $s_\ell = s(\lambda) + s_s$, where s_s is the signal due to scattered light. When the 7-59 filter is in place the signal is $s_f = s(\lambda)t(\lambda) + s'_s$. s'_s is the portion of scattered radiation passing through the 7-59 filter and should be much less than s_s since the 7-59 does not transmit well in most wavelength regions past 5000 Å. The signal with both the 2-60 and 7-59 filters will be approximately $0.88\ s'_s$.

Therefore, a comparison of 7-59 filter transmissions measured with the line source and the continuum source will reveal whether scattered light is a problem. With the line source $t(\lambda) = s_f/s(\lambda)$. But with the continuum source

$s_f/s_\ell = \frac{s(\lambda)t(\lambda) + s'_s}{s(\lambda) + s_s} \leq t(\lambda)$. If s_s is discernable and $s'_s < t(\lambda)s_s$, then s_f/s_ℓ will be less than $t(\lambda)$ measured with the line source.

This test was made, and $t(\lambda)$ measured with the line source was $.826 \pm .008$. s_f/s_ℓ was measured with the continuum source to be $.818 \pm .005$. No signal above the dark current could be seen with the 2-60 and 7-59 filters in place, so $.88\ s'_s$ was below the noise level of the dark current, which was about .005 na. The dark current was about .15 na while s_ℓ and s_f for the continuum source were about 85 and 70 na, respectively.

Therefore, scattered light has not affected the calibration measurements at 3858 Å. Because of the standard lamp's distribution of intensity with wavelength and because of the photomultiplier tube's sensitivity, which falls very rapidly after 6500 Å, we would expect scattered light to be a greater problem, if it existed, at shorter wavelengths than at longer ones, so our calibration of the spectrometer in the wavelength regions of interest was unaffected by scattered light.

3.7 Results

The results for the BR's, A's and log gf's and the uncertainties are listed in Table 5. Table 5 also lists the results of other experimenters as well as the results of semiempirical calculations by Kurucz and Peytremann (1975). Table 6 summarizes the methods used by others in their experiments. A comparison of our results with those of others reveals some interesting discrepancies.

The comparison of absolute transition probabilities shows that those of Corliss and Bozman (1962) (CB) are higher than those reported here. Averaging over the 41 lines in Table 5 which have been measured by CB we find $\langle \log \frac{A_{CB}}{A_{CIT}} \rangle = .70 \pm .23$, where .23 is the standard deviation of the distribution. The magnitude of this discrepancy is similar to that for other Fe group elements.

The values of Allen and Asaad (1957) (AA) are also higher than those reported here, with $\langle \log \frac{A_{AA}}{A_{CIT}} \rangle = .45 \pm .12$ averaged over 19 lines. AA used the gf's of Huldt and Lagerqvist (1952) and Bell et al. (1959) for the Mn I 4030, 4033 and 4034 Å lines to normalize their relative gf's to an absolute scale.

Woodgate's (1966) values are of the same magnitude as ours, with $\langle \log \frac{A_{Wood}}{A_{CIT}} \rangle = -.08 \pm .20$ averaged over 32 lines. He normalized his scale to that of Penkin (1964) for the Mn I 3216 and 3224 Å lines.

Only four of the infrared lines measured by Hefferlin and Gearhart (1964) have been measured at Caltech. The log gf's reported by them are .58-.84 above the upper limits found in this experiment. That is not too surprising, since Hefferlin and Gearhart used measurements of IR lines by Corliss and Bozman to convert their relative gf's to absolute values.

Kurucz and Peytremann (1975) have calculated gf's for many Mn I lines using a scaled Thomas-Fermi-Dirac method and considering configuration interaction. The magnitude of their A's is the same as ours, with $\langle \log \frac{A_{Kur}}{A_{CIT}} = .01 \pm .54$ for the 83 lines in common. However, the large standard deviation indicates that there

are lines for which $\left|\log \frac{A_{Kur}}{A_{CIT}}\right|$ is 1 or greater, so the Kurucz value for any given line cannot be considered trustworthy.

The above experiments all measured relative gf's and normalized them to some absolute scale. If their relative transition probabilities are reliable, then the averages of $\log \frac{A_{other}}{A_{CIT}}$ given above can be used to correct their gf's for transitions not listed in Table 5. Therefore, it is of interest to examine the reliability of the relative gf's of others. The dependence of the gf's on at least three variables must be examined. We have plotted $\frac{A_{other}}{A_{CIT}}$ versus λ to reveal any error in the calibration of detector systems. A plot of $\frac{A_{other}}{A_{CIT}}$ versus the energy of the upper level will reveal any temperature dependence of this ratio, since all of the other experiments depend on the determination of the temperatures of the arcs used. This plot would also reveal an error in the measurement of a lifetime of an excited state, since such an error would shift all of the A_{CIT}'s for lines from that level. The plot of $\frac{A_{other}}{A_{CIT}}$ versus A_{CIT} should reveal whether self-absorption in the sources or nonlinearity of the detection systems has affected the results.

The comparison of our results with others as a function of wavelength is shown in Figures 11 and 12, where $\log \frac{A_{other}}{A_{CIT}}$ is plotted versus wavelength for CB, Woodgate, AA and Kurucz. For CB, Woodgate and AA there appears to be a wavelength dependence; the ratios are higher for lines in the 3800 Å region than for those in the 4400-4800 Å region. We believe that this apparent wavelength dependence is spurious for the following reasons. It is very

unlikely that Woodgate, AA and CB would make the same calibration error. The CIT spectrometer has been calibrated by several different workers using two standard lamps, and the relative sensitivities at 3800 Å and 4400 Å are reproducible. If we examine sets of lines from the same upper level we see no wavelength dependence in $\frac{A_{Wood}}{A_{CIT}}$. The lines available for examination are 3701.728 and 4762.376 from the $z^4F^o_{9/2}$ level and 3692.817, 4709.710 and 4766.426 from the $z^4F^o_{7/2}$ level. Also, Kurucz and Peytremann have calculated f-values for many more lines than the experimenters have measured. Although their f-values may be wrong for lines in certain multiplets, there is no reason for the existence of a wavelength-dependent error in their f-values. Figure 12 shows no systematic wavelength dependence of $\frac{A_{Kur}}{A_{CIT}}$.

The dependence of $\frac{A_{other}}{A_{CIT}}$ on the upper level of the line is shown in Figures 13 and 14. A more likely cause of the apparent wavelength dependence is the fact that the wavelengths of the lines are correlated with the upper levels of the lines. Most of the lines in the 3800 Å region come from the z^6F^o term, while those in the 4400-4800 Å region are from the z^4D^o and z^4F^o terms. For Woodgate and AA the results show the same dependence on E_u, with ratios for lines of the z^4F^o and z^4D^o terms being .20-.28 dex lower than those for the z^6F^o lines. CB shows a similar but much smaller variation, as does Kurucz. In the case of the CB results the spread is large enough to make the comparison inconclusive. The deviation of our results from Kurucz's is similar to that observed by Smith (1976), who compared Kurucz's calculated values

for Fe I, Ti II and V II with experimental values. So it is in the comparison with Woodgate and with AA that the dependence on upper level is most clearly seen.

We have examined the evidence for and against a number of experimental factors that might account for this dependence. They are:

(a) self absorption of z^6F^o lines in the hollow-cathode source, which would reduce the BR's of the strong z^6F^o lines and thus reduce our A-values.

However, the laboratory test of I(3799)/I(3841) for monitor currents varying by a factor of 16 shows no systematic variation of this ratio with monitor current, so there is no variation of this ratio with a variation of N_ℓ, a variation which should occur if self-absorption of the a^6D-z^6F^o lines is a problem. Another indication of the lack of self-absorption is shown in Figure 15, where it is seen that $\log \frac{A_{CB}}{A_{CIT}}$ increases as $\log A_{CIT}$ decreases for lines with the a^6D lower level. This is opposite to the trend one would expect if the hollow cathode source showed self-absorption, and it may indicate that these lines are self-absorbed in the CB arc. Figures 15 and 16 show no systematic trend of $\frac{A_{Wood}}{A_{CIT}}$ or $\frac{A_{Kur}}{A_{CIT}}$ with A_{CIT} for these lines. A third point is that if the fault were self-absorption in the CIT source, it would be necessary for the self-absorption to decrease the $\log A_{CIT}$ by approximately .2 dex, or a factor of 1.6 in the branching ratios, to produce the observed effect. There are four lines for which this could not have happened since their BR's are greater than 62.5%. Self-absorption

could not have reduced these by a factor of 1.6 since the maximum branching ratio is 1.

(b) self-absorption of lines going to the a^4D lower term in the Woodgate and AA sources. This would reduce the observed intensities of the a^4D-z^4F^o and a^4D-z^4F^o lines of Woodgate and AA and thus reduce the A's calculated using these intensities.

However, there is also evidence against hypothesis (b). The same sets of z^4F^o lines which are evidence against a wavelength dependent sensitivity calibration error are evidence against self-absorption since the lines at 3600-3700 Å go to the a^6D term and are weak while most of those at 4670-4770 Å are strong and go to the a^4D term. There is no systematic difference for $\frac{A_{Wood}}{A_{CIT}}$ for these lines. Also, as Figure 15 shows, log $\frac{A_{Wood}}{A_{CIT}}$ decreases as log A_{CIT} decreases for lines with a^4D lower levels, which is the wrong direction if Woodgate's source were to show self-absorption. The plot of log $\frac{A_{AA}}{A_{CIT}}$ versus log A_{CIT} does not indicate anything since AA measure lines with too small a range of A-values for any variation with A to be seen from their results.

The ratio $\frac{A_{CB}}{A_{CIT}}$ for transitions with a^4D lower levels does seem to increase as A_{CIT} decreases, indicating possible self-absorption, but the effect is no greater than that for lines with a^6D lower levels, so this apparent self-absorption by a^4D levels in the CB source should not produce the observed trend for the $\frac{A_{CB}}{A_{CIT}}$ results.

(c) an error in the lifetime measurement for the z^6F^o levels which causes the measured lifetime to be 1.6 times too large.

Beam-foil spectroscopy often yields too large a lifetime because of unrecognized cascades.

However, this explanation does not quite fit all of the facts, either. The lifetime measurement for the z^6F^o levels agrees to within 15% with those of Pinnington and Lutz and Martinson et al. The replenishment ratios R(0) in all z^6F^o lifetime measurements were $< .065$, so there was not much evidence of cascading. For the z^6F^o levels E_u is greater than 5 eV, and the ionization limit for Mn I is 7.432 eV. It is commonly observed in beam-foil spectroscopy experiments that highly-excited levels such as these do not exhibit much cascading.

If the lifetime were too large by a factor of 1.6, the abundance calculated for lines from z^6F^o upper levels would be too large by the same factor. The abundance of manganese calculated with the one z^6F^o line for which we have a Kitt Peak equivalent width (see Chapter 4 and Table 7) agrees very closely with the abundances calculated using z^4F^o and z^4D^o lines. (The standard deviation for the set of abundances is .05 dex.) For the two z^6F^o lines (including the one mentioned just above) for which we can use Moore's W the abundance for 5004.891 is .11 dex lower than the average abundance from the 6 z^6F^o, z^4F^o and z^4D^o lines. The abundance for 5029.779 is .09 above the average. So the abundances calculated from z^6F^o lines are not systematically higher than those calculated using the lines from other terms. Also, the difference between $\langle \log \frac{A_{Kur}}{A_{CIT}} \rangle_{z^6F^o \text{ lines}}$ and $\langle \log \frac{A_{Kur}}{A_{CIT}} \rangle_{z^4F^o \text{ lines}}$ is only .02 dex, not the .2+ dex of the comparison with AA and

Woodgate. If our τ measurement were off by .2 dex or a factor of 1.6 one would expect the difference to be greater for the Kurucz and Peytremann results as well as for the experimental results.

No one of these explanations nicely fits all of the facts concerning the variation of A_{Wood}/A_{CIT} and A_{AA}/A_{CIT} with upper level. Self-absorption of the z^6F^o lines in the hollow cathode lamp seems more unlikely than the other two possible explanations. An error in the lifetime measurement for levels in the z^6F^o term is slightly more probable than self-absorption of lines with a^4D lower levels in the Woodgate and AA arcs. If the lifetime measurement is wrong, then the lifetime of the z^6F^o levels would need to be 1.6-1.8 times lower, or 11.4-10.2 ns rather than 18.3 ns. But the evidence does not clearly point either to a lifetime measurement error or to self-absorption by a^4D levels in the Woodgate or AA arcs.

4. Solar Abundance Results

4.1 Introduction

The goal of this work was to find the solar abundance of manganese through the use of the gf-values measured as explained in Chapters 2 and 3. In addition to the laboratory data we need solar spectra which reveal which Mn I lines appear in the sun and how strong they are. The solar data which we have used come from the tables of Moore et al. (1966) and from the Preliminary Edition of the Kitt Peak Solar Atlas (Brault and Testerman 1972). The former includes approximately 24,000 lines in the region 2935-8770 Å. Much of the data in it is derived from the Utrecht photometric atlas (Minnaert et al. 1940). The Kitt Peak Solar Atlas was recorded as described in Brault et al. (1971) using a double-pass solar spectrometer at the Kitt Peak National Observatory.

4.2 The Curve of Growth

A. Equivalent widths

To find the number density of manganese atoms which are creating an absorption line we need a measure of the intensity of absorption. The measure frequently used is called the equivalent width, W, of the line. W is the width of a line which is perfectly black, has infinitely sharp edges and absorbs from the continuum the same amount of energy as the real line. In other words, W is the area between the absorption line and the continuum. W is usually expressed in milliangstroms.

For weak lines W depends strongly on the placement of the continuum level. The accurate determination of W's is especially difficult for lines of wavelength less than ~ 4000 Å since at shorter wavelengths the continuum is determined in part by the overlapping of many absorption lines and is hard to discern.

For reasons mentioned below, the best lines for abundance analysis are weak, long-wavelength unblended lines. This severely limits the selection of suitable lines. We calculate the abundance of manganese based on four lines for which we have W's obtained from the Kitt Peak atlas by Lennard using the spectrum synthesis method (Lennard, 1974). We also have Moore's (1966) W's for these lines, and we use these and Moore's W's for two other suitable lines to calculate the manganese abundance to see what effect different sets of equivalent widths have.

The uncertainties in the W's have been analyzed by Lennard. An error of 1% of the central depth of the line in the placement of the continuum can lead to a 5% error in the W for the line. The reproducibility uncertainty in deriving W from the recorded Kitt Peak spectrum is negligible. W's taken from different atlases may vary by ± 7%. We assign an uncertainty to the W values of 10%. However, unrecognized blending of lines can produce a W too large by much more than 10%.

B. The curve of growth

The curve of growth is a curve showing the variation of W with Ngf, where N is the number density of atoms and ions of the

element, g is the statistical weight of the lower level and f is the oscillator strength. Mihalas (1970) describes three regions of the curve of growth.

1. For little absorption implying a small N or small gf or both, $\frac{W}{\lambda} \propto Ngf$. In this region only the Doppler-broadened core of the line is absorbing a significant fraction of the radiation.

2. With increasing absorption the curve enters the saturation region in which as much radiation as possible is being absorbed in the Doppler core but the much weaker damping wings do not yet absorb much radiation. The consequence of this is that W grows very slowly with Ngf: $\frac{W}{\lambda} \propto \sqrt{\log Ngf}$.

3. For still greater density or higher gf the damping wings absorb noticeable amounts of radiation, and, in theory $\frac{W}{\lambda} \propto \sqrt{Ngf}$.

In laboratory absorption measurements a curve of growth is generated by measurements of W for one line as N is varied. In the sun N is fixed, and the curve of growth is constructed by plotting $\log \frac{W}{\lambda}$ versus gf for many lines of the same element. Some account must be taken of the temperature gradient in the photosphere, the ionization equilibria, the fact that the same medium which is doing the absorbing is also radiating and the absorption by atoms at different depths in the photosphere. To take these things into account we use the weighting function method of Goldberg, Muller and Aller (1960), hereafter referred to as GMA, in plotting the curve of growth.

Through the weighting function method the curve of growth becomes a curve of log $\frac{W}{\lambda}$ versus log C, where C depends on the gf, wavelength and lower level excitation potential of the line. It is necessary to have a model atmosphere to compute C for each line. The model used in making these computations was that derived by Aller and Pierce (1952) and extended to greater optical depths by Elste (GMA 1960). Parameters based on this atmosphere and used in the computation of C are found in Goldberg and Pierce (1959).

For weak lines $\frac{W}{\lambda} = C \frac{N_{Mn}}{N_H}$, where N_{Mn} is the number density of Mn atoms and ions. So $\log \frac{W}{\lambda} = \log (N_{Mn}/N_H) + \log C$. For lines in the saturation and damping parts of the curve of growth $W/\lambda < CN_{Mn}/N_H$.

To find which lines are weak enough to lie on the linear part of the curve of growth we plotted the curve for all measured lines for which we had Moore's (1966) W's. (See Figure 17.) The transition from the linear to the saturation region was not well defined, however. To determine whether some lines in the region of doubt were weak enough to be used for abundance analysis we used Lennard's (1976) fit of his Ni I data to the theoretical curve of growth from Hunger (1956). Although the horizontal position of the theoretical curve depends on the abundance of the element, its position with respect to the ordinate depends only on ξ_o, the root mean square velocity of an atom in the photosphere. Since the velocity depends only on the temperature of the medium and the mass of the atom, ξ_o will be nearly the same for Mn and Ni, so

the $\frac{W}{\lambda}$ value at which saturation begins should be the same for both elements. The linear part of Lennard's curve of growth ended at $\log \frac{W}{\lambda} = -5.55 \pm .04$, so lines with $\log \frac{W}{\lambda} > -5.51$ were not included in the abundance analysis. Using lines on the linear part of the curve of growth and using the Moore and Kitt Peak equivalent widths, we calculated $\log \frac{N_{Mn}}{N_H} = \log \frac{W}{\lambda} - \log C$.

4.3 Results

A. Abundance results

Table 7 lists the lines with $\log \frac{W}{\lambda} < -5.51$ for which we have W's obtained from the Kitt Peak spectrum by spectrum synthesis. Also listed are the abundances derived from these lines. It is seen that the spread in abundance values is very small except for the line 5260.771, which yields an abundance six standard deviations larger than the average abundance of the other four lines, where the standard deviation is computed from the other four measurements. See Figure 18.

There is no indication of error in the measured gf of the 5260.771 Å line. Self-absorption in the hollow cathode lamp would cause the measured gf of a weak line to be too large, making the abundance too small. The comparison of our lifetime and gf results with those of others and the abundance derived from the other line from the $z\,^4F^o$ term do not indicate an error in the lifetime. It is significant that Lennard had to use a very broad line at this wavelength to give a good fit in the spectrum synthesis fitting to determine W. Therefore, the most likely explanation of

this high value for the abundance is that this line is closely blended with another in the solar spectrum, and it is not possible to get the true W even by spectrum synthesis. For this reason this line has been dropped from further consideration in the abundance calculations.

The solar abundance of manganese calculated from the remaining four lines is $\langle \log \frac{N_{Mn}}{N_H} \rangle + 12.00 \equiv A_{Mn} = 5.44 \pm .05$, where the uncertainty is the standard deviation of the set of calculated abundances.

Using Moore's W's for six lines we get $A_{Mn} = 5.58 \pm .18$, where again the uncertainty is the standard deviation of the set of measurements. See Table 7.

For unclassified lines in Moore (1966) and for those of questionable classification close to wavelengths of lines for which the gf's have been measured in the lab, see Appendix 5 and Tables 8 and 9.

B. The effect of hyperfine structure on the curve-of-growth analysis

^{55}Mn has a nuclear spin of 5/2 and a nuclear magnetic dipole moment of 3.468 nuclear magnetons. Therefore, its spectrum should exhibit hyperfine structure due to the coupling of the nuclear spin and the angular momenta of the upper and lower levels of a transition. The coupling of the nuclear spin $\vec{I}$ and the momentum of the electrons $\vec{J}$ is proportional to $\vec{I} \cdot \vec{J}$ and splits each level characterized by J into a number of levels characterized by F, the quantum number for the total angular momentum $\vec{F} = \vec{I} + \vec{J}$.

Therefore, each line between two levels characterized by J_u and J_ℓ is split into several components, each component representing a transition between levels F_{u_m} and F_{ℓ_n}. The subscripts m and n are to indicate that for both upper and lower levels the quantum number F can have a number of values: $F = I+J, I+J-1, \ldots . |I-J|$.

Abt (1952) first recognized the effect hyperfine structure would have on abundances determined using equivalent widths of lines. He found that the splitting of the line into several components makes the observed line broader and shallower. Therefore, the line will have a larger W before saturation occurs than an unsplit line would have. In other words, the linear part of this line's curve of growth will extend farther than that of an unsplit line with the same gf. This means that a split line can have a certain W with a smaller A_{Mn} than would otherwise be the case. So if hyperfine structure is not taken into account for a line which, if unsplit, would be on the saturation or damping parts of the curve of growth the abundance of Mn calculated from this line will be too high.

Heide (1968) analyzed the effect of hyperfine structure on the solar abundance calculated from 19 lines of Mn I as well as lines from V I, Co I, Cu I and Ba II. The Mn I lines had W's of 20-152 mÅ. Heide used the W's and gf's of Müller and Mutschlecner (1964), correcting the gf's by the procedure of Allen and Corliss (1963). The result was that a different curve of growth had to be constructed for each line, with the behavior in the saturation and

damping regions dependent on the hyperfine structure of that line. The average of A_{Mn} (hfs not accounted for) - A_{Mn} (hfs accounted for) was 0.13. For observations of the center of the solar disk 5 of the total of 46 lines had W's of 20 mÅ or less. For these lines the difference in A_X's with and without consideration of hyperfine structure was at most 0.01 dex. For the 8 lines (including the five above) with W's of 30 mÅ or less the greatest difference in A_X's without and with the consideration of hyperfine structure was 0.03 dex. The difference does not increase monotonically with W because it depends on the hyperfine splitting of each line and the position of the line on the curve of growth, but for weak lines the difference was negligible.

No data were available with which to determine the hyperfine splitting of the lines used in our abundance determinations. However, for lines which have not reached saturation hyperfine structure should not affect the calculated abundance, since the sum of the areas of the components will equal the area that an unsplit unsaturated line would have. In this work care was taken to make sure that all of the lines used were on the linear part of the curve of growth. Therefore, for these weak lines hyperfine structure should not alter the abundance results.

C. Adopted value of the Mn solar abundance

A recent determination of the Ti solar abundance (Whaling et al. 1977) used both Moore's (1966) equivalent widths and those measured at Kitt Peak by the spectrum synthesis method. The

result was that both sets of W's yielded mean A_{Ti} values .02 dex apart, but the standard deviation of the abundances calculated from Moore's W's (W_{CM}) was .25 dex while the corresponding standard deviation for the Kitt Peak W's (W_{KP}) was .13 dex. This indicates that the Kitt Peak W's are more precise, and the abundance determined from these widths is probably nearer to the true abundance than the A_{Mn} calculated from W_{CM}, especially with the small number of lines available in Mn I. For this reason the best value to use for A_{Mn} is 5.44.

The small standard deviation of .05 dex calculated from the four lines used is probably fortuitous since the uncertainty in each log gf is .07-.08 dex, and the uncertainty in log W is .04 dex. Also, there will be a variation in the calculated abundance as different model atmospheres are used, the exact magnitude of which is hard to determine. Whaling et al. (1977) used four model atmospheres which gave a maximum difference of .11 dex in the average A_{Ti} for 15 Ti I lines. None of these models is used in this determination of A_{Mn}, however. Figures 19 and 20 compare the variations of temperature and electron pressure with optical depth for the HSRA, Elste and Holweger model atmospheres with those for the model used by GMA. It is evident that the GMA model does not differ in temperature from the HSRA and Elste models as much as the Holweger model does. In the range log $\tau_{5000} = -1.6$ to log $\tau_{5000} = -.2$ the GMA model does have a higher P_e, however, than any of the other models. This higher P_e will affect both the calculated fraction of Mn which is neutral in these regions and the

continuum opacity, which enters the abundance calculation. Without going through a model atmospheres calculation we cannot say just how much this higher electron pressure will affect the results.

An estimate of the effect can be obtained by studying titanium. Using the equivalent widths and gf values which Whaling et al. listed for the 15 lines with which they calculated A_{Ti}, we have calculated A_{Ti} with the GMA model atmosphere. These lines all had $\log (W/\lambda) < -5.4$ and so are on the linear part of the curve of growth. Our result is $A_{Ti} = 5.01 \pm .11$, where the uncertainty is the standard deviation of the set of A_{Ti} values for the 15 lines. This compares with results of 5.00 (Peytremann model), 4.94 (Elste), 5.05 (Holweger) and 4.97 (HSRA). This indicates that there is probably very little difference between our results for manganese and those which would be obtained using newer model atmospheres. An uncertainty of .08 dex is assigned to account for possible errors in the model atmosphere used.

The .08 dex uncertainty in the log gf's is due primarily to the uncertainties in the lifetimes. These uncertainties would not be eliminated by averaging the A_{Mn} values for several lines of the same upper term, but they should be reduced by averaging over lines from different upper terms. In an average over four lines from three upper terms the uncertainty of .08 dex per line for log gf should be reduced to .05 dex.

The uncertainty in the equivalent width from spectrum synthesis of the Kitt Peak spectrum is, according to Lennard (1974), 10% or .04 dex in log W. This is due mostly to uncertainty in the

placement of the continuum. If the abundance is averaged over lines in different wavelength regions one would expect this uncertainty to be reduced, but if the lines are in the same wavelength region (within 100 Å of each other; see Lennard p. 56) then averaging over them would not decrease the uncertainty due to the continuum placement. Table 7 shows that of the four lines used to determine the abundance, two are in the same wavelength region, so an average over these four lines should reduce the uncertainty due to widths from .04 dex to .02 dex.

Combining these uncertainties we find the solar abundance of manganese with respect to hydrogen to be

$$A_{Mn} = 5.44 \pm .10 \quad .$$

4.4 Comparison with the Results of Others

Table 1 shows the results of other workers for photospheric, meteoritic and coronal abundances. Our final value of $5.44 \pm .10$ is in good agreement with most post-1970 photospheric abundance results. It differs at most by .26 dex from the various coronal and meteoritic abundances except for that of de Boer et al. (1972). It should be noted that de Boer et al. also observed an [Mn XIII] line which yielded an Mn abundance 10 times lower than the Mn[XII] line, but they ignored the [Mn XIII] line because most of the abundances of other elements which they observed were 10 times higher than those of Pottasch (1964), and the Mn[XII] result followed that pattern while the [Mn XIII] result did not.

4.5 Comparison of Abundance Results with Those of Nucleosynthesis Models

One of the motivations for this thesis which were stated in Chapter 1 was to test models of nucleosynthesis. In this section the ratios of Mn, Fe and Ni abundances observed are compared with those predicted by some models of iron-group element nucleosynthesis. The assumptions underlying any comparison of observed abundances with those predicted by different models are listed by Woosley et al. (1973) and Trimble (1975).

Only three or four parameters are required to describe the models, the number of parameters depending on whether the model uses the e process alone or explosive nucleosynthesis. (For descriptions of these processes, see below.) T_9 is the temperature in degrees Kelvin divided by 10^9. ρ is the mass density expressed in g cm^{-3}. η is the neutron excess per nucleon, $\frac{N-Z}{N+Z}$, where N is the total number of neutrons and Z is the total number of protons. The fourth parameter required for explosive nucleosynthesis is χ, the time scale factor. The time scale of an explosion is $\chi \times 446 \rho^{-\frac{1}{2}}$ sec $= \tau$. (A derivation for the case of free implosion or explosion, $\chi = 1$, is given in Fowler and Hoyle (1964), eq. 111.) In an explosion it is assumed that $\rho = \rho_o e^{-t/\tau}$ and $T = T_o e^{-t/3\tau}$, where ρ_o and T_o are the peak density and temperature, respectively, after the material has been shock-heated.

The models which we have compared with the observations are listed in Table 10. Two types of basic processes are considered. In explosive oxygen burning (EOB) and explosive silicon burning

(ESB) the zone is shock-heated to a peak temperature and density, possibly by a supernova shock wave. The zone cools adiabatically as it expands. The initial composition of the zone is taken to represent the products of previous hydrostatic burning processes. In this type of burning the silicon initially present is not exhausted before the burning stops. In the e process, on the other hand, the temperature is so high for so long that proportions of nuclei formed depend only on their binding energies and on the free neutron and proton densities. Coulomb barriers are assumed not to hinder the achievement of statistical equilibrium at these temperatures. All of the silicon above the equilibrium amount is destroyed.

For the e process the end to statistical equilibrium (freeze-out) as the temperature drops can take place under two different sets of conditions. In normal or particle poor freeze-out the density of particles at freeze-out is high enough that α particles are captured as quickly as they are "melted off" of nuclei by (γ, α) reactions. The equilibrium is terminated by a lack of α's. In this type of freeze-out the results depend not on the original composition of the material but only on the η value. In particle-rich or α-rich freeze-out the density is low enough at freeze-out that many α's melted off of nuclei are not recaptured. The α density is high enough that reactions producing α's are suppressed.

The models tested either attempt to use one zone of nucleosynthesis with one process to fit all iron group abundances

(Burbidge et al. 1957) or use more than one zone with different processes, different η's and/or different freeze-out conditions to fit the observed abundance pattern.

Table 10 gives the deviations of abundance ratios observed from those predicted by the models. The smallest deviation of the calculated and observed elemental abundance ratios is shown to be given by Trimble's combination of processes. The original e process of Burbidge et al. (1957) and the 2 zone e process with particle-poor freeze-out of Hainebach (1974) provide the worst fits, indicating that a particle-rich freeze-out of material from the e process may be required to produce the observed abundance ratios.

Burbidge et al. (1957) used the solar abundances of Goldberg et al. (1960) and terrestrial isotope ratios to determine the parameters for the e process which would give the best fit to observed abundances. They normalized all of their iron group abundances to ^{56}Fe. Goldberg et al. report iron, nickel and manganese abundances of 6.57, 5.91 and 4.90, respectively, while the more recent determinations give values of 7.50, 6.33 (Ross and Aller 1976) and 5.44 (this work). Therefore, the discrepancy between the predictions of Burbidge et al. and the recently observed abundances is due in part to the low observed abundances which were used. The other workers used the more recent abundance values to find parameters for their nucleosynthesis models.

The ratio of iron to manganese is important in the area of cosmochemistry, and it is desirable to reduce the uncertainty in this ratio as much as possible. The largest source of uncertainty

in A_{Mn} is the model atmosphere used. If that uncertainty is eliminated, the uncertainties due to the oscillator strengths and equivalent widths combine to give an uncertainty of .05 dex in A_{Mn}, which is the same as the standard deviation of the set of A_{Mn} values for the four lines used. If A_{Mn} and A_{Fe} vary similarly with the model atmosphere the uncertainty due to the model atmosphere can be ignored when the ratio is calculated.

Whether $A_{Fe} - A_{Mn}$ $[= \log(N_{Fe}/N_{Mn})]$ will remain constant with model atmosphere depends on the lines used in calculating A_{Fe} and A_{Mn}. Since different model atmospheres use different runs of temperature and electron pressure with optical depth, it is expected that $\log (N_{Fe}/N_{Mn})$ will remain constant only if iron and manganese have similar ionization potentials and if A_{Fe} and A_{Mn} are determined from lines with similar excitation energies for the lower levels. The ionization potentials of iron and manganese are 7.90 and 7.432 electron volts, respectively. A_{Mn} was calculated from lines with lower level excitation energies of 2.89-3.40 eV. A model atmosphere independent comparison of iron and manganese abundances should use lines having lower levels in this energy range.

Since other model atmospheres were not available to us it was necessary to calculate A_{Fe} with the Goldberg et al. (1960) model atmosphere and the weighting function method. In order to do this we used the log gf's and W's listed in the article by Richter and Wulff (1970)* for ten of the FeI lines with $\log W/\lambda < -5.4$. (The 5320 Å line is excluded because there is evidently a

misprint in the log gf or abundance value or both; the log gf given does not yield the abundance listed. It is likely that the log gf for this line should be -2.65 rather than -1.65.) The average A_{Fe} for the ten lines was 7.52 ± .07. The lower level excitation potentials of these lines are between 2.42 and 4.37 eV. The average A_{Fe} for the three lines with lower level excitation energies in the 2.89-3.40 eV range is 7.50 ± .06. Since this is close to the average over the ten lines, 7.52 ± .07 will be the A_{Fe} value used.

In the averaging over lines some averaging over oscillator strengths and equivalent widths takes place, so in calculating the uncertainty in $A_{Fe} - A_{Mn}$ only the uncertainties in the sets of abundance values will be used. Therefore $A_{Fe} - A_{Mn} = \log (N_{Fe}/N_{Mn}) = 7.52 - 5.44 = 2.08 \pm .09$. It is not clear what effect the 0.5 eV difference in the ionization energies of the two elements would produce if $A_{Fe} - A_{Mn}$ were calculated for different model atmospheres.

---

*J. Richter and P. Wulff, Astron. Astrophys. 9, 37 (1970).

Appendix A - The Equality of Lifetimes of Levels within a Term in the LS Coupling Approximation

In the LS coupling approximation the spacings between levels of a term are much smaller than the spacings between terms. A term is characterized by S and L, the quantum numbers for the total electronic spin and orbital angular momenta, respectively. A term is denoted ^{2S+1}L. Each level of a term has a different J, the total electronic angular momentum quantum number. The set of transitions between terms $^{2S_u+1}L_u$ and $^{2S_\ell+1}L_\ell$ is called a multiplet, and the closeness of levels of the same term means that ω's for different lines of the multiplet are approximately equal.

In this approximation the dipole moment reduced matrix element is

$$(\gamma_\ell S_\ell L_\ell J_\ell \| D \| \gamma_u S_u L_u J_u) = (-1)^{S_\ell + 1 + L_\ell + J_u} (\gamma_\ell L_\ell \| D \| \gamma_u L_u) \times$$

$$\sqrt{(2J_u+1)(2J_\ell+1)} \begin{Bmatrix} L_\ell & J_\ell & S_\ell \\ J_u & L_u & 1 \end{Bmatrix} \delta_{S_\ell S_u}$$

where the term in brackets is a 6-j symbol and γ represents any other quantum numbers characterizing the terms. Hereafter $S_u = S_\ell$ will be called S.

So

$$\left|(\gamma_\ell S L_\ell J_\ell \| D \| \gamma_u S L_u J_u)\right|^2$$

$$= (2J_u+1)(2J_\ell+1) \left|(\gamma_\ell L_\ell \| D \| \gamma_u L_u)\right|^2 \begin{Bmatrix} L_\ell & J_\ell & S \\ J_u & L_u & 1 \end{Bmatrix}^2 .$$

From the properties of 6-j symbols it follows that

$$\sum_{J_\ell} (2J_\ell + 1) \begin{Bmatrix} L_\ell & J_\ell & S \\ J_u & L_u & 1 \end{Bmatrix}^2 = \frac{1}{2L_u + 1}$$

and therefore

$$\sum_{J_\ell} A_{J_u J_\ell} = \frac{4\omega^3}{3\hbar c^3} \frac{1}{2L_u + 1} \left| (\gamma_\ell L_\ell \| D \| \gamma_u L_u) \right|^2 .$$

Therefore, the sum of transition probabilities for decays to a given lower term is the same for each level of the upper term.

Summation over multiplets yields

$$\sum_{L_\ell} \sum_{J_\ell} A_{J_u J_\ell} = \frac{4}{3\hbar c^3} \frac{1}{2L_u + 1} \left[\omega_1^3 \left| (\gamma_{\ell 1} L_{\ell 1} \| D \| \gamma_u L_u) \right|^2 \right.$$

$$\left. + \omega_2^3 \left| (\gamma_{\ell 2} L_{\ell 2} \| D \| \gamma_u L_u) \right|^2 + \ldots \right]$$

which does not depend on J_u. But this sum is over all possible transitions from upper level u, which is $1/\tau_u$. So the lifetime of every level of a term is equal in the LS coupling approximation.

Appendix B - Alignment of Spectrometer with Beam Path

I. Objective: Position the optical axis of the Jarrell-Ash monochromator and lens system perpendicular to the beam path and level with it.

II. Method

A. Take the photomultiplier tube away from the monochromator exit slit.

B. Put the small brass plug with the pinhole in the center into the target chamber entrance port.

C. Align the laser along the optical axis of the monochromator.

1. With the laser mount clamped to the monochromator direct the laser beam to the center of the exit slit.

2. Turn the wavelength drive knob until the wavelength scale reads approximately zero and the laser light is coming out of the entrance slit. At this point light of all wavelengths coming into the exit slit will be focused on the entrance slit by reflections from the mirrors and the grating.

3. Adjust the laser so that the beam spot is hitting the center of the grating as well as the centers of the exit and entrance slits. Now the optical axis of the monochromator is along the laser beam.

D. Align the axis of the lens-holding tube with the optical axis of the spectrometer.

1. Place disks with .05" diameter holes in both ends of the lens tube after taking out the lenses.

2. Shift the tube until the laser beam is coming through both holes.

3. Bolt the tube in place, using shims between the tube and yoke if necessary to maintain the alignment of the tube. Mark the position of the tube on the yoke.

4. Place the lenses in the tube to check that their optical axes are the same as the axis of the tube.

E. Move the monochromator until the laser beam is grazing the front of the target chamber cavity.

F. Place shims under monochromator mount until the laser beam is level with the hole in the brass plug in the target chamber entrance port.

G. Adjust the optical axis to make it perpendicular to the ion beam axis.

1. Clamp a microscope slide to the side of the target chamber.

2. Move the monochromator until the laser beam reflects off of the microscope slide.

3. Remove the lenses and masks from the lens tube.

4. Loosen the locking screw under the platform on the lathe bed. Rotate the platform until the laser beam is perpendicular to the microscope slide, which is shown by the reflected spot's coinciding with the laser beam coming out of the monochromator. The reflected spot should be centered on the monochromator

entrance slit. Tighten the locking screw. The monochromator-lens tube system is now properly aligned with the ion beam path.

Appendix C - Calibration of the Paschen-Runge Spectrometer

I. Purpose of Calibration

To compare the intensities of two lines from the same upper level we need to know the relative efficiency of the spectrometer-detector system at those two wavelengths. This relative efficiency has been found by measuring the response of the spectrometer to light sources of known spectral radiance. The Paschen-Runge spectrometer was used for all branching ratio measurements; it was used with the north entrance slit for first-order measurements of branching ratios, with the south entrance slit for determinations of upper limits of branching ratios of infrared lines and with the north entrance slit for second-order measurements of the upper limits of branching ratios of lines around 2170 Å.

II. Light Sources

A. 3000-10,000 Å calibration: W-filament standard lamp described by Lennard (1974): GE Type 30A/T24/17 commercial lamp calibrated at 35 amp a.c. by the Eppley Laboratory, Inc., Newport, R.I.

B. 2000-3500 Å calibration: D_2 discharge lamp made by Hellma Calls, Inc. Two D_2 discharge lamps were calibrated against a wall-stabilized hydrogen arc at the National Bureau of Standards in Washington, D.C., with the D_2 lamps at 100 v d.c. and $0.300 \pm .002$ amp. The spectrometer's response to a calibrated lamp and an uncalibrated D_2 lamp were measured, and when it was determined that the difference in response to the two lamps was

less than 6% at all wavelengths, we decided to use the uncalibrated lamp for most measurements of spectrometer efficiency. The calibrated lamps were saved for occasional comparison with the uncalibrated lamp.

III. Procedure [also see Lennard (1974)]

A. $n(\lambda)$ = photons incident on detector per sec at λ = $I(\lambda)\mathcal{E}_o(\lambda)\Omega$ where $I(\lambda)$ = photons/sec/stearadian/Å/(cm^2 of source)

$\mathcal{E}_o(\lambda)$ = fraction of photons incident on entrance slit which reach detector.

Ω = geometrical factor.

B. Since we require only relative efficiency, $\mathcal{E}(\lambda)$ define $\mathcal{E}_o(\lambda) = C_1\mathcal{E}_1(\lambda)$, where C_1 is independent of λ.

C. Current from photomultiplier is $(\lambda) = C_2 n(\lambda)\mathcal{E}_2(\lambda)$ where $\mathcal{E}_2(\lambda)$ = efficiency of photomultiplier at λ. This is for photomultipliers operated in the linear region ($i \leq 100$ nA for EMI 9783B in the stepping channel). C_2 = constant.

D. Therefore, $i(\lambda)/I(\lambda) = C_1C_2\Omega\mathcal{E}_1(\lambda)\mathcal{E}_2(\lambda) = \mathcal{E}(\lambda)$ = nanocoulombs/(photon, sec^{-1} $stearad^{-1}$ $Å^{-1}$ cm^{-2}). $i(\lambda)$ is measured, and $I(\lambda)$ is known from the Eppley calibration. To compare efficiencies at two wavelengths

$$\frac{\mathcal{E}(\lambda_1)}{\mathcal{E}(\lambda_2)} = \frac{i(\lambda_1)I(\lambda_2)}{i(\lambda_2)I(\lambda_1)} \quad .$$

In calibration of spectrometer response in second order $\mathcal{E}(\lambda) = \frac{i(\lambda)}{I(\lambda)} \times 2$, since the size of the image of the entrance slit,

which determines the photons per centimeter in the line along the track at the position of the detector, is unchanged for a line source, while the photons per cm of track for a continuum source is halved, since $\frac{d\lambda}{ds}$ = angstroms/cm is halved while $I(\lambda)$ remains the same.

E. The geometry in the calibration was the same as in the BR measurements. The optical path length was kept the same.

F. UV measurements: 2100 Å and 2200 Å second order signals were compared with 3500 Å in first order; then the 3500 Å first order calibration with W fil. standard lamp was compared to $\mathcal{E}(\lambda)$ at 4400 Å and 4500 Å to find $\frac{\mathcal{E}(2170\ \text{Å, 2nd order})}{\mathcal{E}(4450\ \text{Å, 1st order})}$

G. The uncertainty in NBS standards is 3-8%. We have assumed the same uncertainty for the Eppley calibrations for the W filament lamp. An uncertainty of 5% has been assigned to each $\mathcal{E}(\lambda)$ used, so the uncertainty in $\mathcal{E}(\lambda_1)/\mathcal{E}(\lambda_2)$ is 7% for λ_1 and λ_2 not in the same λ region. We have used $\sigma\left[\frac{\mathcal{E}(\lambda_1)}{\mathcal{E}(\lambda_2)}\right] = 0$ for lines in the same multiplet as the strongest line from the branch and $\sigma\left[\frac{\mathcal{E}(\lambda_1)}{\mathcal{E}(\lambda_2)}\right] =$ 7% for lines in other multiplets. In these measurements the lines from other multiplets were always at least 400 Å from the strongest line from the branch.

For the D_2 discharge lamp calibration combined with the tungsten filament lamp calibration $\sigma\ \frac{\mathcal{E}(2170\ \text{Å, 2nd order})}{\mathcal{E}(4450\ \text{Å, 1st order})} \approx 19\%$, but this is not critical since only an upper limit was measured for the BR's of lines in the 2170 Å region.

Appendix D - The Effect of Using One Monitor Line for All BR Measurements for Lines from the Same Term

The object of these calculations is to find

$$\frac{\Delta(s_{u\ell}/M_{u'\ell'})/(s_{u\ell}/M_{u'\ell'})}{\Delta M_{u'\ell'}/M_{u'\ell'}} ,$$

the relative change in the scan signal-to-monitor signal ratio compared with the relative change in the monitor signal, which I can measure directly. $s_{u\ell}$ = signal from stepping PMT.

$$\frac{s_{u\ell}}{M_{u'\ell'}} = \frac{K \frac{1}{U_o} A_{u\ell} g_u e^{-E_u/kT}}{K' \frac{1}{U_o} A_{u'\ell'} g_{u'} e^{-E_{u'}/kT}} = \frac{K g_u A_{u\ell} e^{-E_u/kT}}{K g_{u'} A_{u'\ell'} e^{-E_{u'}/kT}}$$

where K, K' are constants and $U_o = \sum_i g_i e^{-E_i/kT}$ = partition function.

For $u = u'$ there is no dependence on T in the ratio $s_{u\ell}/M_{u\ell}$ but for $u \neq u'$ this ratio will change with T.

$$\frac{d(s_{u\ell}/M_{u'\ell'})}{dT} = \frac{K g_u A_{u\ell}}{K' g_{u'} A_{u'\ell}} e^{-(E_u - E_{u'})/kT} \frac{E_u - E_u}{kT^2} = \frac{s}{M} \frac{E_u - E_{u'}}{kT^2}$$

$$\frac{d(s_{u\ell}/M_{u'\ell'})}{s_{u\ell}/M_{u'\ell'}} = \frac{E_u - E_{u'}}{kT^2} dT$$

$$\frac{dM_{u'\ell'}}{dT} = \frac{K'}{U_o} A_{u'\ell'} g_{u'} e^{-E_{u'}/kT} \frac{E_{u'}}{kT^2}$$

$$+ K' A_{u'} g_{u'} e^{-E_{u'}/kT} \left(\frac{-1}{U_o^2}\right) \sum_i g_i \frac{E_i}{kT^2} e^{-E_i/kT}$$

$$= M_{u'\ell'} \left[\frac{E_{u'}}{kT^2} - \frac{1}{kT^2} \frac{\Sigma g_i E_i e^{-E_i/kT}}{\Sigma g_i e^{-E_i/kT}} \right]$$

$$\frac{dM_{u'\ell'}}{M_{u'\ell'}} = \frac{dT}{kT^2} \left[E_{u'} - \frac{\Sigma g_i E_i e^{-E_i/kT}}{\Sigma g_i e^{-E_i/kT}} \right]$$

So

$$\frac{[d(s_{u\ell}/M_{u'\ell'})/s_{u\ell}]/M_{u'\ell'}}{dM_{u'\ell'}/M_{u'\ell'}} = \frac{E_u - E_{u'}}{E_{u'} - \dfrac{\Sigma g_i E_i e^{-E_i k/T}}{\Sigma g_i e^{-E_i/kT}}} .$$

For the z^6F^o term using line 3834.368 as the monitor the maximum $|E_u - E_{u'}| = 210\ cm^{-1}$. $E_{u'} \approx 43,000\ cm^{-1}$.

See Chapter 2, section VII for the estimate of temperature used in hollow-cathode lamp. For the lamp temperatures used

$$\frac{\Sigma g_i E_i e^{-E_i/kT}}{\Sigma g_i e^{-E_i/kT}} < 3000\ cm^{-1} .$$

So

$$\left| \frac{d(s_{u\ell}/M_{u'\ell'})/(s_{u\ell}/M_{u\ell'})}{dM_{u'\ell'}/M_{u'\ell'}} \right| \leq .005 \ ,$$

indicating that it was safe to use one line as monitor for the whole term; the ratios of populations of levels of the term were very nearly constant.

If the monitor line is blended with a line from another level u'' of the same term the signal from the monitor PMT is

$$M_{u'\ell'} = K' \frac{1}{U_o} g_{u'} A_{u'\ell'} e^{-E_{u'}/kT} + \alpha K' \frac{1}{U_o} g_{u''} A_{u''\ell''} e^{-E_{u''}/kT}$$

where α = measure of how well the lines are resolved by the monitor system. For no blending $\alpha = 0$. For the monitor line from the same level as the line being scanned, $u' = u$. $M_{u'\ell'}$ is measured at the peak of the $u'\ell'$ line. By a calculation similar to the one presented above we get

$$\left| \frac{d(s_{u\ell}/M_{u'\ell'})}{(s_{u\ell}/M_{u'\ell'})} \right| \leq \left| \frac{dM}{M} \right| \left| \frac{\Delta E_{max}}{E_{u'} - \frac{\sum g_i E_i e^{-E_i/kT}}{\sum g_i e^{-E_i/kT}}} \right|$$

where ΔE_{max} = greater of $|E_u - E_{u'}|$ and $|E_u - E_{u''}|$. In this case ΔE_{max} is always < 340 cm^{-1} so

$$\left| \frac{d(s_{u\ell}/M_{u'\ell'})}{s_{u\ell}/M_{u'\ell'}} \right| < \left| \frac{dM_{u'\ell'}}{M_{u'\ell'}} \right| \times .0085 \ .$$

Appendix E - Lines in The Solar Spectrum (Moore et al. 1966) Not Identified as Mn I

There are some lines in Moore which are at wavelengths very close to those of lines for which the gf's have been measured in the lab. However, these lines either are identified Mn I?, or have some other identity assigned to them, or are unidentified. It is logical to inquire whether the tentatively identified and the unidentified lines are indeed Mn I and whether the identification of some lines in Moore could have been in error. One piece of information which may help is the abundance calculated from each line. The comparison of this abundance with that calculated from lines positively identified as Mn I may give an indication of the likelihood that the line is due to Mn. Table 8 lists the lines investigated and the abundances calculated from them. Each line is discussed below. The wavelengths labeling each paragraph are from Catalan et al. (1964).

4987.066

Other members of this multiplet are seen, and this line is definitely in the Kitt Peak spectrum $|\Delta\lambda| = |\lambda_{CM} - \lambda_{Cat}|$ of the line is 19 mÅ, which is not extraordinarily large. (See Table 9.) However, the high abundance obtained from Moore's W indicates that this line may be closely blended with another line. The Kitt Peak spectrum shows this line badly blended with nearby lines, so Moore's W may be very uncertain.

7174.420

The other members of this multiplet are very weak. $|\Delta\lambda|$ of 30 mÅ is a large but not impossible difference. Moore does not list anything within .25 Å of 7055.583, another member of the multiplet. There is a weak unclassified line 58 mÅ from 7088.288, which is also in the multiplet, but this distance is quite large compared to $|\Delta\lambda|$'s for known Mn I lines. The high abundance indicates that this line is due at least in part to something other than Mn I.

6413.947

Although this line yields an abundance close to the average of those calculated from W_{CM} and although $|\Delta\lambda|$ is only 15 mÅ, this line is probably the CN band member which Moore lists. There are many other CN 5,1 vibrational band members in this wavelength region.

6443.511

$|\Delta\lambda|$ between this line and that listed in Moore is 39 mÅ, which is larger than any of the wavelength differences listed in Table 9. It should be easy to tell which lines are atmospheric and which are solar lines. Moore's location of many other members of the same vibration-rotation band of H_2O in this wavelength region makes a strong case for her identification of this line.

6349.795

The abundance calculated from this line's W_{CM} is quite high, and its $|\Delta\lambda|$ of 45 mÅ is large. However, since it is well-separated

from other lines its width was measured from the Kitt Peak spectrum by the method of counting squares. Using this width (2.9 ± .2 mÅ) we find an abundance of $A_{Mn} = 5.72$. Given the crudeness of the W measurement and the difficulty of discerning where the line ended and the continuum began, we consider this abundance to be close to those calculated from other lines, so this may be an Mn I line.

6378.969

The very reasonable abundance plus the fact that Moore sees lines at 6440.934 and 6349.715 Å, 39 and 45 mÅ, respectively, from other multiplet members as listed in Catalan's spectrum are indications that this may be Mn I. The W has been measured by counting squares under the line from a tracing of the Kitt Peak spectrum. W was found to be 2.5 mÅ, yielding an A_{Mn} of 5.64. This is a reasonable value, especially since the continuum level is difficult to determine in this method of W measurement. This A_{Mn} value from the Kitt Peak W adds to the evidence that this may be Mn I.

6382.195

This line is definitely in the Kitt Peak spectrum. The Utrecht Atlas shows a shallow (1%-1.5%) depression of the continuum about 150 mÅ across at this wavelength. The W for this line has been measured by counting squares under a tracing of the line from the Kitt Peak spectrum. The W is 2.6 mÅ, but again it was hard to tell where the continuum stopped and the line began.

With this W the calculated A_{Mn} is 5.66, which is not extraordinarily large. Therefore, this line also may be Mn I.

Comment on Table 9

Table 9 shows that most of the Catalan wavelengths are within 10 mÅ of the Moore wavelengths. However, two of the lines which we use for abundance determination, 5029.779 and 5388.538, are 36 and 34 mÅ, respectively, from lines listed in Moore as Mn I. Moore classifies these lines as $a^4D\text{-}z^6F^o$ and $a^4P\text{-}z^4D^o$, respectively, which is consistent with Catalan's classification of the lines. It is not clear why these two Catalan wavelengths are so far from those of Moore. In the solar atlases these lines appear to be only slightly blended and of the widths we would expect from Mn I lines with a^4D and a^4P lower levels, so there is support for their identification and classification by Moore. One possible explanation is that there are misprints or slight wavelength measurement errors in Catalan et al.

These lines should not be dismissed from consideration in abundance determinations simply because of the wavelength disagreement, because if our gf's are correct and if the classification of the lines is correct the lines must appear in the solar spectrum with the appropriate equivalent widths (or larger ones, if other lines are blended with these). They could not be absent from the solar spectrum. For this reason we use these lines and suspect Catalan et al. of some misprints or wavelength measurement errors.

References

1. A. Abt, Astrophys. J. 115, 199 (1952).
2. C. W. Allen and A. S. Asaad, Mon. Not. R. Astron. Soc. 117, 36 (1957).
3. C. W. Allen and C. H. Corliss, Mon. Not. R. Astron. Soc. 126, 37 (1963).
4. L. H. Aller and A. K. Pierce, Astrophys. J. 116, 176 (1952).
5. S. Bashkin, Nuc. Instr. and Methods 28, 88 (1964).
6. S. Bashkin, Chapter IV of Progress in Optics XII, E. Wolf, ed. (North-Holland, 1974).
7. G. D. Bell, M. H. Davis, R. B. King and P. M. Routley, Astrophys. J. 129, 437 (1959).
8. E. Biemont, Solar Phys. 44, 269 (1975).
9. D. E. Blackwell, B. S. Collins and A. Petford, Solar Phys. 23, 292 (1972).
10. A. E. Blaugrund, Nuc. Phys. 88, 501 (1966).
11. J. W. Brault, C. D. Slaughter, A. K. Pierce and R. S. Aikens, Solar Phys. 18, 366 (1971).
12. J. W. Brault and L. Testerman, "Preliminary Edition of the Kitt Peak Solar Atlas" (unpublished 1972).
13. E. M. Burbidge, G. R. Burbidge, W. A. Fowler and F. Hoyle, Rev. Modern Phys. 29, 547 (1957).
14. A. G. W. Cameron, Space Sci. Rev. 15, 121 (1973).
15. M. A. Catalan, W. F. Meggers and O. Garcia-Riquelme, J. Res. Natl. Bur. Std. 68A, 9 (1964).

16. W. J. Claas, Recherches Astronomiques de l'Observatoire d'Utrecht XII, Part 1 (1951).

17. C. L. Cocke, A. Stark, J. C. Evans, Astrophys. J. 184, 653 (1973).

18. C. Corliss and W. Bozman, Natl. Bur. Std. Monograph No. 53 (1962).

19. L. J. Curtis, H. G. Berry and J. Bromander, Physica Scripta 2, 216 (1970).

20. K. S. DeBoer, H. Olthoff and S. R. Pottasch, Astron. Astrophys. 16, 417 (1972).

21. L. Delbouille, L. Neven and G. Roland, Atlas Photométrique du Spectre Solaire de λ3000 a λ10,000 Å (Institut d'Astrophysique, Univ. de Liege, 1973).

22. G. Elste, Astrophys. J. 148, 857 (1967).

23. H. Falk and H. Lucht, J. Quant. Spectrosc. Rad. Trans. 16, 909 (1976).

24. W. A. Fowler and F. Hoyle, Astrophys. J. Supp. 9, 201 (1964).

25. R. H. Garstang, private communication (1977).

26. O. Gingerich, R. W. Noyes, W. Kalkofen and Y. Cuny, Solar Phys. 18, 347 (1971).

27. L. Goldberg, E. A. Müller and L. H. Aller, Astrophys. J. Supp. 5, 1 (1960).

28. L. Goldberg and A. K. Pierce, Handbuch der Physik 52 (Springer-Verlag, Berlin, 1959).

29. K. L. Hainebach, W. D. Arnett, S. E. Woosley and D. D. Clayton, Astrophys. J. 193, 157 (1974).

30. R. Hefferlin and J. Gearhart, J. Quant. Spectrosc. Rad. Trans. 4, 9 (1964).

31. K. v. d. Heide, Zeit. f. Astrophys. 69, 220 (1968).

32. H. Holweger, Zeit. f. Astrophys. 65, 365 (1967).

33. L. Huldt and A. Lagerqvist, J. Opt. Soc. Am. 42, 142 (1952).

34. K. Hunger, Zeit. f. Astrophys. 39, 38 (1956).

35. P. Hvelplund and B. Fastrup, Phys. Rev. 165, 408 (1968).

36. L. Inglesias y R. Velasco, Publicaciones del Instituto de Optica "Daza de Valdés", Madrid, no. 23 (1964).

37. L. Kay, Phys. Lett. 5, 36 (1963).

38. R. B. King and A. S. King, Astrophys. J. 87, 24 (1938).

39. R. B. King, B. R. Parnes, M. H. Davis and K. H. Olsen, J. Opt. Soc. Am. 45, 350 (1955).

40. R. L. Kurucz and E. Peytremann, A Table of Semi-Empirical gf Values, Smithsonian Astrophysical Observatory Special Report 362 (1975).

41. D. L. Lambert, Mon. Not. R. Astron. Soc. 138, 143 (1968).

42. W. N. Lennard, Ph.D. Thesis, California Institute of Technology (1974).

43. J. Lindhard, M. Scharff and H. E. Schiott, Kgl. Danske Videnskab. Selskab. Mat.-Fys. Medd. 33, no. 14 (1963).

44. G. D. Magnuson, C. E. Carlston, P. Mahadevan and A. R. Comeaux, Rev. Sci. Instr. 36, 136 (1965).

45. T. E. Margrave, Solar Phys. 27, 294 (1972).

46. I. Martinson, L. J. Curtis, J. Brzozowski and R. Buchta, Physica Scripta 8, 62 (1973).

47. I. Martinson, L. J. Curtis, P. L. Smith and E. Biemont, Physica Scripta 16, 35 (1977).

48. D. Mihalas, Stellar Atmospheres (W. H. Freeman and Co., San Francisco, 1970).

49. M. Minnaert, G.F.W. Mulders and J. Houtgast, Photometric Atlas of the Solar Spectrum, 3332 Å to 8771 Å (Amsterdam, Schnabel, 1940).

50. C. E. Moore, A Multiplet Table of Astrophysical Interest, rev. ed. (Princeton University Observatory, 1945).

51. C. E. Moore, M.G.J. Minnaert and J. Houtgast, The Solar Spectrum 2935 Å-8770 Å, Natl. Bur. Std. Monograph 61 (1966).

52. C. E. Moore, Atomic Energy Levels, Natl. Bur. Std. Circular 467, Vol. II (1971).

53. E. A. Müller and J. P. Mutschlecher, Astrophys. J. Supp. 9, 1 (1964).

54. G. M. Nikolsky, R. A. Gulyaev and K. I. Nikolskaya, Solar Phys. 21, 332 (1971).

55. V. I. Ostrovsky and N. P. Penkin, Optical Transition Probabilities, Israel Program for Scientific Translation, Vol. I, 332 (1957).

56. B. E. J. Pagel, Space Sci. Rev. 15, 1 (1973).

57. N. P. Penkin, J. Quant. Spectrosc. Rad. Trans. 4, 41 (1964).

58. E. Peytremann, Ph.D. Thesis, Municipal Observatory of Geneva (1970).

59. E. H. Pinnington and H. O. Lutz, Can. J. Phys. 52, 1253 (1974).

60. S. R. Pottasch, Mon. Not. R. Astron. Soc. 128, 73 (1964).

61. J. E. Ross and L. H. Aller, Science 191, 1223 (1976).

62. R. A. Sawyer, Experimental Spectroscopy, 3rd ed. (Dover Publications, New York, 1963).

63. H. E. Suess and H. C. Urey, Rev. Modern Phys. 28, 53 (1956).

64. P. L. Smith, Ph.D. Thesis, California Institute of Technology (1972).

65. P. L. Smith, Mon. Not. R. Astron. Soc. 177, 275 (1976).

66. I. I. Sobel'man, Introduction to the Theory of Atomic Spectra (Pergamon Press, New York, 1972).

67. S. Tolansky, High Resolution Spectroscopy (Methuen and Co., London, 1947).

68. V. Trimble, Rev. Modern Phys. 47, 877 (1975).

69. H. C. Urey, Quart. J. R. Astron. Soc. 8, 23 (March, 1967).

70. H. C. Urey, Annal. N.Y. Acad. Sci. 194, 35 (1972).

71. J. E. Vernazza, E. H. Avrett and R. Loeser, Astrophys. J. Supp. 30, 1 (1976).

72. B. Warner, Mon. Not. R. Astron. Soc. 138, 229 (1968).

73. W. D. Watson, Astrophys. J. 158, part 2, L189 (1969).

74. W. Whaling, R. B. King and M. Martinez-Garcia, Astrophys. J. 158, 389 (1969).

75. W. Whaling, J. M. Scalo and L. Testerman, Astrophys. J. 212, 581 (1977).

76. B. Woodgate, Mon. Not. R. Astron. Soc. 134, 287 (1966).

77. S. E. Woosley, W. D. Arnett and D. D. Clayton, Astrophys. J. Supp. 26, 231 (1973).

78. S. E. Woosley, Astrophys. Space Sci. 39, 103 (1976).

Table 1

Manganese abundance results. $A_{Mn} = \log \frac{N_{Mn}}{N_H} + 12.00$, where I is the number density of each element. W stands for the equivalent width of an absorption line in the solar spectrum; gf is the oscillator strength, and hfs stands for hyperfine structure. Square brackets enclosing Mn XII or Mn XIII indicate an electric-dipole-forbidden transition. Refer to pages 4, 7 and 72.

Table 1

Worker(s)	Date	A_{Mn}	Comments
Suess & Urey	1956	5.23	chondritic meteorites
Goldberg, Müller & Aller	1960	4.90	Mn I, gf's from Allen and Asaad (1957) W's 49-165 mÅ, Utrecht and Michigan atlases Aller-Pierce (1952) model atmosphere curve of growth analysis
Müller & Mutschlecner	1964	4.80	Mn I, Corliss and Bozman (1962) gf's
		4.95	Mn I, Allen and Asaad gf's W's 5-152 A, Michigan Atlas their own model atmosphere curve of growth
Pottasch	1964	5.7	corona, 1 line apiece from [Mn XII] and [Mn XIII] theoretical gf's
Urey	1967	5.45	Type I carbonaceous chondrites
Warner	1968	4.88	Mn II, measured relative gf's normalized to scale of gf's calculated by Coulomb approximation W's 0.5-17 mÅ, Moore et al. Lambert (1968) model atmosphere
Heide	1968	4.79	Mn I, Corliss and Bozman gf's corrected by method of Allen and Corliss (1963) W's 20-152 mÅ, Müller and Mutschlecner Holweger (1967) model atmosphere hfs accounted for
Nikolsky, Gulyaev, Nikolskaya	1971	5.70	corona, [Mn XIII], theoretical gf's

Table 1 (Continued)

Worker(s)	Date	A_{Mn}	Comments
Blackwell, Collins, Petford	1972	5.42	Mn I, absorption measurements of relative gf's normalized to scale of Ostrovsky and Penkin (1957) W's 41-80 mÅ measured at Gornergrat, Switzerland HSRA model atmosphere (Gingerich et al. 1971) hfs accounted for
Urey	1972	5.62	Type I carbonaceous chondrites
		5.44	Type II carbonaceous chondrites
Margrave	1972	5.41	Mn I, Corliss and Bozman gf's corrected by Takens' (1970) procedure W's 30-78 mÅ, line profiles measured at Kitt Peak HSRA model atmosphere hfs accounted for
De Boer, Olthof, Pottasch	1972	6.9	corona, 1 [Mn XII] line, theoretical gf
Martinson, Curtis, Brzozowski, Buchta	1973	5.4	Mn I, Woodgate (1968) gf's W's from Müller and Mutschlecner
Cameron	1973	5.47	Type I carbonaceous chondrites
Pinnington and Lutz	1974	5.34	Mn I and II, lifetime measurements and Corliss and Bozman branching ratios abundance determined by comparing their $A_{u\ell}$'s with those of other authors

Table 1 (Concluded)

Worker(s)	Date	A_{Mn}	Comments
Biemont	1975	5.37	Mn I, semi-empirical scaled Thomas-Fermi method for calculating gf's W's 16-130 mA from Delbouille et al. (1973), profiles fitted hfs accounted for with 1 of the 5 multiplets used
Martinson, Curtis, Smith, Biemont	1977	5.4	Mn II, measured gf's W's 111-235 mA, Delbouille et al. HSRA, Holweger, Vernazza (1976) model atmospheres

Table 2

Comparison of calculated and observed Doppler shifts for λ4451.575 Å. The calculated velocity was obtained by subtracting the energy lost in nuclear collisions (Lindhard 1963) and in electronic collisions (Hvelplund and Fastrup 1968) from the known incident energy. The uncertainty in the calculated velocities is due to the ±40% uncertainty in the thickness of the carbon foils. Refer to page 20.

Foil Thickness ($\mu g/cm^2$) ±40%	Incident Beam Energy (keV)	Calculated Doppler Shift (Å)	Observed Doppler Shift (Å)
10	308	13.8 ± 0.7	14.2 ± 0.5
10	512	18.7 ± 0.6	19.3 ± 0.6
5	512	19.3 ± 0.2	19.4 ± 0.7

Table 3

Results of beam-foil measurements of lifetimes. In column 1 the weaker components of the blends are listed in parentheses. The relative intensities listed in column 2 are with respect to the most intense line from the term, which is given an intensity of 10. The uncertainty in the foil thickness is 40%. The $\langle\tau(\text{ns})\rangle$ refers to an average of measurements over all lines from the term. R(0) is the replenishment ratio of Curtis et al. (1970). P_2 and P_1 are fitting parameters in the fit $I(x) = P_1 e^{M_1 x} + P_2 e^{M_2 x}$, where I(x) is the number of counts at position x for a certain integrated beam current. In the τ_{others} column superscript a refers to Martinson et al. (1973) and superscript b refers to Pinnington and Lutz (1974). Refer to pages 25, 28 and 33.

Table 3

λ(Å)	Relative Intensity	Upper Level	E_u (eV)	Beam Energy (keV)	Foil Thickness ($\mu g/cm^2$)	τ (ns)	⟨τ(ns)⟩	R(0)	P_2/P_1	τ_{others} (ns)
4451.575	10	$z^4D^o_{7/2}$	5.65	512	10	12.73		0	0	
				307	10	12.99	13.3	.004	.004	11 ± 2^a
(4453.013)	(1.7)	$z^4D^o_{5/2}$	5.70	307	10	13.07	±2.0	.004	.004	11.5 ± 2.0^b
				512	10	14.44		.002	.01	
				512	10	12.82		.04	.06	
				512	5	13.27		.005	.005	
				307	10	13.91		.006	.005	
3806.715	10	$z^6F^o_{11/2}$	5.35	307	10	18.91		.05	.05	17 ± 4^a
				512	10	19.26		.04	.04	16 ± 3^b
(3809.593	(1.7)	$z^6F^o_{7/2}$	5.37	512	5	18.57		.06	.07	
							18.1 ±2.7			
3823.508	7.6	$z^6F^o_{9/2}$	5.36	307	10	16.08		.00005	.02	18 ± 4^a
				512	10	18.41		.003	.005	
(3823.891)	(2.0)	$z^6F^o_{5/2}$		512	5	18.77		0	0	16 ± 3^b
3834.368	5.2	$z^6F^o_{7/2}$	5.37	307	10	17.01		.008	.008	
				512	10	18.55		0	0	
(3833.865)	(1.8)	$z^6F^o_{3/2}$	5.39	512	5	18.45		0	0	
3841.074	3.0	$z^6F^o_{5/2}$	5.38	307	10	17.20		.03	.06	
(3839.779)	(1.4)	$z^6F^o_{1/2}$	5.39							
(3843.988)	(1.2)	$z^6F^o_{3/2}$	5.39							
4762.376	10	$z^4F^o_{9/2}$	5.47	307	10	17.80		0	0	15 ± 3^a
				307	10	15.33	16.4	.02	.02	
(4761.527)	(2.7)	$z^4F^o_{3/2}$	5.53	307	10	16.24	±2.5	0	0	15 ± 5^b
				307	10	16.12		0	0	
(4765.856)	(4.2)	$z^4F^o_{5/2}$	5.52	512	5	16.46		0	0	
(4766.426)	(6.3)	$z^4F^o_{7/2}$	5.50							

Table 4

Specifications of the Paschen-Runge spectrometer and associated optical and electronic components. Refer to pages 37 and 39.

For measurements at $\lambda < 8460$ Å: north entrance slit (Figure 7)

concave mirror: 10 cm diameter, 52 cm focal length
magnification = 4 in the arrangement used

entrance slits: 25 μ, 50 μ, 100 μ widths, interchangeable
50 μ slits used for most measurements to give trapezoidal line shape since the exit slit on the stepping channel was 25 μ
height = 1 mm for quantitative measurements

grating: 600 lines/mm
18 cm wide × 7 cm high
5 m radius of curvature
blazed at 6000 Å
dispersion in first order = 3.33 cos θ_r Å/mm at plane of exit slit, where θ_r = angle between diffracted ray and normal to grating

Rowland circle: 5 m diameter
steel tape scale along rails for wavelength determination from position of exit slit

detectors: scanning channels

$\lambda < 6600$ Å: refrigerated (dry ice) EMI 9783B photomultiplier tube, modified S-5 photocathode
25 μ exit slit, fixed
scanning speeds 10 Å/min, 1 Å/min and 0.1 Å/min

8460 Å > λ > 6600 Å:

refrigerated RCA 4832 photomultiplier tube
Ga-As photocathode
20 μ exit slit, fixed
scanning speeds 7.40 Å/min and .35 Å/min

Table 4 (Continued)

monitor channel
unrefrigerated EMI 9783B
continuously variable exit slit set to 200 μ
scanning speed 7.59 Å/min with 10 rpm motor
located on the -1 order part of the track to avoid interference with 1st or 2nd order measurements

filters:

neutral density filters
purpose: reduce signal reaching scan channel
types: Balzer 1%, 10%, 20% and 50% transmission filters. The 10% filter was used in most measurements of very strong lines
short wavelength cutoff filters
purpose: eliminate second order lines
types: Schott WG 335, Corning 4-97 and 9-53 most frequently used
Baird-Atomic 2100 Å interference filter
purpose: eliminate 1st order lines in the 2100-2200 Å measurement

For measurements at $\lambda > 8460$ Å: south entrance slit (Figure 8)

concave mirror listed above
-40 cm focal length glass lens
2 plane front-surface mirrors
1 M focal length convex lens

entrance slit:

continuously variable, set to 300 μ width
height = 1 mm for 4451 Å measurements
= 2 mm for 9050-9244 Å measurements

detector:

Hamamatsu R406 photomultiplier tube, refrigerated (dry ice)
S-1 photocathode
carriage designed to turn the PMT mount so the exit slit faces the grating
continuously variable exit slit set to 400 μ
scanning speed 9.1 Å/min

filters:

Corning 3-69 in front of scan PMT and Corning 4-97 in front of monitor PMT for IR measurements

Table 4 (Concluded)

Electronics

current amplifiers: Analog Devices 144-A FET input op amp with feedback resistors and capacitors
Semiconductor Circuits, Inc., LCD 15 v. power supply
same design for monitor and scan channels

strip-chart recorder: 2-channel Honeywell Electronik 194
photomultiplier tube power supply: Kiethley 224
hollow cathode lamp power supply: Regatron 209B
exit slit carriage drive motors: monitor carriage and S-1 phototube carriage: Bodine Type KYC 1, 3 and 10 rpm motors
RCA 4832 carriage: fast scan Bodine Type KYC 1 rpm motor
slow scan Insco 06710-300H multi-speed generator
stepping carriage: Slosyn HS-50 stepping motor, 1.8°/step
stepping motor driven by oscillator at
2.02 Hz = 1.0 Å/min
20.2 Hz = 10.0 Å/min

Table 5

Branching ratios, transition probabilities and oscillator strengths. The wavelengths are from Catalan et al. (1964). In the column labeled "Results of others, log gf" a denotes Allen and Asaad (1957), b denotes Woodgate (1966), c Corliss and Bozman (1962), d Kurucz and Peytremann and e Hefferlin and Gearhart (1964). Refer to pages 54-56.

Table 5

Upper Level	Lower Level	λ(Å)	BR	$A(10^7 sec^{-1})$	$\log_{10}$ gf	Comments	Results of Others, $\log_{10}$ gf
$z^6F^o_{11/2}$	$a^6D_{9/2}$	3806.715	1.00	5.5 ± .8	.16 ± .06		.79,[a] 0.0,[b] .97,[c] .26[d]
$z^6F^o_{9/2}$	$a^6D_{9/2}$	3790.214	.092 ±.004	.51 ± .08	-.96 ±.07		-1.01,[b] -0.10,[c] -.95,[d]
	$a^6D_{7/2}$	3823.508	.889 ±.004	4.9 ±.7	.03 ±.06		.66,[a] -0.02,[b] .81,[c] .14[d]
	$a^4D_{7/2}$	4965.856	.0203 ±.0016	.11 ± .02	-1.38 ±.07		-0.75,[c] -1.44[d]
	$a^4G_{11/2}$	5504.224	1.11×10^{-3} $\pm.09 \times 10^{-3}$	6.1×10^{-3} $\pm 1.0 \times 10^{-3}$	-2.56 ±.08		-2.49[d]
	$a^4G_{9/2}$	5510.190	1.2×10^{-4} $\pm.7 \times 10^{-4}$	7.8×10^{-4} $\pm 4.1 \times 10^{-4}$	-3.45 ±.25		-3.30[d]
$z^6F^o_{7/2}$	$a^6D_{9/2}$	3776.537	3.3×10^{-3} $\pm.1 \times 10^{-3}$	.018 ±.003	-2.51 ±.07		-2.41,[b] -2.78[d]
	$a^6D_{7/2}$	3809.593	.238 ±.008	1.3 ±.2	-0.64 ±.07	report results (a, b, c) but they were unable to resolve this from 3809.485. They get -.02,[a] -.45,[b] .34[c]	-.59[d]
	$a^6D_{5/2}$	3834.368	.737 ±.008	4.1 ±.6	-0.14 ±.06		-0.04,[b] 0.45,[c] -.04[d]
	$a^4D_{7/2}$	4942.396	9.4×10^{-4} $\pm.9 \times 10^{-4}$	5.2×10^{-3} $\pm.9 \times 10^{-3}$	-2.82 ±.08		-3.27[d]
	$a^4D_{5/2}$	5004.891	.013 ±.001	.074 ±.013	-1.66 ±.08		-1.00,[c] -1.64[d]

Table 5 (Continued)

Upper Level	Lower Level	λ(Å)	BR	$A(10^7 sec^{-1})$	$\log_{10} gf$	Comments	Results of Others, $\log_{10} gf$
	$a^4G_{9/2}$	5481.345	$\leq 6.8 \times 10^{-3}$ $\pm .7 \times 10^{-3}$	$\leq .037$ $\pm .007$	≤ -1.87 $\pm .08$	blended with 5481.396 (λ_{Kurucz})	-2.68[d]
$z^6F^o_{5/2}$	$a^6D_{7/2}$	3799.256	.024 $\pm .001$	.13 $\pm .02$	-1.77 $\pm .07$		-1.77,[b] -0.78,[c] -1.84[d]
	$a^6D_{5/2}$	3823.891	.382 $\pm .006$	2.1 $\pm .3$	-0.56 $\pm .07$		.01,[a] -.33,[b] .10,[c] -.48[d]
	$a^6D_{3/2}$	3841.074	.577 $\pm .007$	3.2 $\pm .5$	-.37 $\pm .06$		.16,[c] -.28,[d]
	$a^4D_{5/2}$	4987.066	7.1×10^{-4} $\pm .6 \times 10^{-4}$	3.9×10^{-3} $\pm .7 \times 10^{-3}$	-3.05 $\pm .08$		-3.70[d]
	$a^4D_{3/2}$	5029.779	9.8×10^{-3} $\pm .9 \times 10^{-3}$	.054 $\pm .01$	-1.91 $\pm .08$		-1.95[d]
	$a^4G_{7/2}$	5460.645	$\leq 8.5 \times 10^{-3}$ $\pm 1.0 \times 10^{-3}$	$\leq .047$ $\pm .009$	≤ 1.90 $\pm .08$	blended with 5460.555 (λ_{Kurucz})	-3.00[d]
$z^6F^o_{3/2}$	$a^6D_{5/2}$	3816.746	.076 $\pm .003$	.42 $\pm .06$	-1.44 $\pm .07$		-1.33,[b] -.54,[c] -1.43[d]
	$a^6D_{3/2}$	3833.865	.55 $\pm .01$	3.0 $\pm .5$	-.57 $\pm .07$		.08,[a] -.34,[b] .02,[c] -.50[d]
	$a^6D_{5/2}$	3843.988	.37 $\pm .01$	2.0 $\pm .3$	-.74 $\pm .07$		-.21,[a] -.59,[b] -.12,[c] -.66[d]

Upper Level	Lower Level	λ(Å)	BR	A(10^7 sec^{-1})	$\log_{10}$ gf	Comments	Results of Others, $\log_{10}$ gf
	$a^4D_{1/2}$	5042.567	4.6×10^{-3} $\pm .4 \times 10^{-3}$	.026 ±.004	-2.41 ±.08		-2.40[d]
$z^6F^o_{1/2}$	$a^6D_{3/2}$	3829.679	.188 ±.007	1.0 ±.2	-1.34 ±.07		-1.19,[b] -.36,[c] -1.30[d]
	$a^6D_{1/2}$	3839.779	.812 ±.007	4.5 ±.7	-.70 ±.06		-.07,[a] -.59,[b] -.12,[c] -.63[d]
$z^4F^o_{9/2}$	$a^6D_{9/2}$	3670.505	9.0×10^{-3} $\pm .7 \times 10^{-3}$	.055 ±.010	-1.95 ±.08		-.48,[c] -1.93[d]
	$a^6D_{7/2}$	3701.728	.013 ±.001	.080 ±.014	-1.78 ±.08		-1.99,[b] -.60,[c] -1.82[d]
	$a^4D_{7/2}$	4762.376	.924 ±.004	5.6 ±.9	.28 ±.07		.54,[a] .29,[b] .60,[c] .21[d]
	$a^4G_{11/2}$	5255.330	.049 ±.004	.30 ±.05	-.90 ±.08		-.20,[c] -.89[d]
	$a^4G_{9/2}$	5260.771	3.9×10^{-3} $\pm .3 \times 10^{-3}$	.024 ±.004	-2.01 ±.08		-2.02[d]
	$b^4D_{7/2}$	7174.420	7.6×10^{-4} $\pm .8 \times 10^{-4}$	4.6×10^{-3} $\pm .9 \times 10^{-3}$	-2.44 ±.08		-2.18[d]
$z^4F^o_{7/2}$	$a^6D_{9/2}$	3639.148	6.1×10^{-4} $\pm .6 \times 10^{-4}$	3.7×10^{-3} $\pm .7 \times 10^{-3}$	-3.23 ±.08		-3.38[d]
	$a^6D_{7/2}$	3669.837	9.9×10^{-3} $\pm .8 \times 10^{-3}$	.060 ±.010	-2.01 ±.08		-2.09[d]

Table 5 (Continued)

Upper Level	Lower Level	λ(Å)	BR	$A(10^7 sec^{-1})$	$\log_{10} gf$	Comments	Results of Others, $\log_{10} gf$
	$a^6D_{5/2}$	3692.817	7.2×10^{-3} $\pm .6 \times 10^{-3}$	.044 ±.008	-2.14 ±.08		-2.26,[b] -2.31[d]
	$a^4D_{7/2}$	4709.710	.198 ±.006	1.2 ±.2	-.49 ±.07		-.69,[b] -.05,[c] -.48[d]
	$a^4D_{5/2}$	4766.426	.721 ±.007	4.4 ±.7	.08 ±.07		.45,[a] .09,[b] .45,[c] -.01[d]
	$a^4G_{9/2}$	5196.603	.056 ±.004	.34 ±.06	-.96 ±.08		-.43,[c] -.99[d]
	$a^4G_{7/2}$	5197.229	7.5×10^{-3} $\pm .6 \times 10^{-3}$	.046 ±.008	-1.83 ±.08		-1.88[d]
	$b^4D_{7/2}$	7055.583	7.6×10^{-4} $\pm 1.6 \times 10^{-4}$	4.7×10^{-3} $\pm 1.2 \times 10^{-3}$	-2.56 ±.12		-2.29[d]
$z^4F^o_{5/2}$	$a^6D_{7/2}$	3646.707	7.9×10^{-4} $\pm .8 \times 10^{-4}$	4.8×10^{-3} $\pm .9 \times 10^{-3}$	-3.24 ±.08		-3.28[d], b reports results, but with hotter sources and worse resolution than mine, I suspect they see some nearby Mn II lines. They get -3.19[b]
	$a^6D_{5/2}$	3669.398	$\leq 5.3 \times 10^{-3}$ $\pm .5 \times 10^{-3}$	≤.032 ±.006	≤-2.41 ±.08	looks very wide in my spectrum, probably blended	-2.54[d]
	$a^6D_{3/2}$	3685.215	3.2×10^{-3} $\pm .3 \times 10^{-3}$	.020 ±.003	-2.62 ±.08		-2.89[d]
	$a^4D_{7/2}$	4671.688	.0167 ±.0007	.10 ±.02	-1.70 ±.07		-2.05,[b] -.75,[c] -1.59[d]

Table 5 (Continued)

Upper Level	Lower Level	λ(Å)	BR	$A(10^7 sec^{-1})$	$\log_{10}$ gf	Comments	Results of Others, $\log_{10}$ gf
	$a^4D_{5/2}$	4727.462	.261 ±.007	1.6 ±.2	-.50 ±.07		-.14,[a] -.77,[b] .01,[c] -.48[d]
	$a^4D_{3/2}$	4765.856	.643 ±.008	3.9 ±.6	-.10 ±.07		.24,[a] -.24,[b] .25,[c] -.20[d]
	$a^4G_{7/2}$	5150.937	.061 ±.005	.37 ±.06	-1.05 ±.08		-.42,[c] -1.09[d]
	$a^4G_{5/2}$	5149.155	8.2×10^{-3} $\pm.6 \times 10^{-3}$	.050 ±.009	-1.92 ±.08		-1.98[d]
$z^4F^o_{3/2}$	$a^6D_{5/2}$	3653.514	1.2×10^{-3} $\pm.1 \times 10^{-3}$	7.1×10^{-3} $\pm1.2 \times 10^{-3}$	-3.24 ±.07		-3.68[d]
	$a^6D_{3/2}$	3669.198	1.6×10^{-3} $\pm0.4 \times 10^{-3}$	9.6×10^{-3} $\pm 2.7 \times 10^{-3}$	-3.11 ±.13		-3.20[d]
	$a^6D_{1/2}$	3678.470	1.5×10^{-3} $\pm.1 \times 10^{-3}$	9.1×10^{-3} $\pm 1.6 \times 10^{-3}$	-3.13 ±.07		-3.68[d]
	$a^4D_{5/2}$	4701.150	.028 ±.001	.16 ±.03	-1.66 ±.07		-2.09,[b] -.53,[c] -1.61[d]
	$a^4D_{3/2}$	4739.110	.270 ±.007	1.6 ±.2	-.66 ±.07		-1.07,[b] -.12,[c] -.66[d]
	$a^4D_{1/2}$	4761.527	.623 ±.008	3.7 ±.6	-.30 ±.07		-.42,[b] .03,[c] -.38[d]
	$a^4G_{5/2}$	5117.935	.075 ±.006	.44 ±.07	-1.16 ±.07		-.32,[c] -1.19[d]

Table 5 (Continued)

Upper Level	Lower Level	λ(Å)	BR	$A(10^7 sec^{-1})$	$\log_{10} gf$	Comments	Results of Others, $\log_{10} gf$
$z\,^4D^o_{7/2}$	$a\,^6D_{9/2}$	3483.084	$\leq 2.2 \times 10^{-3}$	$\leq 1.6 \times 10^{-2}$	≤ -2.63		$-.47^d$
	$a\,^6D_{7/2}$	3511.188	3.7×10^{-4} $\pm .3 \times 10^{-4}$	2.8×10^{-3} $\pm .5 \times 10^{-3}$	-3.39 $\pm .08$		$-.82^d$
	$a\,^4D_{7/2}$	4451.575	.772 $\pm .006$	5.8 $\pm .9$	.14 $\pm .07$		$.52,^a$ $.23,^b$ $.69,^c$ $-.20^d$
	$a\,^4D_{5/2}$	4502.223	.175 $\pm .004$	1.3 $\pm .2$	$-.50$ $\pm .07$		$-.13,^a$ $-.72,^b$ $.18,^c$ $-.68^d$
	$a\,^5P_{5/2}$	5388.538	7.6×10^{-3} $\pm .8 \times 10^{-3}$	.057 $\pm .010$	-1.70 $\pm .08$		-1.93^d
	$b\,^4D_{7/2}$	6491.697	.022 $\pm .002$	.17 $\pm .03$	-1.07 $\pm .08$		$-.29,^c$ -1.28^d
	$b\,^4D_{5/2}$	6519.381	.015 $\pm .001$	.11 $\pm .02$	-1.24 $\pm .08$		-2.04^d
	$b\,^4P_{5/2}$	8380.77	$< 2.6 \times 10^{-3}$	$< .02$	< -1.79		-2.23^d
	$a\,^4F_{9/2}$	9243.29	$< 5.8 \times 10^{-3}$	$< .044$	< -1.35		$-1.88,^d$ $-.77 \pm .13^e$
	$a\,^6S_{5/2}$	2184.912	$< 4 \times 10^{-3}$	$< .03$	< -2.76		$-.632^d$
$z\,^4D^o_{5/2}$	$a\,^6D_{7/2}$	3488.309	7.6×10^{-4} $\pm 1.5 \times 10^{-4}$	5.7×10^{-3} $\pm 1.4 \times 10^{-3}$	-3.20 $\pm .11$		-1.41^d
	$a\,^6D_{5/2}$	3509.067	$< 4.0 \times 10^{-4}$ $\pm .4 \times 10^{-4}$	$< 3.0 \times 10^{-3}$ $\pm .5 \times 10^{-3}$	< -3.47 $\pm .08$	blended in my spectrum, probably in b's also, who reports -3.16	-1.38^d

Table 5 (Continued)

Upper Level	Lower Level	λ(Å)	BR	$A(10^7 sec^{-1})$	$\log_{10}$ gf	Comments	Results of Others, $\log_{10}$ gf
	$a^6D_{3/2}$	3523.530	3.5×10^{-4} $\pm .4 \times 10^{-4}$	2.6×10^{-3} $\pm .5 \times 10^{-3}$	-3.53 ±.08		-1.55[d]
	$a^4D_{7/2}$	4414.887	.303 ±.008	2.3 ±.4	-.40 ±.07		-.51,[b] .34,[c] -.57[d]
	$a^4D_{5/2}$	4464.679	.421 ±.009	3.2 ±.5	-.25 ±.07		.28,[a] -.33,[b] .28,[c] -.40[d]
	$a^4D_{3/2}$	4498.897	.239 ±.007	1.8 ±.3	-.49 ±.07		-.05,[a] -.71,[b] .21,[c] -.53[d]
	$a^4P_{5/2}$	5334.872	6.8×10^{-4} $\pm .6 \times 10^{-4}$	5.1×10^{-3} $\pm .9 \times 10^{-3}$	-2.88 ±.08		-4.35[d]
	$a^4P_{3/2}$	5348.078	8.1×10^{-3} $\pm .7 \times 10^{-3}$	.061 ±.011	-1.81 ±.08		-1.90[d]
	$b^4D_{7/2}$	6413.947	4.2×10^{-3} $\pm .5 \times 10^{-3}$	.031 ±.006	-1.94 ±.08		-1.99[d]
	$b^4D_{5/2}$	6440.973	≤.014 ±.001	≤.10 ±.02	≤-1.42 ±.08	blended in my measurement, probably in c's also	-.44,[c] -1.36[d]
	$b^4D_{3/2}$	6443.511	5.8×10^{-3} $\pm .8 \times 10^{-3}$	.044 ±.009	-1.79 ±.09		-1.75[d]
	$a^4F_{7/2}$	9172.09	$< 5.5 \times 10^{-3}$	<.042	< -1.50		-1.86,[d] -.82±.12[e]
	$a^6S_{5/2}$	2176.014	<.013	<.092	< -3.41		-1.35[d]

Table 5 (Continued)

Upper Level	Lower Level	λ(Å)	BR	$A(10^7 sec^{-1})$	$\log_{10}$ gf	Comments	Results of Others, $\log_{10}$ gf
$z^4D^o_{3/2}$	$a^6D_{5/2}$	3491.548	1.5×10^{-4} $\pm .3 \times 10^{-4}$	1.1×10^{-3} $\pm .3 \times 10^{-3}$	-4.08 ±.11		-2.96[d]
	$a^6D_{3/2}$	3505.863	3.4×10^{-4} $\pm .4 \times 10^{-4}$	2.6×10^{-3} $\pm .5 \times 10^{-3}$	-3.72 ±.08		-2.68[d]
	$a^6D_{1/2}$	3514.330	$< 2.6 \times 10^{-4}$	$< 2.0 \times 10^{-3}$	< -3.83		-2.27[d]
	$a^4D_{5/2}$	4436.358	.415 ±.007	3.1 ±.5	-.43 ±.07		-.08,[a] .17,[c] -.52[d]
	$a^4D_{3/2}$	4470.142	.297 ±.006	2.2 ±.3	-.57 ±.07		-.07,[a] -.82,[b] .15,[c] -.70[d]
	$a^4D_{1/2}$	4490.078	.251 ±.008	1.9 ±.3	-.64 ±.07		-.27,[a] -.97,[b] .09,[c] -.69[d]
	$a^4P_{1/2}$	5317.082	4.4×10^{-3} $\pm .5 \times 10^{-3}$	.033 ±.006	-2.26 ±.08		-2.27[d]
	$b^4D_{5/2}$	6382.196	8.1×10^{-3} $\pm 1.5 \times 10^{-3}$	.061 ±.015	-1.83 ±.11		-1.78[d]
	$b^4D_{3/2}$	6384.686	.014 ±.001	.11 ±.02	-1.58 ±.08		-.78,[c] -1.61[d]
	$b^4D_{1/2}$	6378.969	7.6×10^{-3} $\pm .7 \times 10^{-3}$	.057 ±.010	-1.86 ±.08		-1.82[d]
	$a^4F_{5/2}$	9114.02	$< 4.2 \times 10^{-3}$	< 0.32	< -1.80		-1.99,[d] -1.22±.17[e]

Table 5 (Concluded)

Upper Level	Lower Level	λ(Å)	BR	A(10^7 sec^{-1})	$\log_{10}$ gf	Comments	Results of Others, $\log_{10}$ gf
$z\,^4D^o_{3/2}$	$a\,^6D_{1/2}$	3503.727	4.5×10^{-3} $\pm .4 \times 10^{-3}$	.034 ±.006	-2.91 ±.08		-3.74[d]
	$a\,^4D_{3/2}$	4453.013	.541 ±.009	4.1 ±.6	-.62 ±.07		-.20,[a] -.86,[b] .06,[c] -.70[d]
	$a\,^4D_{1/2}$	4472.793	.419 ±.009	3.2 ±.5	-.72 ±.07		-.28,[a] -1.15,[b] -.02,[c] -.79[d]
	$a\,^4P_{3/2}$	5283.407	3.0×10^{-4} $\pm .4 \times 10^{-4}$	2.2×10^{-3} $\pm .4 \times 10^{-3}$	-3.73 ±.08		
	$a\,^4P_{1/2}$	5292.869	1.8×10^{-3} $\pm .2 \times 10^{-3}$	.014 ±.002	-2.94 ±.08		-2.74[d]
	$b\,^4D_{3/2}$	6349.795	.015 ±.001	.11 ±.02	-1.86 ±.08		-1.86[d]
	$b\,^4D_{1/2}$	6344.133	.016 ±.002	.12 ±.02	-1.85 ±.08		-1.80[d]
	$a\,^4F_{3/2}$	9084.29	$< 5.1 \times 10^{-3}$	<.039	< -2.02		-2.18,[d] -1.18 ±.24[e]

Table 6

Experiments by others. This table describes experiments by other workers who have measured transition probabilities for some of the same Mn I lines listed in this work. All of these experiments yielded sets of relative transition probabilities which were normalized to the absolute transition probabilities of the workers mentioned in column 5. In columns 4 and 5, I refers to the intensity of the spectral line in emission, λ to the wavelength of the line and E_u to the energy of the upper level of the line. Refer to pages 33 and 54.

Table 6

Experimenters	Light Source	Detector and Calibration	Temperature Determination	Absolute gf's Used to Normalize Scale	$\sigma_{\log gf}$
Allen and Asaad (1957)	d.c. arc in air Cu electrodes with Mn as impurity concentration of Mn < .05%	film calibrated with C arc, tungsten filament lamp and Fe arc and King and King (1938) relative gf values	plot log $(I\lambda^3/gf)$ vs E_u for lines of Fe, Ni, Cr, Mn and Co Co and Fe results used to determine T with Co and Fe used King et al. (1955) and King and King (1938) relative gf values, respectively T = 4300°K	Huldt and Lagerqvist (1952) and Bell et al. (1959) values for lines at 4030, 4033 and 4034 Å	0.2
Corliss and Bozman (1962)	d.c. arc in air Cu electrodes with Mn as impurity with 1 atm Mn per 1000 atoms of Cu	film calibrated with tungsten filament lamp and H arc lamp	plot log $(gf/I\lambda^3)$ vs. E_u 31 sets of relative gf's from 5 laboratories for 20 elements were used T = 5100 ± 110°K	Normalization function $C = (gf_{absolute}/I\lambda^3) \times (Np/u)\exp(-E/kT)$ computed for many elements using many published sets of $gf_{absolute}$. p = persistence of atoms in arc relative to that of Cu atoms u = partition function average C over 20 elements to normalize scale Bell et al. (1959) absolute gf of 4030 Å line for Mn I	relative gf's .13-.17 absolute gf's .24-.29

Table 6 (Concluded)

Experimenters	Light Source	Detector and Calibration	Temperature Determination	Absolute gf's Used to Normalize Scale	$\sigma_{\log gf}$
Woodgate (1966)	d.c. rotating walled arc with C electrodes wall was tube of sintered SiO_2 and Mn_3O_4 wall composition of 1%, 10%, 20% Mn_3O_4 used	film calibrated with C arc characteristic curve found with free-burning Fe arc and step wedge	emission-absorption method: lines measured in emission, then in absorption of continuum from flash tube coaxial with arc plot $\ell n(I/W\bar{\upsilon}^5)$, which $= C' - \frac{hc\bar{\upsilon}}{kT}$, vs $\bar{\upsilon}$, where $\bar{\upsilon} = 1/\lambda$, W = equivalent width of line in absorption, C' = constant slope of line gives T T = 8240 - 8830° = for the spectra studied	Penkin (1964) gf's for 3216, 3224 Å lines	.03-.09
Hefferlin and Gearhart (1964)	d.c. arc in air fused Mn rods as electrodes	cooled (dry ice) 7102 PMT calibrated with tungsten filament lamp	plot log $(I\lambda^3/gf)$ vs. E_u for different zones of arc and take average several references used for relative gf's with which to determine T T = 5340 ±50°K	Corliss and Bozman gf's for 14 lines at $\lambda > 6900$ Å	.12-.24

Table 7

Solar abundance results. The wavelengths are from Catalan et al. (1964). The equivalent widths (W) are from the Preliminary Edition of the Kitt Peak Solar Atlas (KP) and from Moore et al. (1966) (CM). Log C has been calculated from the parameters of Goldberg and Pierce (1959) for the model atmosphere of GMA (1960), the excitation energy of the lower level of the line and the measured gf of the transition. Refer to pages 60, 66 & 67.

λ(Å)	Upper Level	Lower Level	W_{KP}(mÅ)	W_{CM}(mÅ)	log gf	log C	log (W_{KP}/λ)	log (W_{CM}/λ)	A_{Mn}(KP)	A_{Mn}(CM)
5004.891	$z^6F^o_{7/2}$	$a^4D_{5/2}$	14.3	14	-1.66	0.98	-5.54	-5.55	5.48	5.47
5029.779	$z^6F^o_{5/2}$	$a^4D_{3/2}$		12	-1.91	0.71		-5.62		5.67
5260.771	$z^4F^o_{9/2}$	$a^4G_{9/2}$	7.69	3.5	-2.01	0.42	-5.83	-6.18	5.75	5.40
4671.688	$z^4F^o_{5/2}$	$a^4D_{7/2}$	12.92	11	-1.69	0.97	-5.56	-5.63	5.47	5.40
5388.538	$z^4D^o_{7/2}$	$a^4P_{5/2}$	4.92	5	-1.70	0.50	-6.04	-6.03	5.46	5.47
5348.078	$z^4D^o_{5/2}$	$a^4P_{3/2}$	2.89	4.5	-1.81	0.36	-6.27	-6.08	5.37	5.57
5317.082	$z^4D^o_{3/2}$	$a^4P_{1/2}$		3.5	-2.26	-0.05		-6.18		5.89

A_{Mn}(KP) (with 5260.771 included in average) = 5.51 ± .14

A_{Mn}(KP) (without 5260.771) = 5.44 ± .05

A_{Mn}(CM) (with 5260.771) = 5.55 ± .18

A_{Mn}(CM) (without 5260.771) = 5.58 ± .18

Table 8

Lines not identified as Mn I in Moore et al. (1966). λ_{Cat} is the wavelength of an Mn I line listed in Catalan et al. (1964). ID_{Cat} is the transition which Catalan et al. associate with the line. λ_{CM} is the wavelength of a line in Moore et al., and ID_{CM} is the atom or molecule which Moore et al. list as producing that line. W is the equivalent width of the line in mÅ. In the column "Source of W" CM refers to Moore et al., KP to widths measured from the Kitt Peak atlas by spectrum synthesis and KP-sq to widths measured from the Kitt Peak atlas by our counting squares contained by a tracing of the line. A_{Mn} is the abundance of manganese calculated for each line. Refer to pages 67 and 87.

λ_{Cat}	ID_{Cat}	λ_{CM}	ID_{CM}	W	Source of W	A_{Mn}
4987.066	$a^4D_{5/2}$-$z^6F^o_{5/2}$	4987.085	—	1.5	CM	5.89
7174.420	$b^4D_{7/2}$-$z^4F^o_{9/2}$	7174.45	Mn I?	3	CM	6.26
6413.947	$b^4D_{7/2}$-$z^4D^o_{5/2}$	6413.932	CN	1.94	KP	5.60
6443.511	$b^4D_{3/2}$-$z^4D^o_{5/2}$	6443.55	Atm H_2O	3.32	KP	5.67
6349.795	$b^4D_{3/2}$-$z^4D^o_{1/2}$	6349.75	—	4.5 2.9	CM Kp-sq	5.91 5.72
6378.969	$b^4D_{1/2}$-$z^4D^o_{3/2}$	6378.953	—	1.5 2.5	CM Kp-sq	5.42 5.64
6382.195	$b^4D_{5/2}$-$z^4D^o_{3/2}$	—	—	2.6	Kp-sq	5.63

Table 9

Comparison of wavelengths listed in Moore et al. (1966) and Catalan et al. (1964) for Mn I lines. These are the lines among those for which we have measured gf's which are unblended enough in the Utrecht atlas (Minnaert et al. (1940) to make an accurate determination of wavelength straightforward. λ_{Cat} is the wavelength listed in Catalan et al. λ_{CM} is the wavelength listed in Moore et al. Refer to pages 67 and 87-90.

λ_{Cat}(Å)	λ_{CM}(Å)	$\lambda_{CM}-\lambda_{Cat}$(mÅ)	Upper Level
3823.508	3823.514	+6	$z^6F^o_{9/2}$
5004.891	5004.894	+3	$z^6F^o_{7/2}$
5029.779	5029.815	+36	$z^6F^o_{5/2}$
3816.746	3816.745	-1	$z^6F^o_{3/2}$
3839.779	3839.785	+6	$z^6F^o_{1/2}$
3701.728	3701.729	+1	$z^4F^o_{9/2}$
4762.376	4762.375	-1	
5255.330	5255.325	-5	
3669.837	3669.839	+2	$z^4F^o_{7/2}$
3692.817	3692.816	-1	
4709.710	4709.718	+8	
4766.426	4766.423	-3	
4671.688	4671.687	-1	$z^4F^o_{5/2}$
4765.856	4765.864	+8	
4739.110	4739.113	+3	$z^4F^o_{3/2}$
4761.527	4761.528	+1	
5117.935	5117.942	+7	
4451.575	4451.588	+13	$z^4D^o_{7/2}$
4502.223	4502.221	-2	
5388.538	5388.504	-34	
4498.897	4498.900	+3	$z^4D^o_{5/2}$
5348.078	5348.070	-8	

Table 9 (Concluded)

λ_{Cat}(Å)	λ_{CM}(Å)	$\lambda_{CM}-\lambda_{Cat}$(mÅ)	Upper Level
4436.358	4436.356	-2	$z\,^4D^o_{3/2}$
4470.142	4470.138	-4	
4453.013	4453.006	-7	$z\,^4D^o_{1/2}$

$\lambda_{CM}-\lambda_{Cat} = 1.1 \pm 11.3$ mÅ averaged over 25 lines

Table 10

Nucleosynthesis results: theory and observation. The A_{Mn} value used is the result of this thesis work. The values for iron and nickel have been taken from the table of Ross and Aller (1976). In column 3, T_9 is the temperature in °K divided by 10^9. ρ is the density in g/cc. η is the neutron excess, (N-Z)/(N+Z), where N and Z are the total numbers of neutrons and protons, respectively. EOB stands for Explosive Oxygen Burning. ESB stands for Explosive Silicon Burning. In the last column $L_i(o)$ stands for the observed L_i while $L_i(c)$ is the L_i calculated from the theory. Refer to pages 73 & 75.

Authors	Date	Process	$L_1 = \log\left(\frac{N_{Fe}}{N_{Mn}}\right)$	$L_2 = \log(N_{Fe}/N_{Ni})$	$L_3 = \log(N_{Ni}/N_{Mn})$	$\sqrt{\sum_{i=1}^{3} [L_i(o) - L_i(c)]^2}$
this work (Mn) and Ross and Aller (Fe, Ni)	1978 1976	observed	2.06 ± .14	1.22 ± .12	0.84 ± .14	
Burbidge et al.	1957	e process $T_9 = 3.78$ $\rho \sim 10^5$ $\eta = .07$	1.20	0.87	0.33	1.06
Woosley et al.	1973	composite of equal parts by mass of EOB, ESB and e process ($\eta = .002$, $T_9 = 5.5$, $\rho = 2\times10^7$) with α-rich freeze-out	2.45	1.34	1.11	0.49
Hainebach et al.	1974	two zone e process $T_9 = 5$, $\rho = 5\times10^7$, .966 of nucleons in $\eta = .0037$ zone .034 of nucleons in $\eta = .0769$ zone	1.85	1.66	0.19	0.81
Trimble	1975	combination of C burning, EOB, ESB, e processes with α-rich and α-poor freeze-out	1.94	1.41	0.53	0.38

Figure 1

Schematic diagram of the beam path and apparatus used in the measurement of lifetimes of excited states of atoms by beam-foil spectroscopy. The RCA 8575 monitors the beam current passing through the foil. When the integrated current from the 8575 reaches a preset amount, a pulse from the current integrator moves the beam stop into the beam path and stops counting by the timing scaler and the photon-counting scaler. Refer to pages 14 and 17.

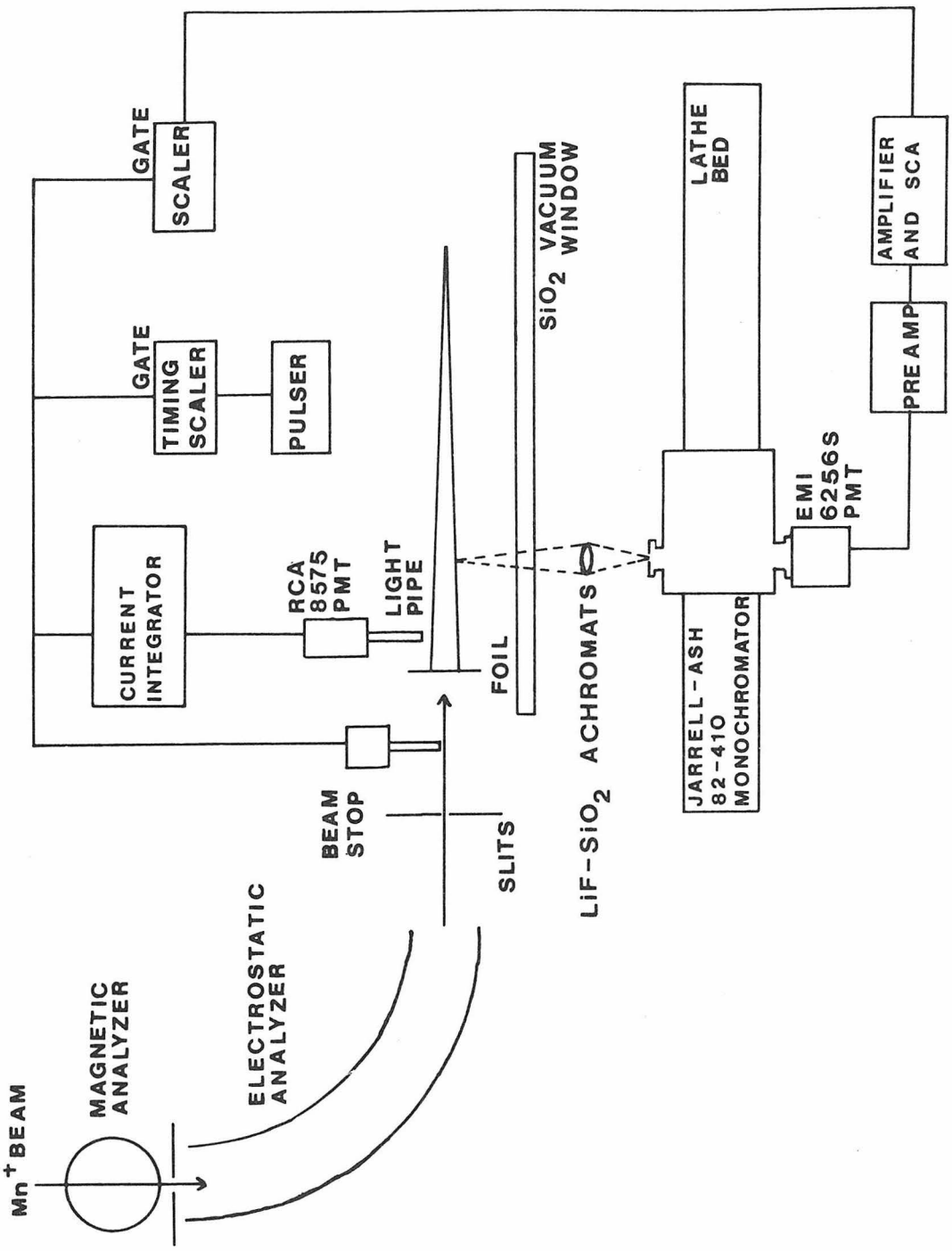
Mn+ BEAM
MAGNETIC ANALYZER
ELECTROSTATIC ANALYZER
BEAM STOP
SLITS
LiF-SiO2 ACHROMATS
FOIL
LIGHT PIPE
RCA 8575 PMT
CURRENT INTEGRATOR
GATE
TIMING SCALER
PULSER
GATE
SCALER
SiO2 VACUUM WINDOW
JARRELL-ASH 82-410 MONOCHROMATOR
LATHE BED
EMI 6256S PMT
PREAMP
AMPLIFIER AND SCA

Figure 2

Furnace of the ion source in the 2MV Van de Graaff terminal. The heating coil, another .025" diameter tungsten wire coil, is not shown. Electrons are emitted from the filament, accelerated by an electric field between the filament and the wall of the furnace and strike atoms of manganese vapor, ionizing some of them. The ions are accelerated through the hole in the bottom of the furnace. Refer to page 14.

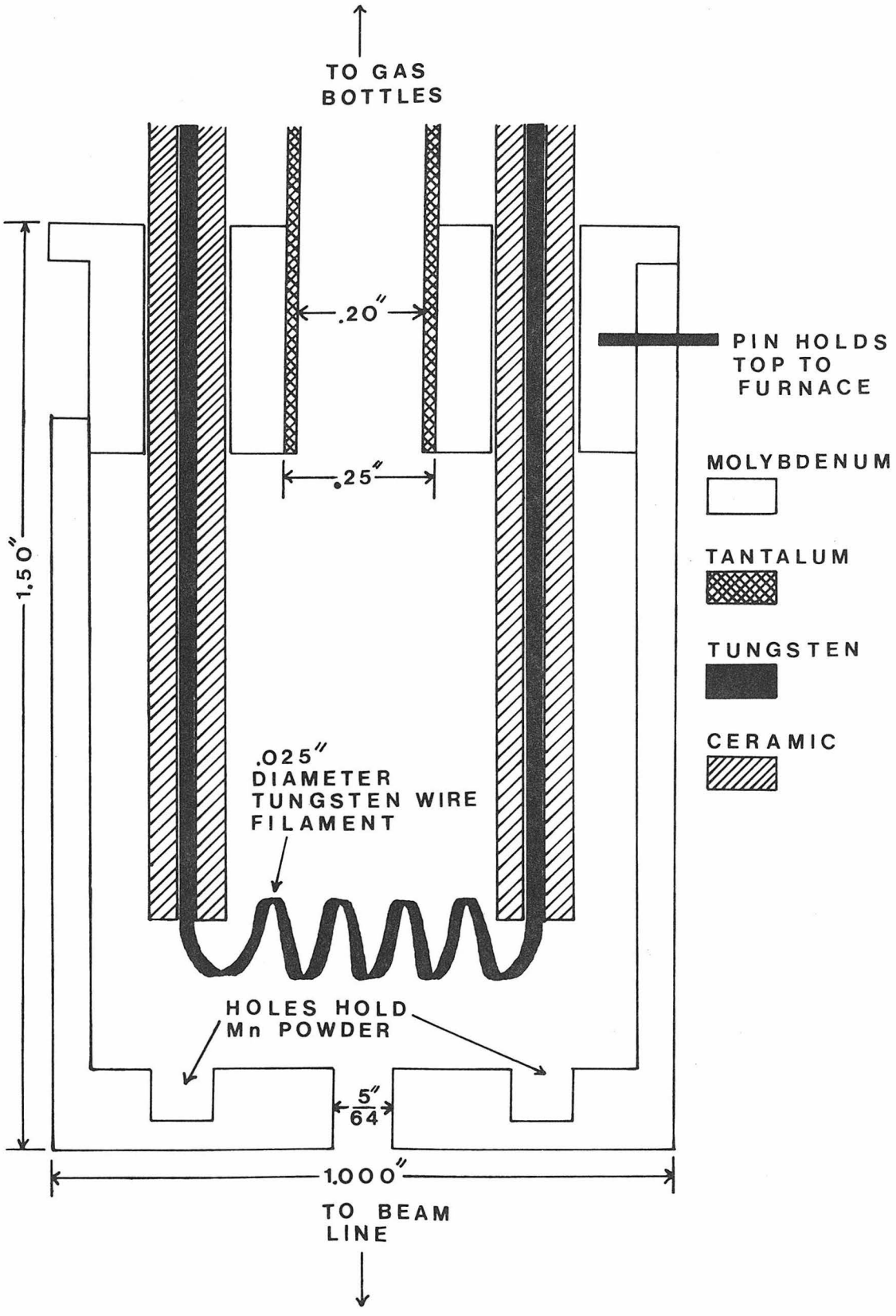
TO GAS BOTTLES
.20″
.25″
1.50″
PIN HOLDS TOP TO FURNACE
MOLYBDENUM
TANTALUM
TUNGSTEN
CERAMIC
.025″ DIAMETER TUNGSTEN WIRE FILAMENT
HOLES HOLD Mn POWDER
5/64″
1.000″
TO BEAM LINE

Figure 3

Sketch of the optical path of the Jarrell-Ash 82-410 .25 m Ebert monochromator. Refer to page 16.

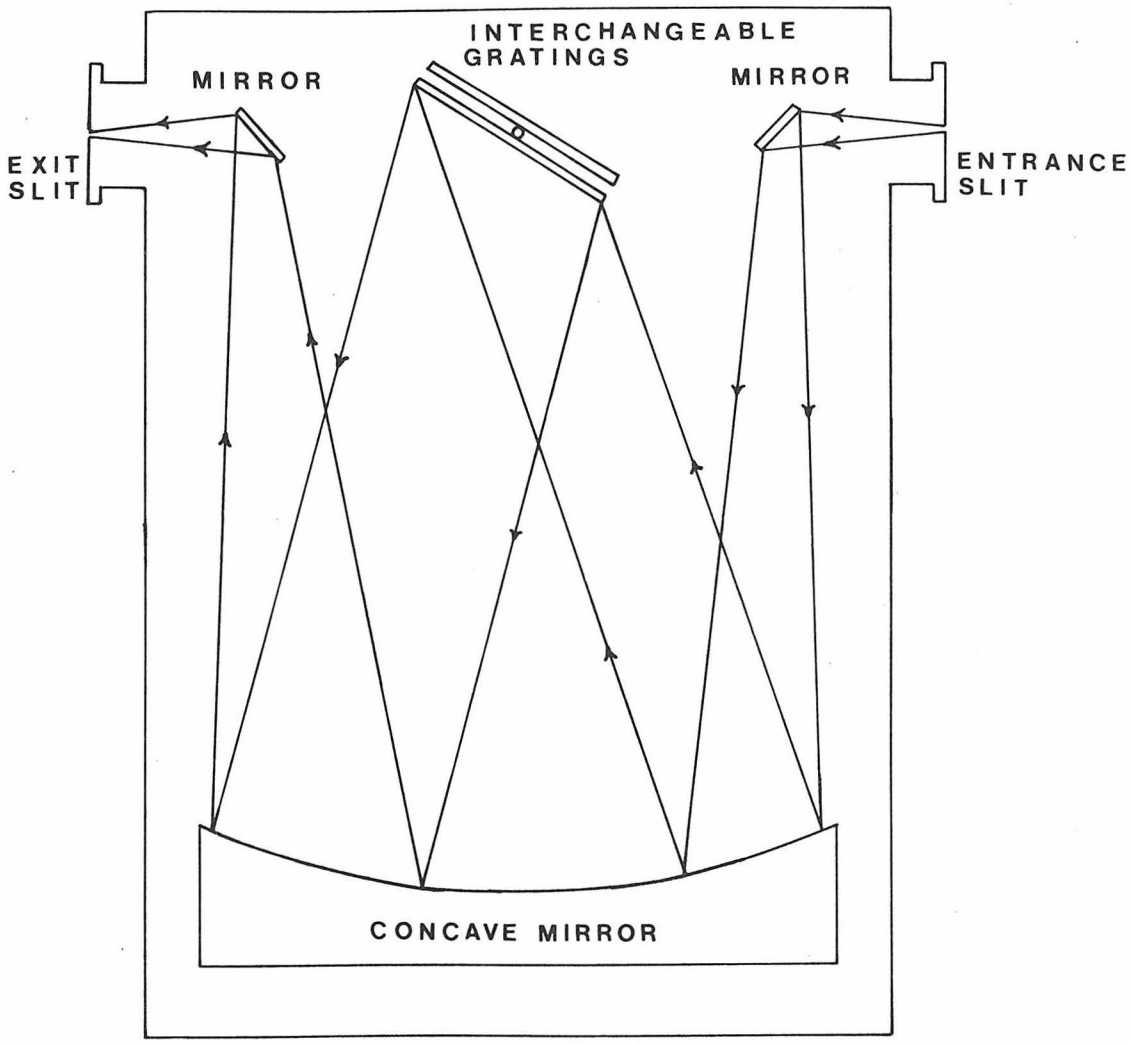
INTERCHANGEABLE
GRATINGS
MIRROR
MIRROR
EXIT
SLIT
ENTRANCE
SLIT
CONCAVE MIRROR

Figure 4

Light decay curve for lifetime measurement. The line used was at 3806.715 Å (upper level $z^6F^o_{11/2}$) and was blended with 3809.593 (upper level $z^6F^o_{7/2}$). The beam-dependent background readings were made at 3975 Å. The incident beam energy was 512 keV. The foil thickness was 10 $\mu g/cm^2$, and 150 μ slits were used with the 2360 grooves/mm grating. This combination of grating and slits gave an instrumental full width at half maximum of 2.8 Å. The Doppler width is 3.05 Å. The small dots are counts at 3807 Å. The squares are counts at 3795 Å. The lifetime calculated from this decay curve was 19.26 ± 1.16 ns. Refer to pages 18 and 26.

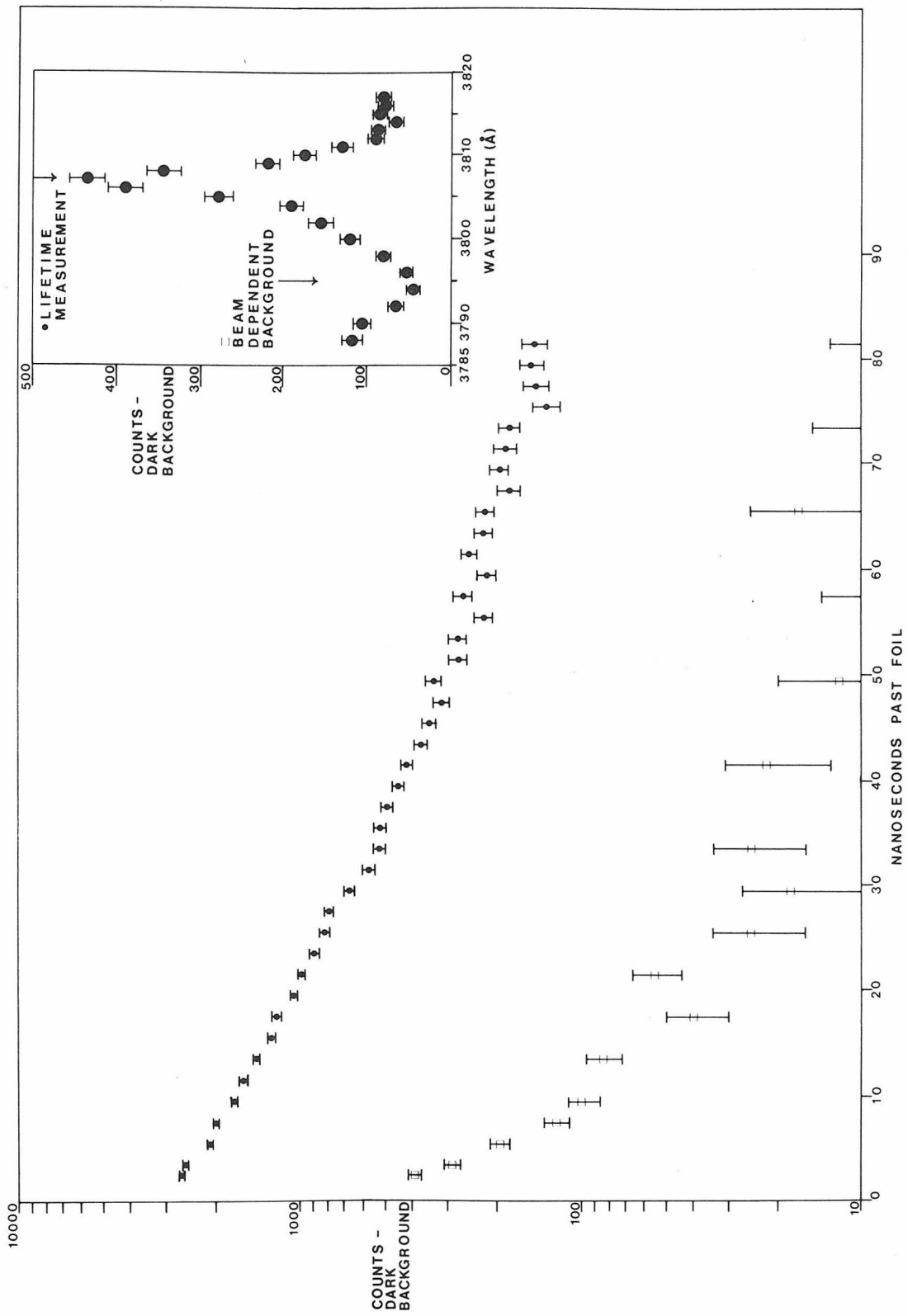
• LIFETIME MEASUREMENT
□ BEAM DEPENDENT BACKGROUND
COUNTS - DARK BACKGROUND
WAVELENGTH (Å)
3785 3790 3800 3810 3820
0 100 200 300 400 500
10000 1000 100 10
0 10 20 30 40 50 60 70 80 90
NANOSECONDS PAST FOIL

Figure 5

Results of total intensity measurements to test the equality of lifetimes of levels within a term. Since all of the strongest lines from upper levels of the same term were within a 40 Å region, there was no need to correct the signal $s_{u\ell}$ for filter transmission or spectrometer response. The error bars correspond to the spread in the day's measurements of s/M values for each line. The slopes of the lines correspond to temperatures of 1424 ± 128°K (z^6F^o), 5308 ± 1293°K (z^4F^o) and 5156 ± 1146°K (z^4D^o). Refer to page 32.

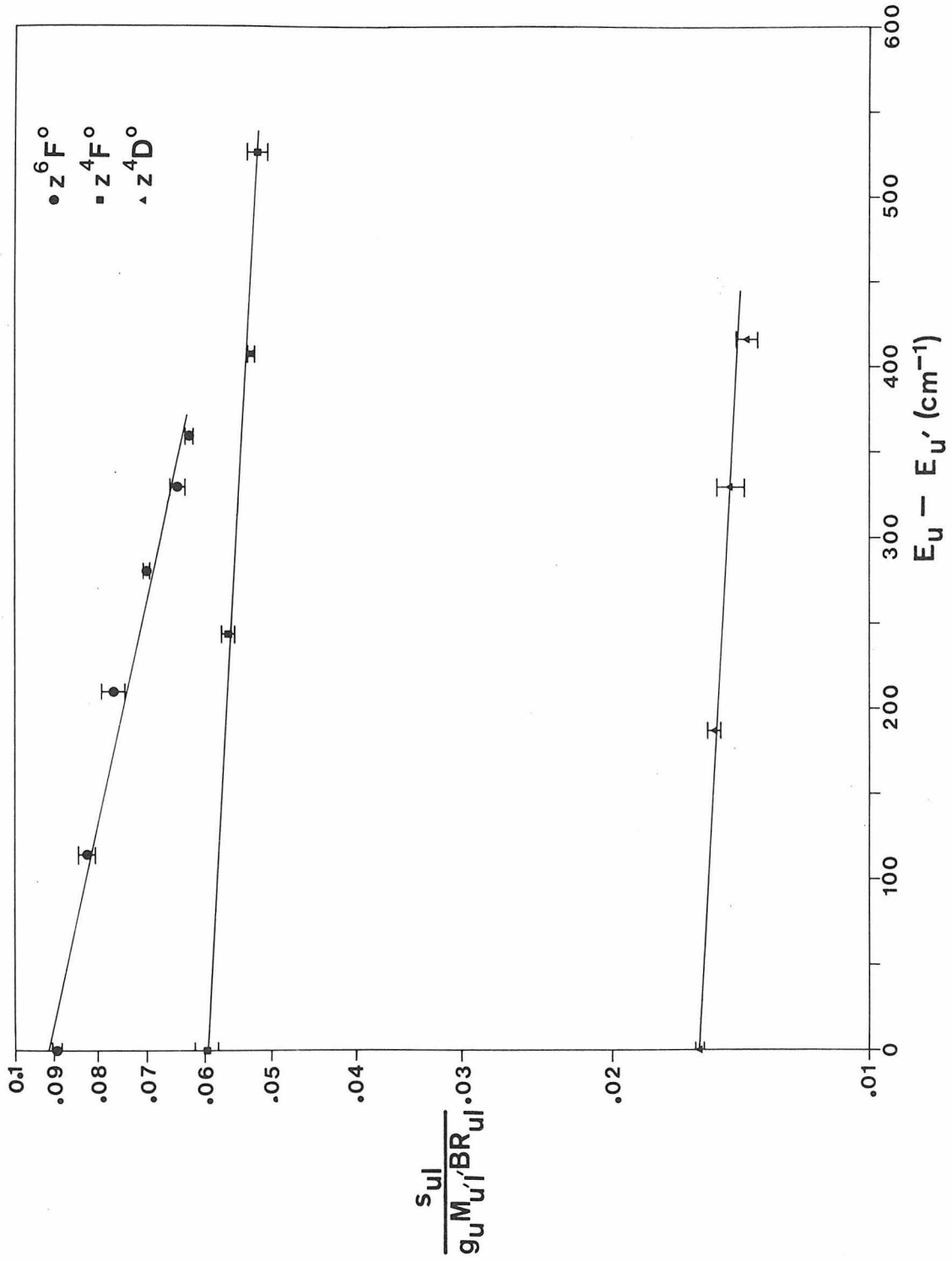
• z ^{6}F°
▪ z ^{4}F°
▲ z ^{4}D°
$\frac{S_{ul}}{g_u M_{u'l'} BR_{ul}}$
$E_u - E_{u'}$ (cm^{-1})
.1
.09
.08
.07
.06
.05
.04
.03
.02
.01
0
100
200
300
400
500
600

Figure 6

The hollow cathode light source. The tube which feeds the carrier gas into the source is not shown. Refer to page 35.

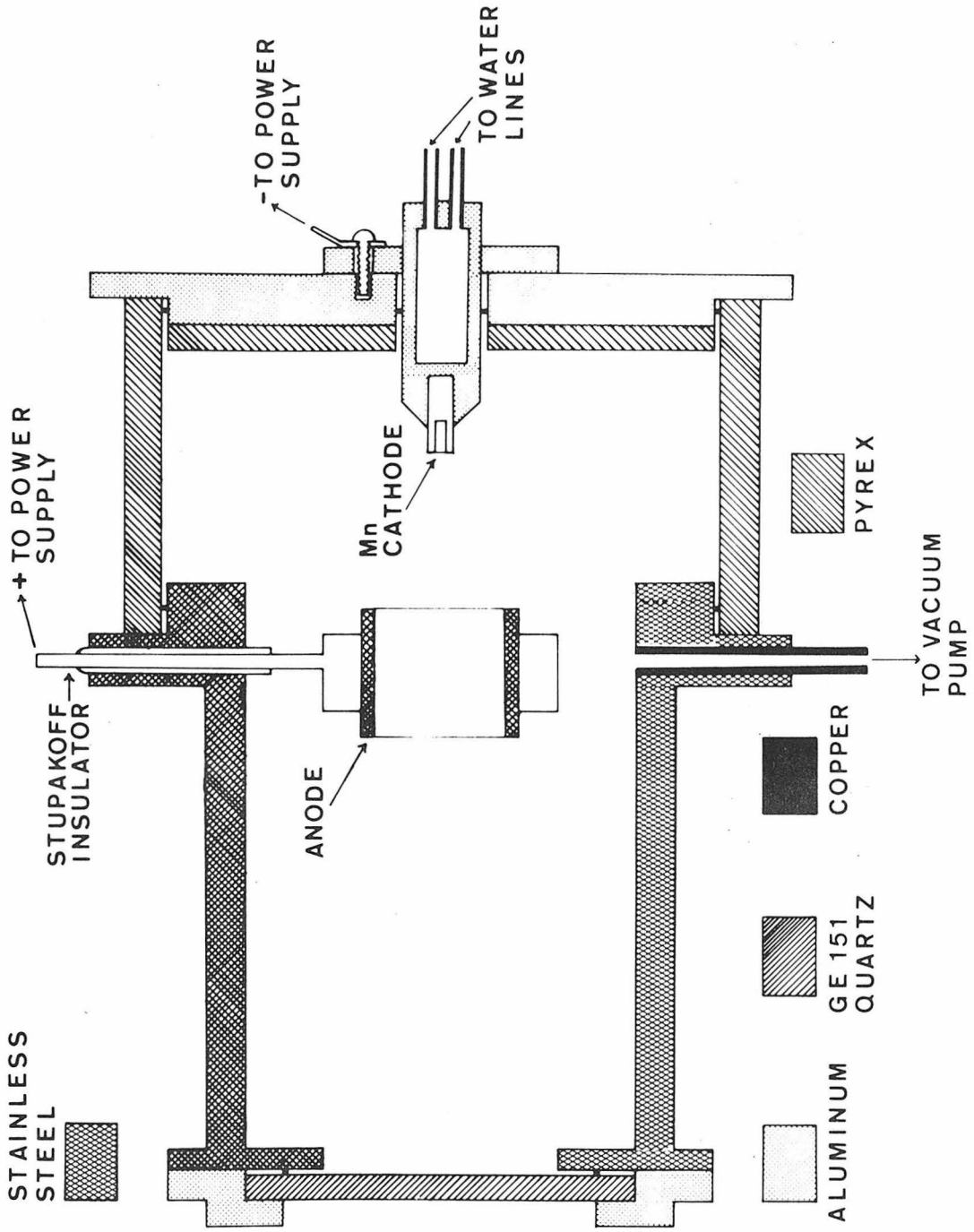
-TO POWER SUPPLY
TO WATER LINES
+ TO POWER SUPPLY
Mn CATHODE
PYREX
STUPAKOFF INSULATOR
ANODE
TO VACUUM PUMP
COPPER
GE 151 QUARTZ
STAINLESS STEEL
ALUMINUM

Figure 7

The Paschen-Runge spectrometer with the north slit as the entrance slit. The entrance slit usually used was 50 μ × 1 mm, but a 25 μ × 1 mm slit was sometimes used to resolve closely-spaced lines. The scan channel usually used was a refrigerated EMI 9783B photomultiplier. The monitor channel was an unrefrigerated EMI 9783B. Refer to pages 37 and 104.

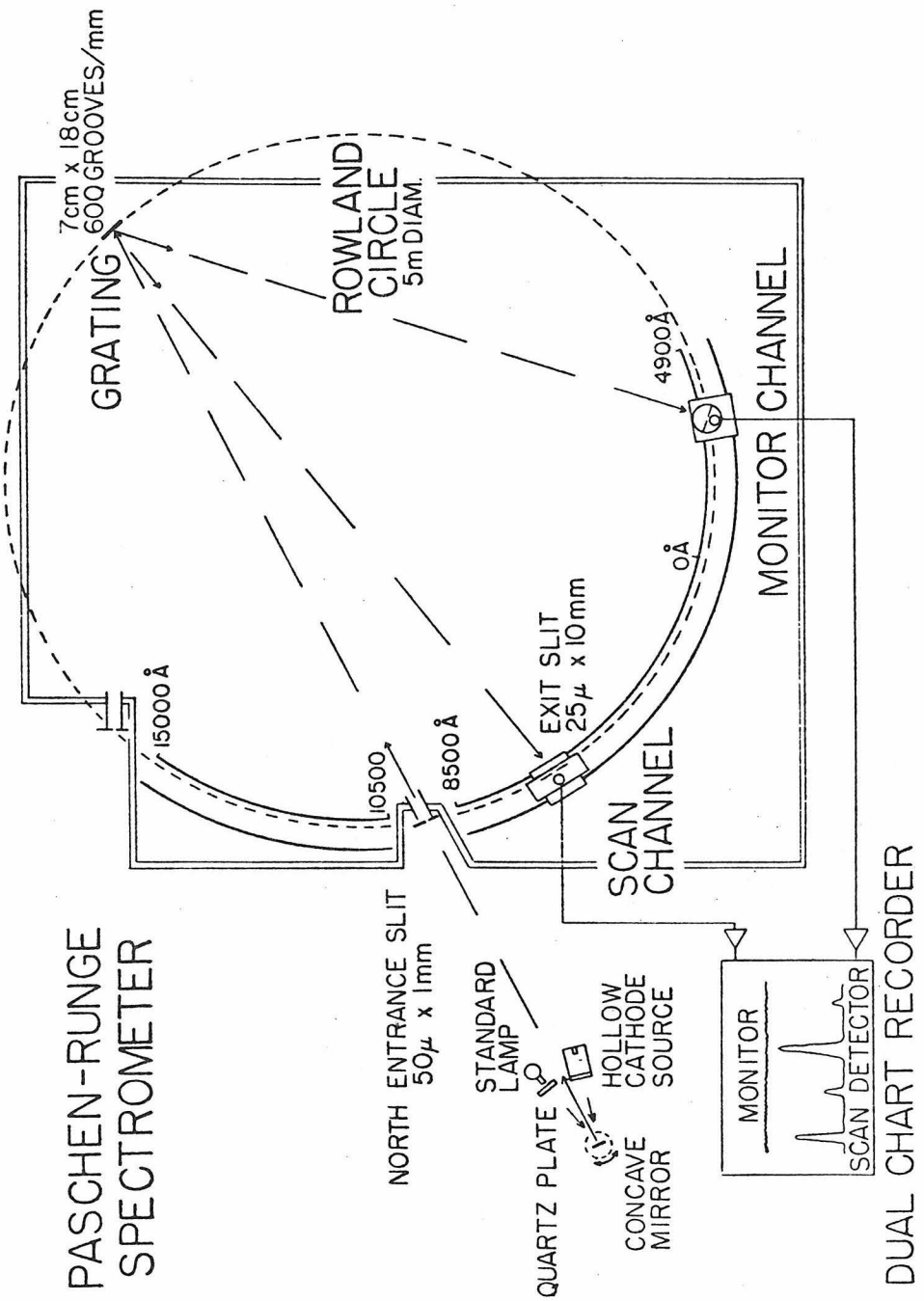
PASCHEN-RUNGE SPECTROMETER
7cm x 18cm 600 GROOVES/mm
GRATING
ROWLAND CIRCLE 5m DIAM.
15000 Å
10500
8500 Å
NORTH ENTRANCE SLIT 50μ x 1mm
EXIT SLIT 25μ x 10mm
0Å
4900Å
SCAN CHANNEL
MONITOR CHANNEL
STANDARD LAMP
QUARTZ PLATE
HOLLOW CATHODE SOURCE
CONCAVE MIRROR
MONITOR
SCAN DETECTOR
DUAL CHART RECORDER

Figure 8

The Paschen-Runge spectrometer with the south slit as the entrance slit. Refer to pages 38 and 105.

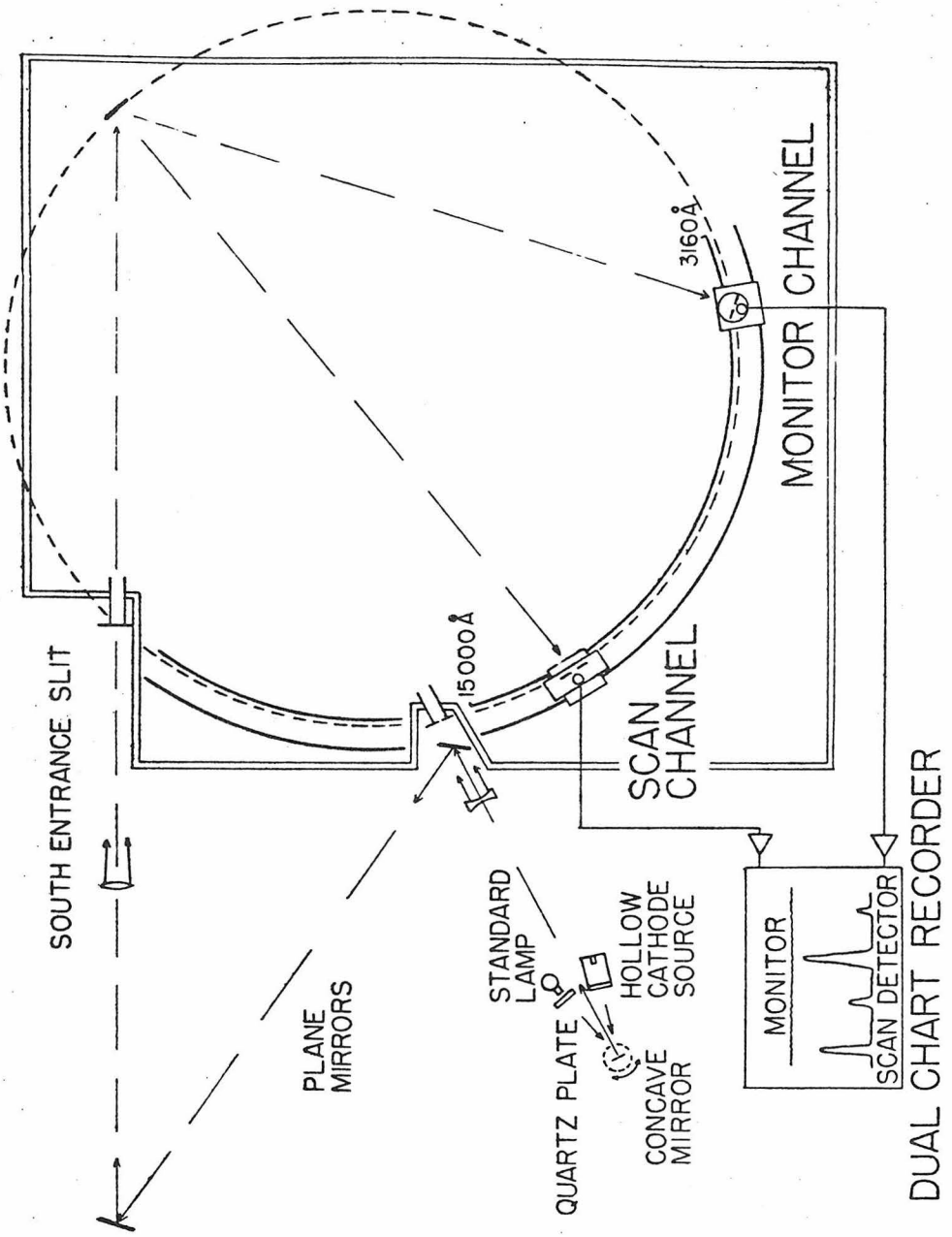
SOUTH ENTRANCE SLIT
PLANE MIRRORS
15000Å
3160Å
SCAN CHANNEL
MONITOR CHANNEL
STANDARD LAMP
HOLLOW CATHODE SOURCE
QUARTZ PLATE
CONCAVE MIRROR
MONITOR
SCAN DETECTOR
DUAL CHART RECORDER

Figure 9

Rapid (10 Å/min scanning speed, 1 min/inch chart speed) scan of the spectrum from 3844 Å to 3806 Å. The light source was the hollow cathode discharge, the cathode being an aluminum cathode with manganese powder placed in the cavity. The carrier gas was helium. Refer to page 39.

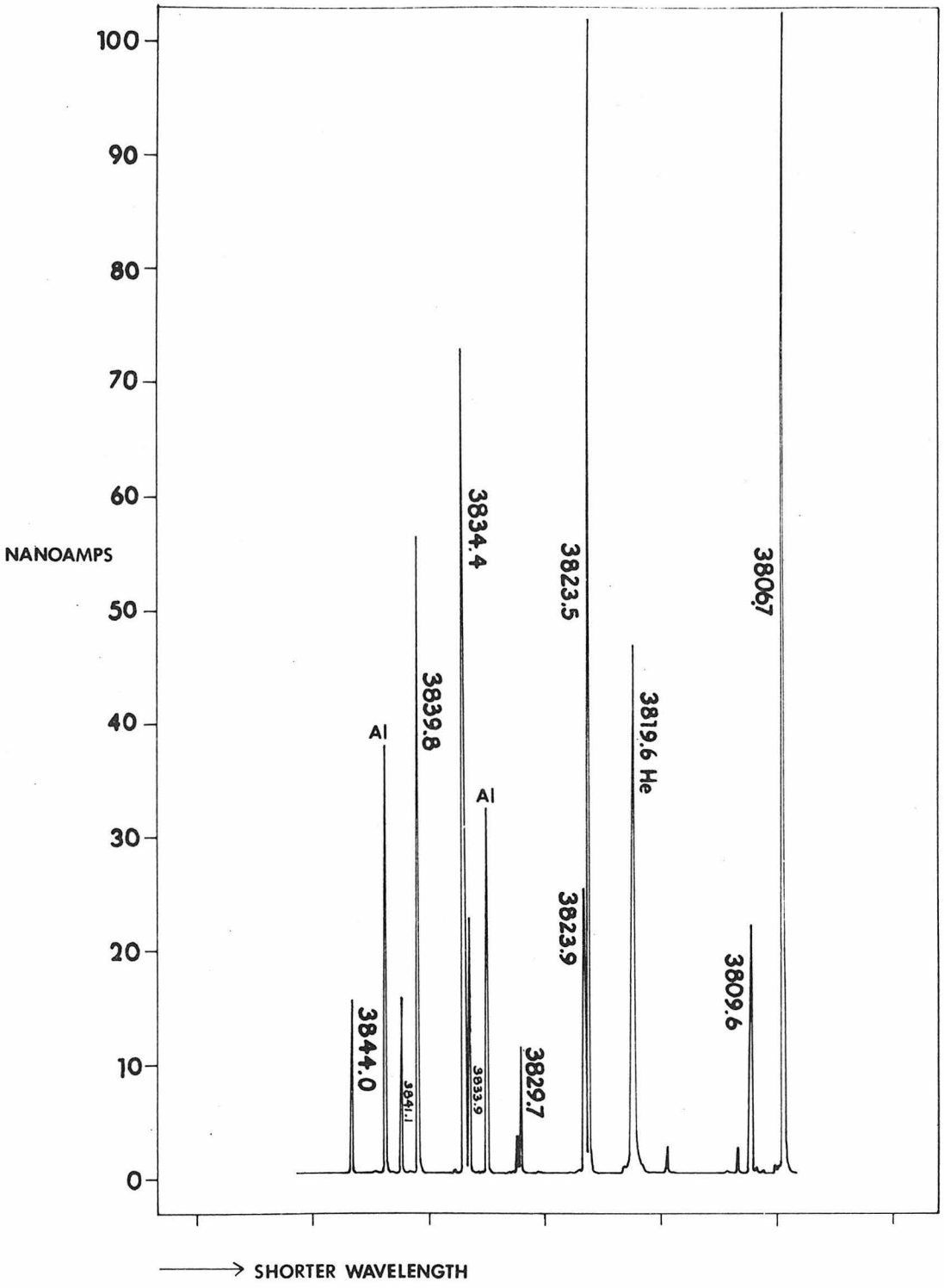
100
90
80
70
60
50
40
30
20
10
0
NANOAMPS
3844.0
Al
3841.1
3839.8
3834.4
3833.9
Al
3829.7
3823.9
3823.5
3819.6 He
3809.6
3806.7
SHORTER WAVELENGTH

Figure 10

Slow scan over the $z^6F^o_{11/2}$ 3806.715 Å line. The scanning speed was 1 Å/min, and the chart speed was 20 sec/inch. The monitor channel was set at the peak of the same line. A 10% neutral density filter was placed in front of the scan channel to keep the signal below 100 na. The observed full width at half maximum agrees well with theoretical FWHM calculated from the entrance slit width (nominally 50 μ, actually 43.8 ± 1.2 μ) and the reciprocal dispersion of the spectrometer in Å/mm. Refer to pages 40 and 42.

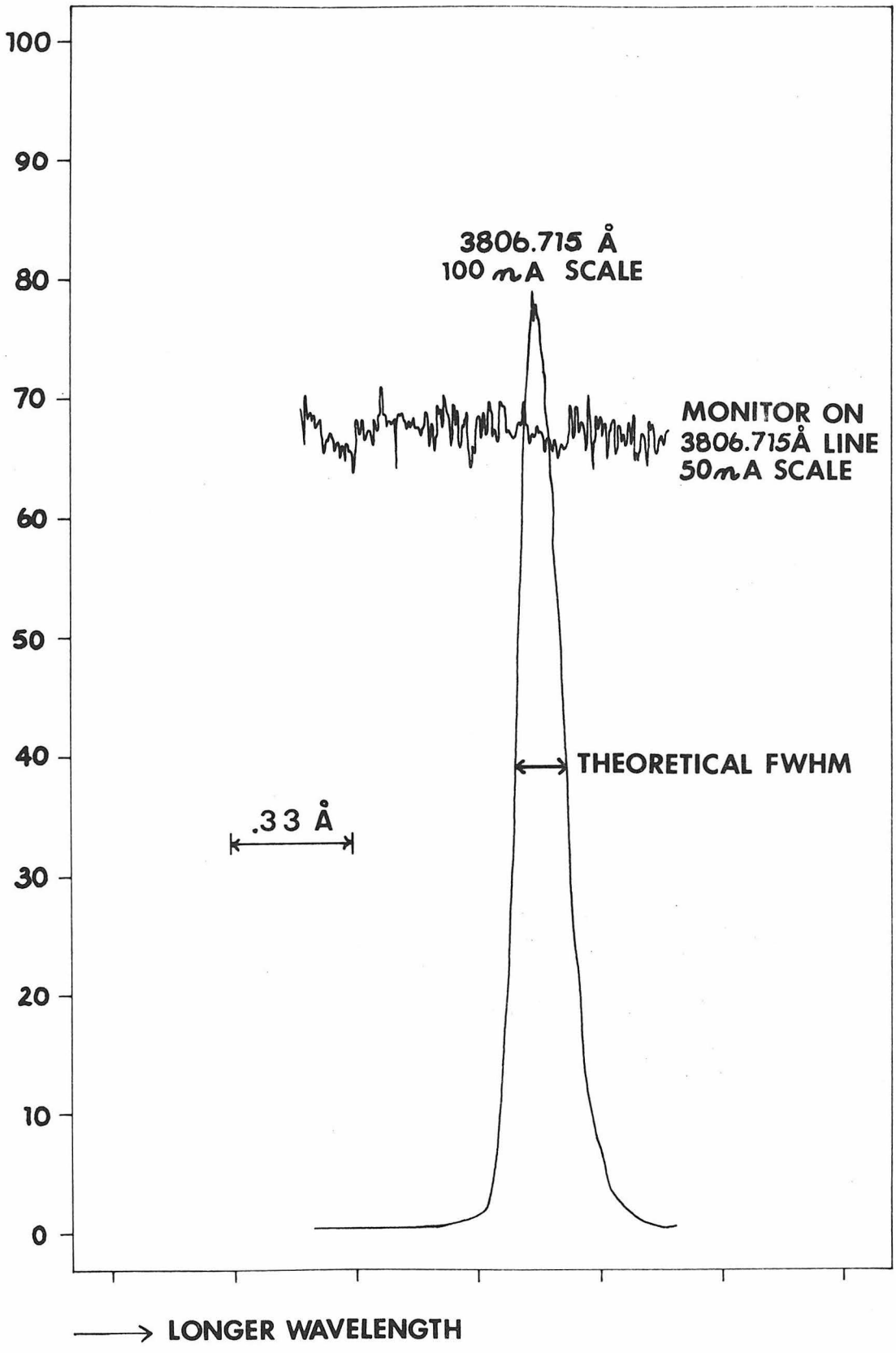
100
90
80
70
60
50
40
30
20
10
0
3806.715 Å
100 mA SCALE
MONITOR ON
3806.715Å LINE
50mA SCALE
THEORETICAL FWHM
.33 Å
LONGER WAVELENGTH

Figure 11

Comparison with respect to wavelength of the transition probabilities of Corliss and Bozman (CB 1962) and Woodgate (1966) with those of this thesis. Refer to page 56.

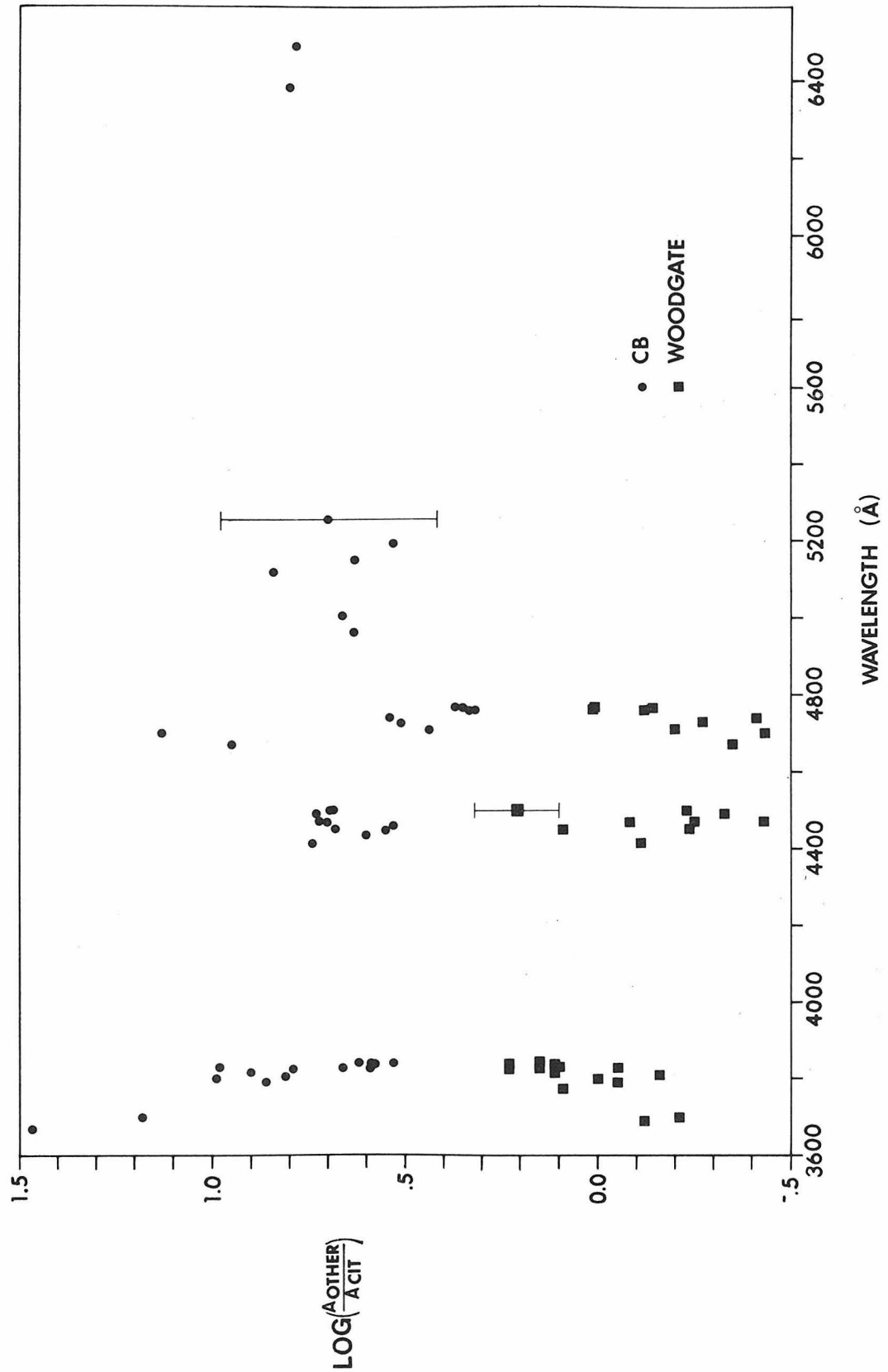
1.5
1.0
.5
0.0
-.5
3600
4000
4400
4800
5200
5600
6000
6400
WAVELENGTH (Å)
CB
WOODGATE
LOG(A OTHER / A CIT)

Figure 12

Comparison with respect to wavelength of the transition probabilities of Kurucz and Peytremann (1975) and Allen and Asaad (AA 1957) with those of this thesis. Refer to pages 56-57.

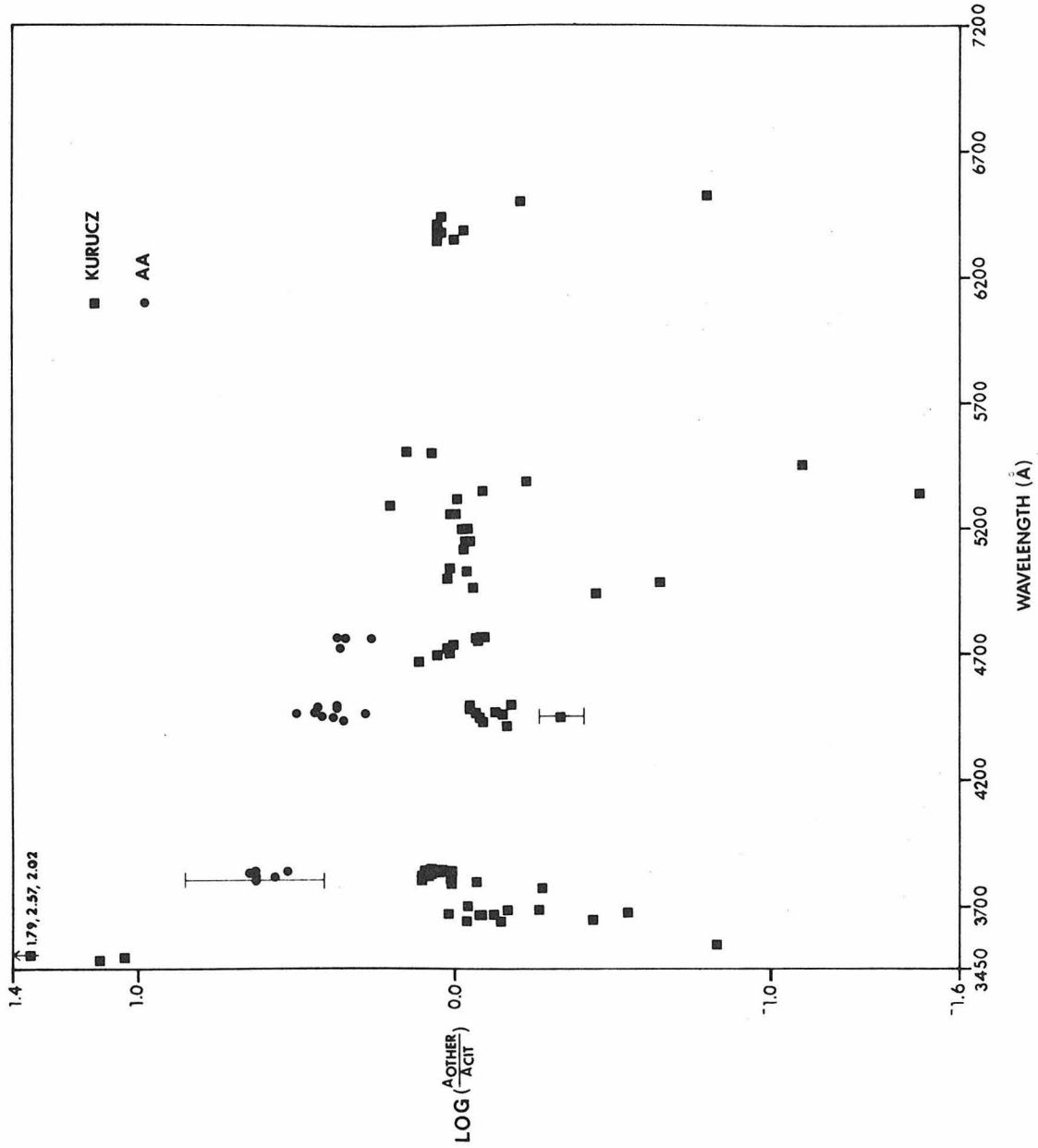
KURUCZ
AA
1.79, 2.57, 2.02
1.4
1.0
0.0
-1.0
-1.6
3450
3700
4200
4700
5200
5700
6200
6700
7200
WAVELENGTH (Å)
LOG (A_OTHER / A_CIT)

Figure 13

Transition probabilities of Corliss and Bozman (CB 1962), Woodgate (1966) and this thesis compared with respect to upper level. The error bar on an arrow represents the standard deviation of the values for the relevant term, not the standard deviation of the mean. Refer to page 57.

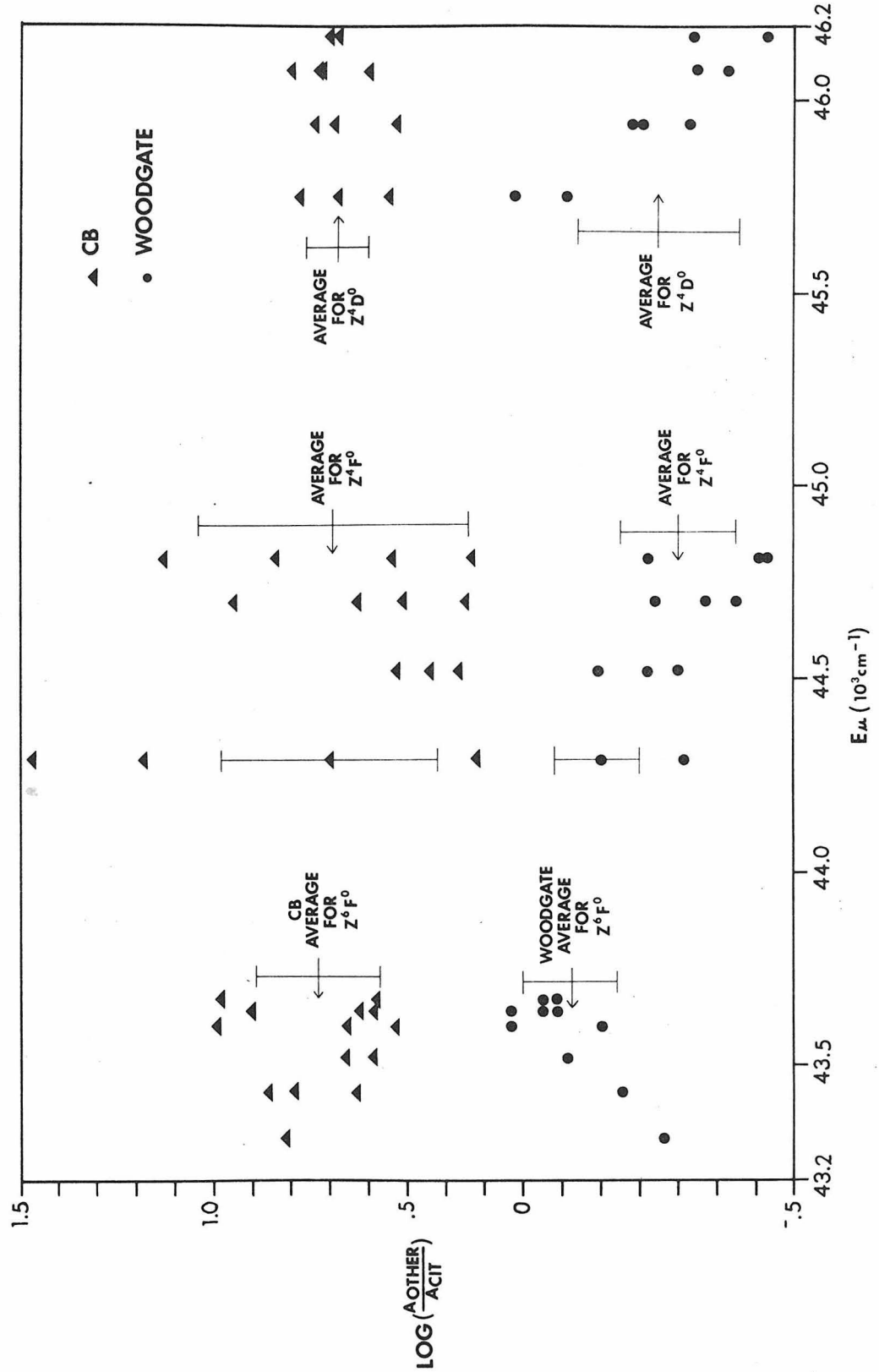
CB
WOODGATE
AVERAGE FOR Z^4D^0
AVERAGE FOR Z^4F^0
CB AVERAGE FOR Z^6F^0
WOODGATE AVERAGE FOR Z^6F^0
AVERAGE FOR Z^4F^0
AVERAGE FOR Z^4D^0
$LOG(\frac{A_{OTHER}}{A_{CIT}})$
E_μ ($10^3 cm^{-1}$)
1.5
1.0
.5
0
-.5
43.2
43.5
44.0
44.5
45.0
45.5
46.0
46.2

Figure 14

Transition probabilities of Allen and Asaad (AA 1957), Kurucz and Peytremann (1975) and this thesis compared with respect to upper level. The error bar on an arrow represents the standard deviation of the values for the relevant term, not the standard deviation of the mean. The means and standard deviations for the Kurucz points are calculated from the points in the interval $-.5 \leq \log \frac{A_{Kurucz}}{A_{CIT}} \leq +.5$, which excludes points off of the graph and the two $z\,^4D^o$ points for which $\log \frac{A_{Kurucz}}{A_{CIT}} > 1$. Refer to page 57.

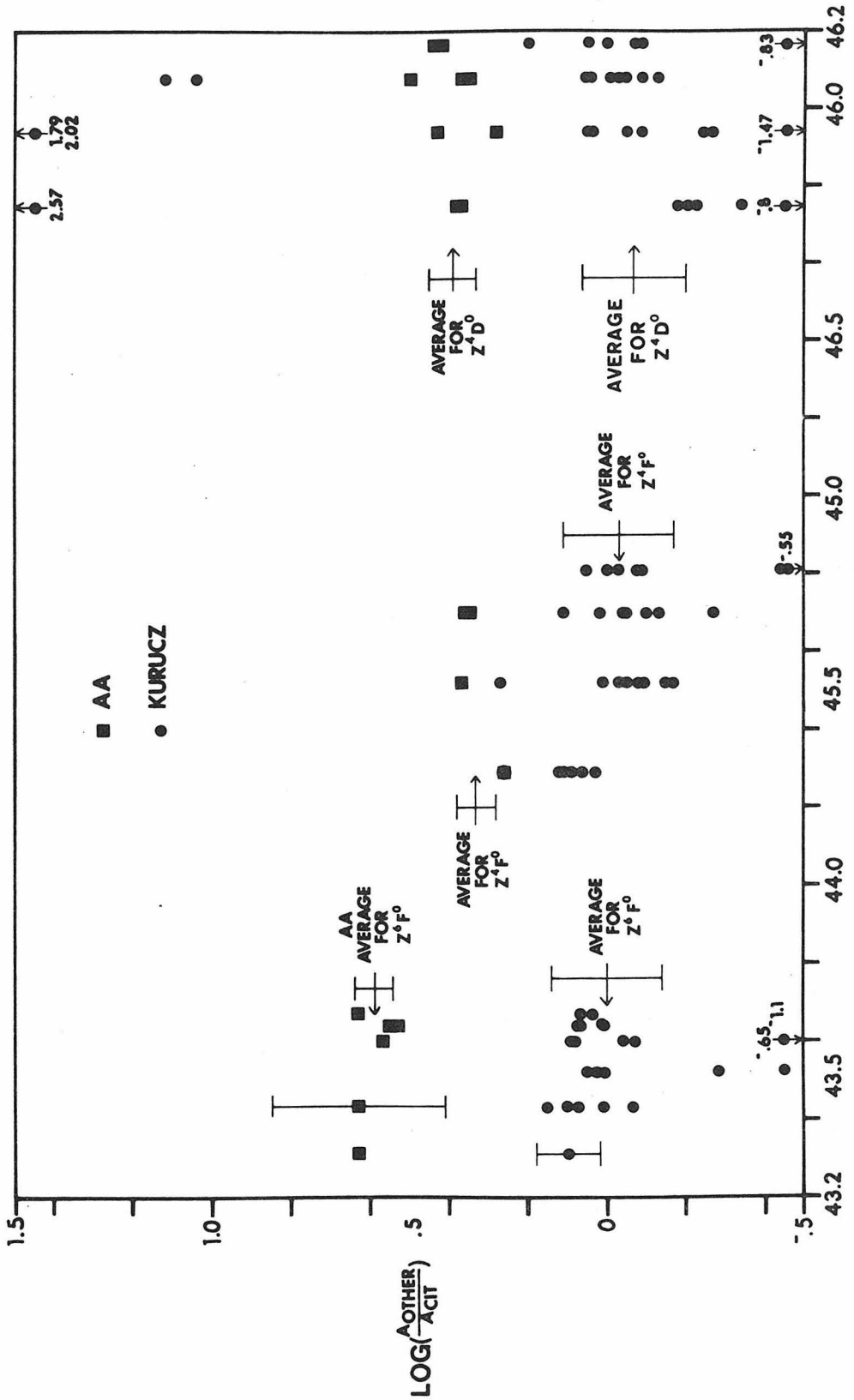
AA
KURUCZ
AA AVERAGE FOR Z^6F^0
AVERAGE FOR Z^4F^0
AVERAGE FOR Z^6F^0
AVERAGE FOR Z^4F^0
AVERAGE FOR Z^4D^0
AVERAGE FOR Z^4D^0
2.57
1.79
2.02
.65
1.1
.55
1.47
.83
$LOG(\frac{A_{OTHER}}{A_{CIT}})$
E_{AA} (10^3 cm^{-1})
1.5
1.0
.5
0
-.5
43.2
43.5
44.0
45.5
45.0
46.5
46.0
46.2

Figure 15

Transition probabilities of Corliss and Bozman (CB 1962), Woodgate (1966) and this thesis compared with respect to the transition probability. The symbols designate the terms containing the lower levels of the lines. Refer to pages 58-59.

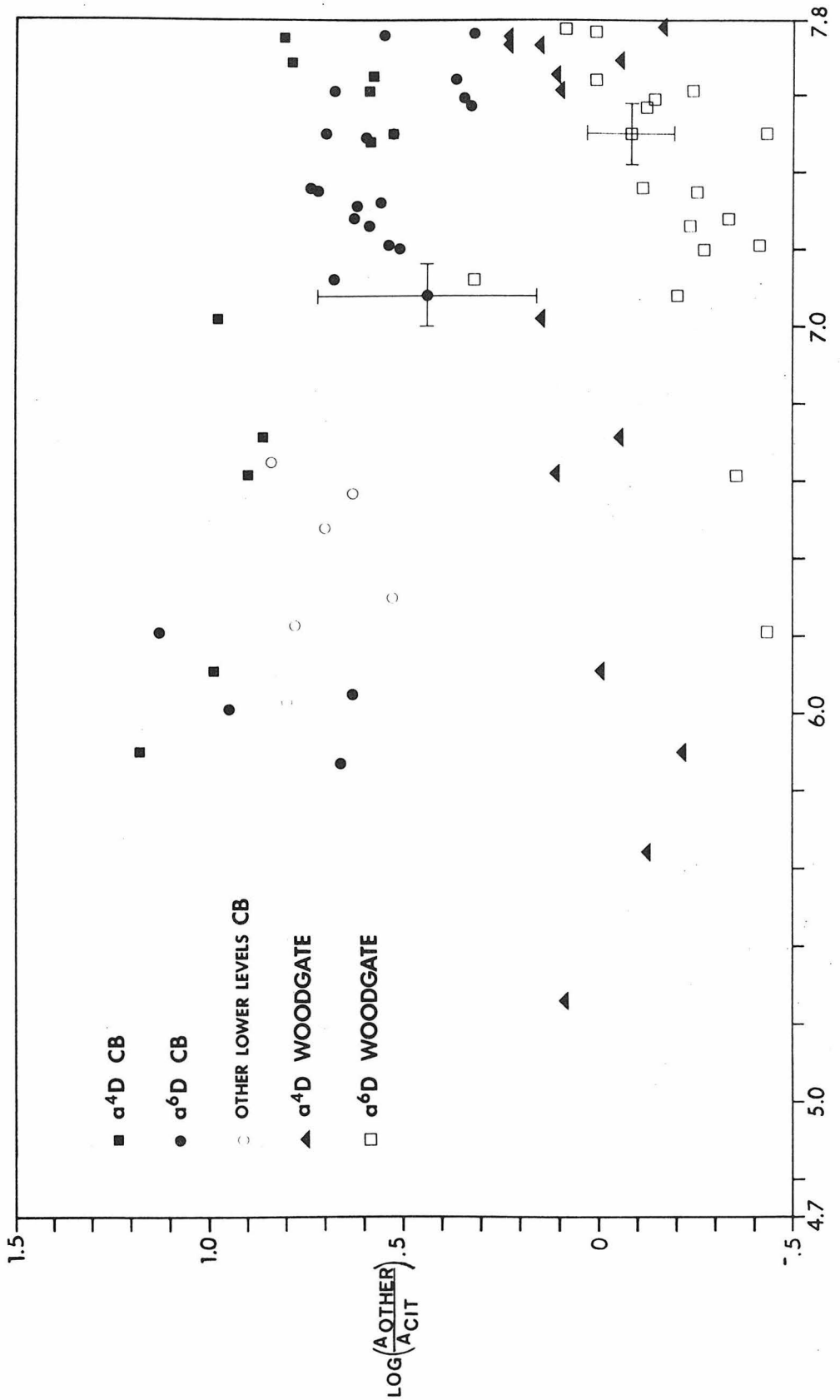
a⁴D CB
a⁶D CB
OTHER LOWER LEVELS CB
a⁴D WOODGATE
a⁶D WOODGATE
LOG (A OTHER / A CIT)
LOG A CIT
1.5
1.0
.5
0
-.5
4.7
5.0
6.0
7.0
7.8

Figure 16

Transition probabilities of Kurucz and Peytremann (1975) and this thesis compared with respect to transition probability. The symbols designate the terms containing the lower levels of the lines. Refer to page 58.

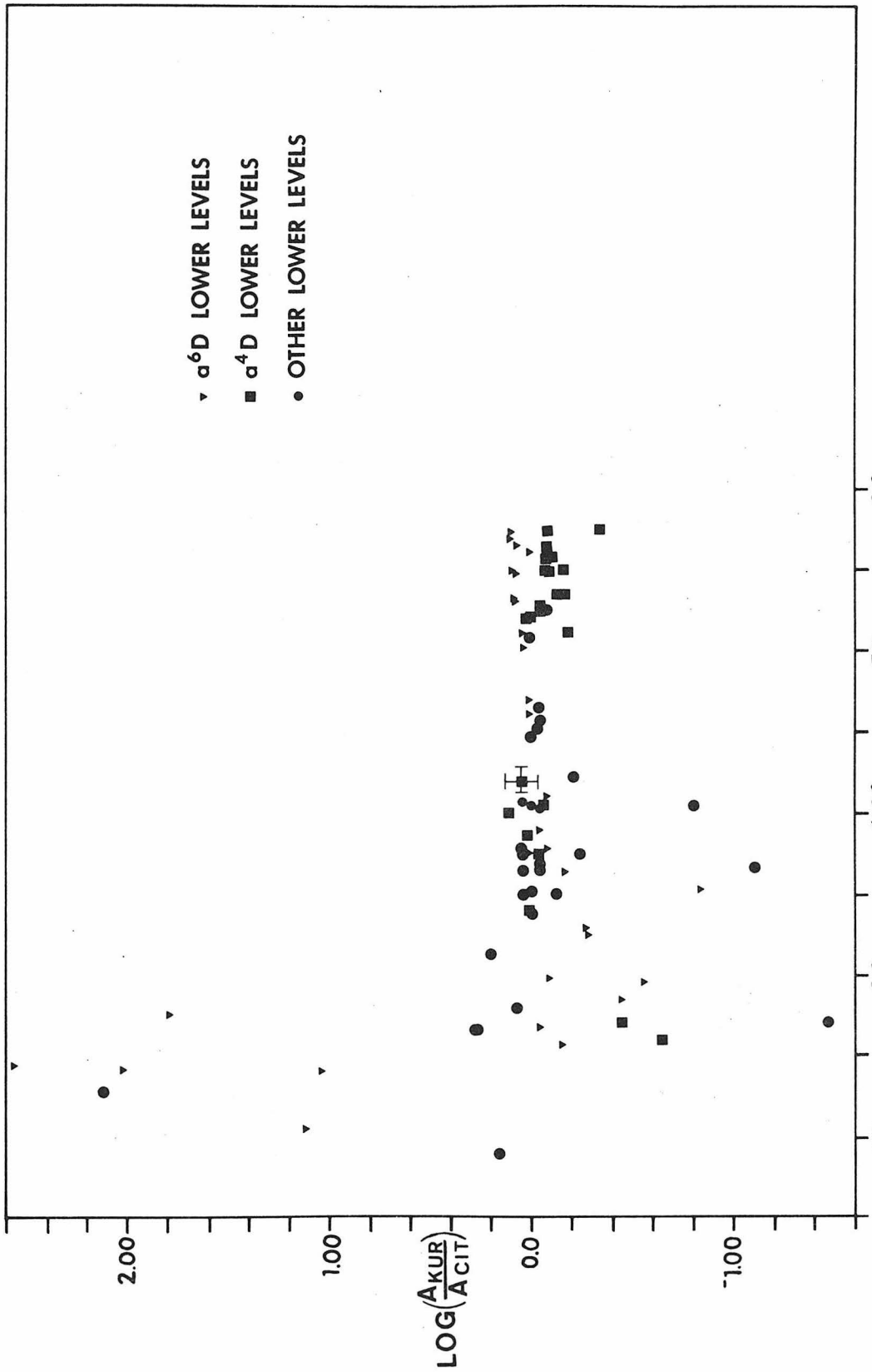
a⁶D LOWER LEVELS
a⁴D LOWER LEVELS
OTHER LOWER LEVELS
LOG(A_KUR/A_CIT)
2.00
1.00
0.0
-1.00
4.0
5.0
6.00
7.0
8.0
LOG A_CIT

Figure 17

The curve of growth. The symbols designate upper terms of lines in the solar spectrum. Equivalent widths, W, are from The Solar Spectrum (Moore et al. 1966). Log C is calculated with the parameters of Goldberg and Pierce (1959), which are used in the method of weighting functions applied to the model atmosphere of Goldberg et al. (1960). The point at the extreme right represents the line at $\lambda_{Catalan} = 3834.368$ Å ($a^6D_{5/2}$-$z^6F^o_{7/2}$). Moore assigns this line a W of 21 mÅ and a wavelength of 3834.371 Å. However, this line is badly blended in the solar spectrum with a huge (W = 624 mÅ) Fe I line at 3834.233 Å, and the listed equivalent width could be wrong. An error in the assigned W is the most likely explanation for the position of this point on the graph. Refer to page 65.

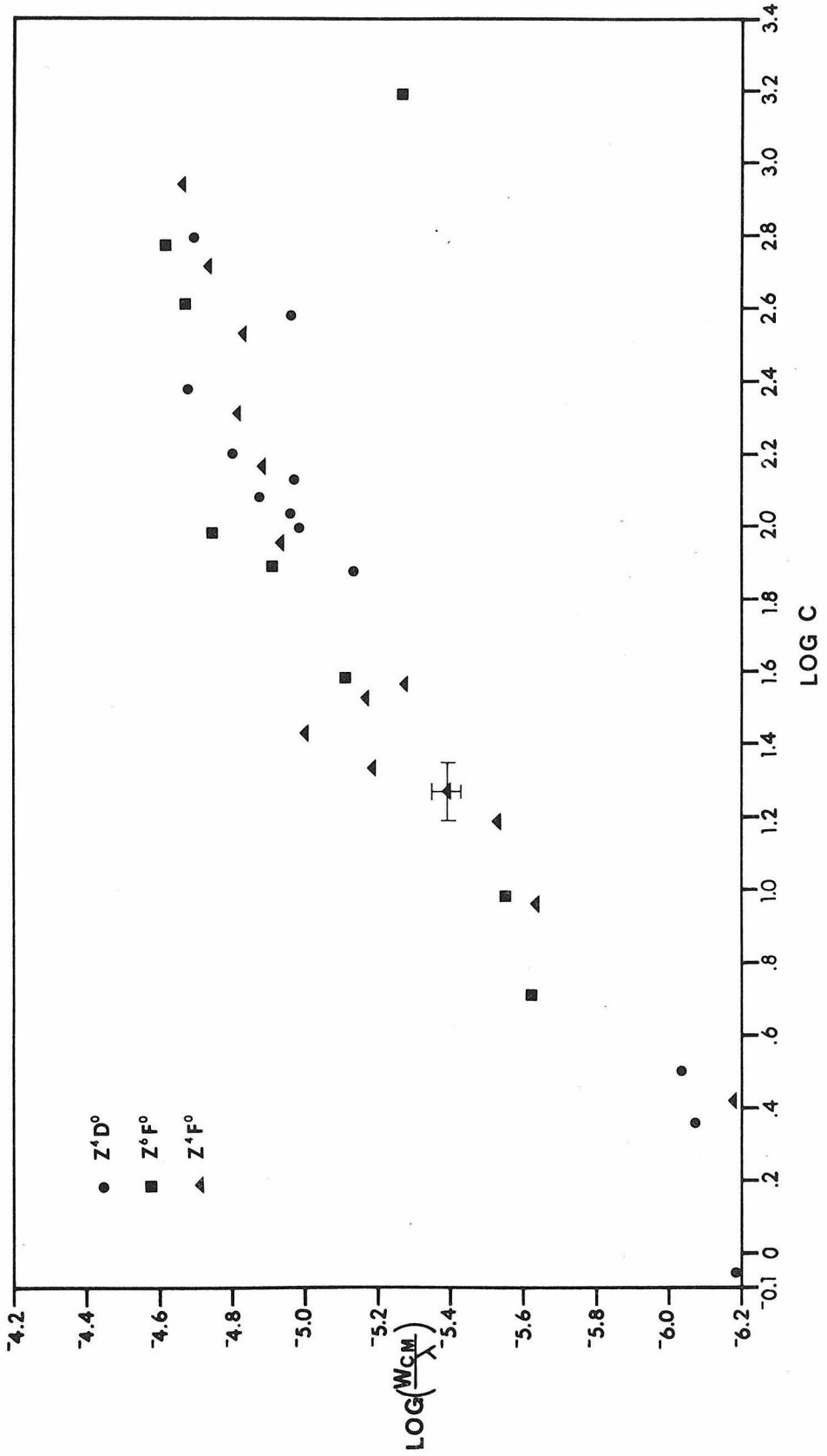
Z¹D°
Z°F°
Z¹F°
LOG C
LOG(W_CM/λ)
-4.2
-4.4
-4.6
-4.8
-5.0
-5.2
-5.4
-5.6
-5.8
-6.0
-6.2
-0.1
0
.2
.4
.6
.8
1.0
1.2
1.4
1.6
1.8
2.0
2.2
2.4
2.6
2.8
3.0
3.2
3.4

Figure 18

$A_{Mn} = \log\left(\frac{N_{Mn}}{N_H}\right) + 12.0$ plotted versus log (W_{CM}/λ) and log (W_{KP}/λ), where W_{CM} is the equivalent width of the line in the solar spectrum assigned by Moore et al. (1966) and W_{KP} is the equivalent width of the line in the Preliminary Edition of the Kitt Peak Solar Atlas (Brault and Testerman 1972). The lines are those listed in Table 7. The empty squares represent the line 5260.771. The horizontal lines are drawn at the average A_{Mn} for the lines, with 5260.771 excluded from the average. Refer to page 66.

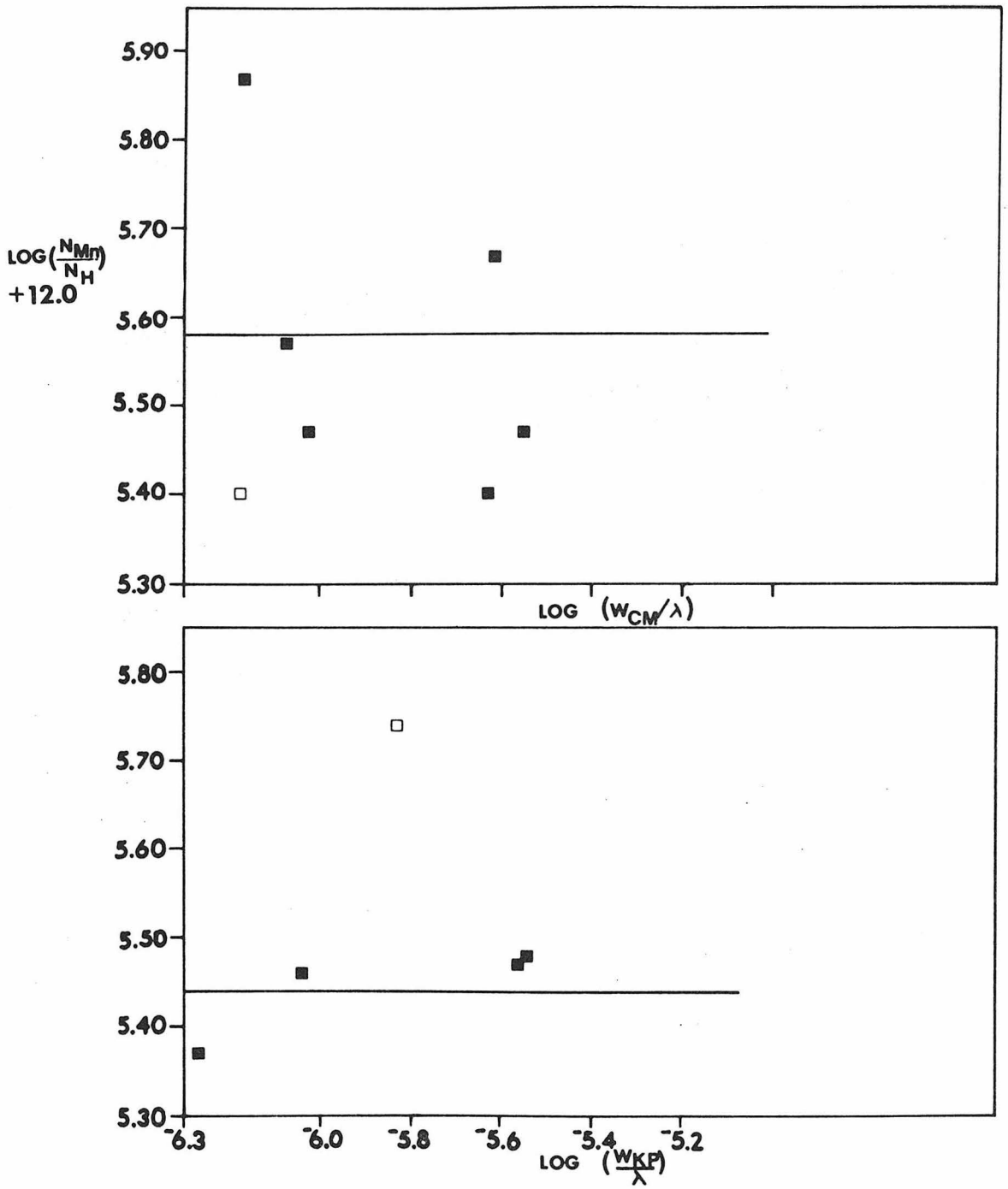
5.90
5.80
5.70
5.60
5.50
5.40
5.30
LOG $(\frac{N_{Mn}}{N_H})$ +12.0
LOG (W_{CM}/λ)
5.80
5.70
5.60
5.50
5.40
5.30
-6.3
-6.0
-5.8
-5.6
-5.4
-5.2
LOG $(\frac{W_{KP}}{\lambda})$

Figure 19

$\theta[5040/T(^{\circ}K)]$ versus log τ_{5000}, where τ_{5000} is the optical depth at 5000 Å, for the HSRA (Gingerich et al. 1971), Elste (1967), Holweger (1967) and GMA (1960) model atmospheres. Holweger actually use $\overline{\tau}$, the Rosseland mean optical depth, but he states that $\overline{\tau}$ is approximately equal to τ_{5000}. Refer to page 70.

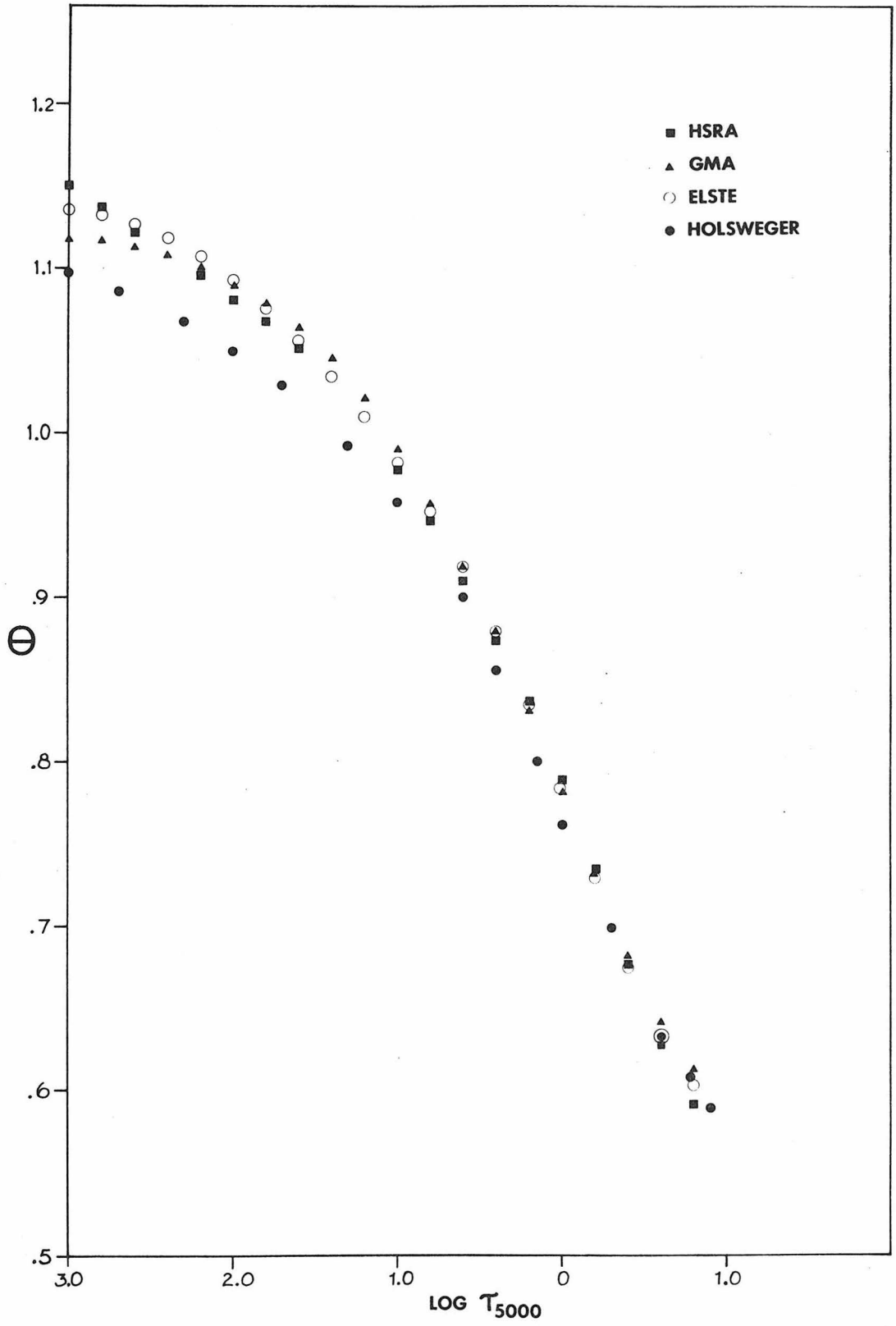
HSRA
GMA
ELSTE
HOLSWEGER
1.2
1.1
1.0
.9
.8
.7
.6
.5
Θ
3.0
2.0
1.0
0
1.0
LOG τ_{5000}

Figure 20

Log Pe, where Pe is the electron pressure in dynes/cm^2, versus log τ_{5000} for the same four model atmospheres used for Figure 19. The same comment regarding Holweger's optical depth scale applies here. Refer to page 70.

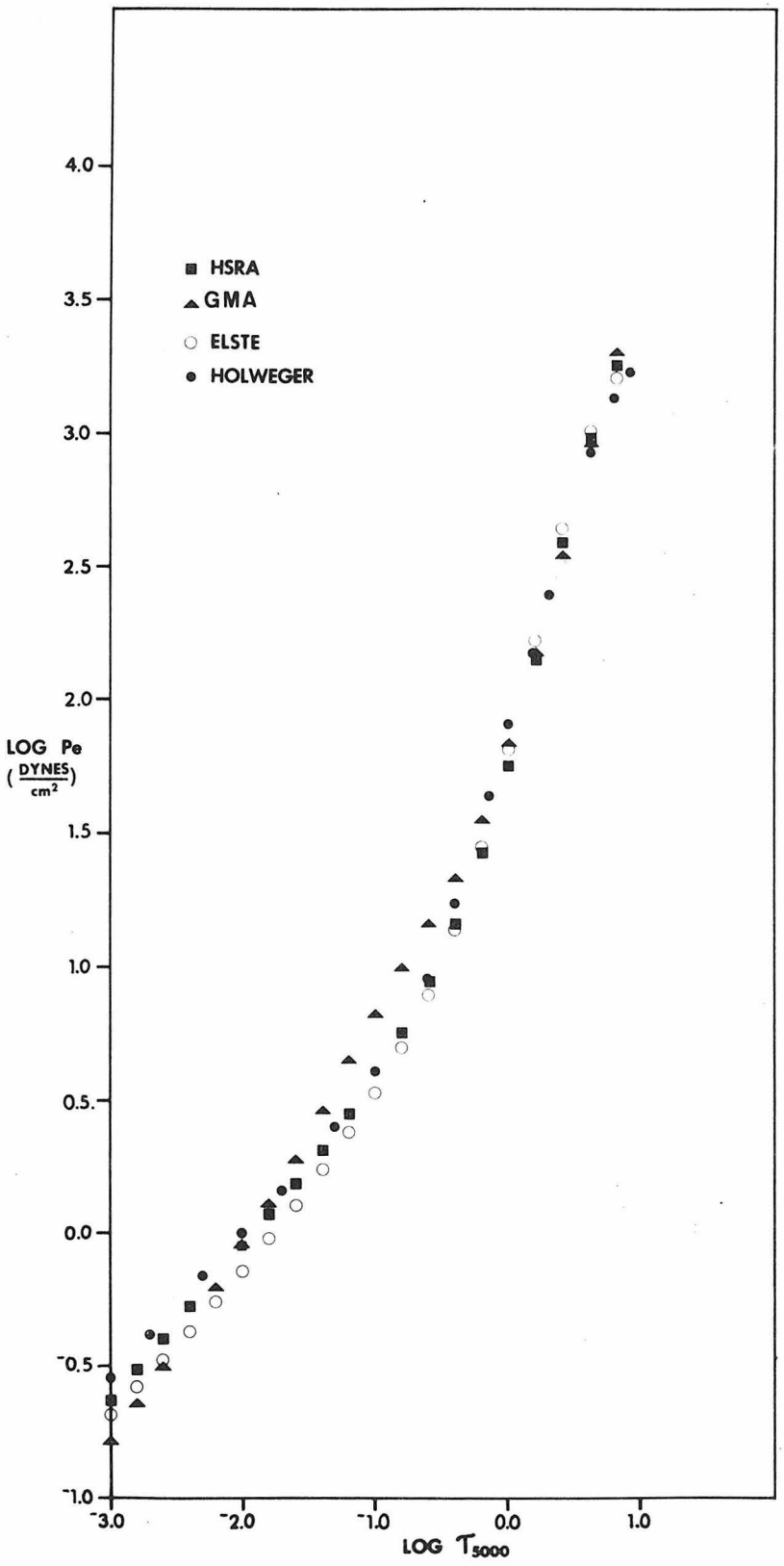
HSRA
GMA
ELSTE
HOLWEGER
4.0
3.5
3.0
2.5
2.0
1.5
1.0
0.5
0.0
-0.5
-1.0
LOG Pe
(DYNES/cm²)
-3.0
-2.0
-1.0
0.0
1.0
LOG τ5000